



Flinders
UNIVERSITY

Vibration Cancellation in Plate Structures

by

Qingqing Chen, M.Eng. (Electronics)

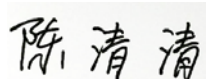
Supervisor: Fangpo He

Date of submission: May, 2016

Submitted to the School of Computer Science, Engineering, and Mathematics in the Faculty of Science and Engineering in partial fulfilment of the requirements for the degree of master of engineering (electronics) at Flinders University – Adelaide Australia

Declaration

I certify that this thesis does not incorporate without acknowledgment any material previously submitted for a degree or diploma in any university; and that to the best of my knowledge and belief it does not contain any material previously published or written by another person except where due reference is made in the text.

Handwritten signature of Qingqing Chen in black ink on a light gray background.

Qingqing Chen

May, 2016

Acknowledgement

First, I'd like to say thank you to my supervisor, Fangpo He, I'm inspired by her dedicated work style and encouraging persistence, she is very open to communicate with me whenever I have problems for the project. I really appreciate her valuable input and encouragement to this challenging project.

And I'm thankful to ph.D. student Peng Zhang, for his generosity in helping me during the project.

Also, I want to say thank you to all related staff that helped a lot in many ways, thank you for your patience and kindness.

Finally, special thanks to my husband and my parents, thanks for your selfless support all the way from China to Australia.

Abstract

In a mechanical system, unwanted vibration is usually considered as noise because it can affect the accuracy of the system or even damage the entire system. The task of vibration cancellation therefore plays an important role in the design of the mechanical system.

In this project, a multi-input multi-output (MIMO) vibration cancellation problem is demonstrated using a laboratory plate structure, which consists of one base plate, three sensor/actuator pairs, one disturbance transducer, and one top plate. The vibration to be controlled on the top plate is introduced by the disturbance transducer that is mounted on the base plate. The main goal of this project is to control the first three modes of the vibration on the top plate while the external vibration caused by the disturbance transducer persistently exists.

Theoretical analysis method and physical experiment method are utilized to derive the transfer function matrix of the plate. Modal analysis software, ModalVIEW, is used to obtain the frequency response function (FRF) of the plate as well as the parameters of the transfer functions including natural frequencies, damping ratios, and mode shapes. For the purpose of the controller design, the measured model of the plate is truncated to the first three modes and a model correction technique based on spatial H_2 norm is applied to the truncated model to minimize the truncation error.

Based on the transfer function matrix obtained in the modeling stage, positive position feedback (PPF) control technique is selected to design the controllers because of its quick roll-off property at higher frequencies and its stability of the corresponding closed-loop system. The plate structure is considered, respectively, as a group of individual SISO systems or a single interconnected MIMO system for the design and implementation of the PPF controllers. Natural frequencies of the PPF controllers are set to be the same as the target modes in order to add extra damping according to the PPF design principle. Selection of the damping ratios and controller gains is considered as a spatial H_∞ optimization problem. SISO and MIMO PPF controllers are designed, respectively, for the corresponding SISO and MIMO models of the plate.

The designed SISO-PPF and MIMO-PPF controllers are validated via simulation and experiment separately. It is seen that the simulated PPF controlled system can achieve the desired control effects, and the current experimental results can achieve on average a 30.1%

of vibration attenuation. With further tuning of the parameters of the PPF controllers as well as the mathematical models of the plate structure, it is anticipated that the experimental vibration attenuation can be further improved.

List of Figures

Figure 1.1 Laboratory model used in this vibration cancellation project	2
Figure 2.1 Initial laboratory model of this project	5
Figure 2.2 An example of passive vibration control.....	9
Figure 2.3 An example of active vibration control	10
Figure 2.4 Block diagram of feedback control	10
Figure 2.5 Block diagram of feedforward control	11
Figure 3.1 Comparison of previous and current plate structure.....	13
Figure 3.2 Electromagnetic transducer used as sensor and actuator.....	14
Figure 3.3 Cross section of the electromagnetic transducer	14
Figure 3.4 PCB of interface board	15
Figure 3.5 Working principle of self-sensing technique.....	16
Figure 3.6 Block diagram to compute induced voltage	17
Figure 3.7 NI DAQ 9234 module and BNC connector assignments.....	17
Figure 3.8 Input circuitry for each channel.....	18
Figure 3.9 Effect of build-in gain in dSPACE.....	21
Figure 4.1 Input and output in plate structure.....	23
Figure 4.2 Block diagram of 3-input 3-output system.....	24
Figure 4.3 Hardware connection for manual measurement	29
Figure 4.4 Manually measured FRF curves	30
Figure 4.5 Block diagram and physical setup for performing measurement in ModalVIEW .	31
Figure 4.6 ModalVIEW software measured FRF curves.....	32
Figure 4.7 Comparison of manually measured and ModalVIEW measured FRF curves	33
Figure 4.8 Plate structure in ModalVIEW software	34
Figure 4.9 Simulated transducer positions in ModalVIEW software	34
Figure 4.10 Hardware connection for modelling.....	35
Figure 4.11 Input and output signals.....	36
Figure 4.12 FRF curve of G11, G21, G31 generated in ModalVIEW.....	37
Figure 4.13 FRF curve of G12, G22, G32 generated in ModalVIEW.....	38
Figure 4.14 FRF curve of G13, G23, G33 generated in ModalVIEW.....	39
Figure 4.15 Modal analysis window in ModalVIEW software	40
Figure 4.16 Modal estimate parameter setting window.....	41

Figure 4.17 Comparison of FRF curves of all modes and significant modes-input from transducer 1	46
Figure 4.18 Comparison of FRF curves of all modes and significant modes-input from transducer 2	47
Figure 4.19 Comparison of FRF curves of all modes and significant modes-input from transducer 3	48
Figure 4.20 Comparison of FRF of true model and truncated model	52
Figure 4.21 Comparison of FRF of true model and corrected model	56
Figure 5.1 Block diagram of PPF control system	58
Figure 5.2 Configuration of standard H_∞ method	63
Figure 5.3 Block diagram for PPF controller evaluation	64
Figure 5.4 H_∞ optimized SISO-PPF controller for mode 1	65
Figure 5.5 Control effects of SISO-PPF Mode 1	65
Figure 5.6 H_∞ optimized SISO-PPF controller for mode 2	66
Figure 5.7 Control effects of SISO-PPF Mode 2	66
Figure 5.8 H_∞ optimized SISO-PPF controller for mode 3	67
Figure 5.9 Control effects of SISO-PPF Mode 3	67
Figure 5.10 Control effects of SISO-PPF three modes control on corrected model	68
Figure 5.11 Control effects of SISO-PPF three modes control on true model	69
Figure 5.12 H_∞ optimized MIMO-PPF controller for mode 1	70
Figure 5.13 Control effects of MIMO-PPF mode 1	71
Figure 5.14 H_∞ optimized MIMO PPF controller for mode 2	73
Figure 5.15 Control effects of MIMO PPF-Mode 2	73
Figure 5.16 H_∞ optimized MIMO-PPF controller for mode 3	75
Figure 5.17 Control effects of MIMO-PPF mode 3	76
Figure 5.18 Control effects of MIMO-PPF three modes control on corrected model	77
Figure 5.19 Control effects of MIMO-PPF First three modes on true model	79
Figure 6.1 Hardware setup and block diagram of control experiment	81
Figure 6.2 FRF curves of each transducer - Open-loop	82
Figure 6.3 SIMULINK model of SISO PPF control experiment	83
Figure 6.4 Configuration of subsystem	83
Figure 6.5 Control signal generated in dSPACE	84
Figure 6.6 Comparison of FRF curves of open-loop and SISO-PPF closed-loop	85
Figure 6.7 SIMULINK model of MIMO PPF control experiment	87

Figure 6.8 Comparison of FRF curves of open-loop and MIMO PPF closed-loop.....	88
Figure A.0.1 Schematic circuit of interface board.....	94
Figure A.0.2 Component layout of interface board.....	95
Figure A.0.3 Create a new project in ModalVIEW.....	96
Figure A.0.4 Blank structure view window.....	97
Figure A.0.5 Structure editor window.....	97
Figure A.0.6 Select plate structure.....	98
Figure A.0.7 Measure property window.....	98
Figure A.0.8 Measure window.....	99
Figure A.0.9 Select front end.....	99
Figure A.0.10 DAQ setup window-Channel page.....	100
Figure A.0.11 DAQ setup window-Acquisition page.....	100
Figure A.0.12 Measurement scheme window-Measurement page.....	101
Figure A.0.13 Measurement scheme window-post-process page.....	101
Figure A.0.14 Measurement scheme window-Measurement set page.....	102
Figure A.0.15 FRF window.....	102
Figure A.0.16 Zoom in 20-60 Hz range.....	103
Figure A.0.17 Mode estimation window.....	103
Figure A.0.18 Structure window.....	104
Figure A.0.19 Modal parameters.....	104

List of Tables

Table 3.1 Mapping of A/D converters to DS1103 I/O pins.....	19
Table 3.2 Mapping of D/A converters to DS1103 I/O pins.....	20
Table 3.3 A/D and D/A channels used in dSPACE.....	20
Table 4.1 Input and output combinations for FRF measurement	29
Table 4.2 Modal analysis result	41
Table 4.3 Modal parameters	44
Table 5.1 Routh- Hurwitz array of PPF control system.....	59
Table 5.2 Parameters for SISO-PPF controller-Mode 1	64
Table 5.3 Vibration control result for SISO-PPF mode 1.....	65
Table 5.4 Parameters for SISO-PPF controller-Mode 2	66
Table 5.5 Vibration control result for SISO-PPF mode 2.....	66
Table 5.6 Parameters for SISO PPF-controller Mode 3	67
Table 5.7 Vibration control result for SISO-PPF mode 3.....	68
Table 5.8 Vibration control result for SISO-PPF first three modes control	68
Table 5.9 Parameters for MIMO-PPF Controller-Mode 1.....	70
Table 5.10 Vibration control result for MIMO PPF mode 1	71
Table 5.11 Parameters for MIMO-PPF controller-Mode 2	72
Table 5.12 Vibration control result for MIMO-PPF mode 2.....	74
Table 5.13 Parameters for MIMO-PPF controller mode 3	74
Table 5.14 Vibration control result for MIMO-PPF mode 3.....	76
Table 5.15 Vibration control result for MIMO PPF first three modes	77
Table 6.1 Result of experiment of SISO-PPF controlled system.....	86
Table 6.2 Result of experiment of MIMO-PPF controlled system.....	89
Table A.1 Component list of interface board.....	95

Contents

Declaration.....	i
Acknowledgement	iii
Abstract.....	v
List of Figures	vii
List of Tables	x
Chapter 1 : Introduction	1
1.1 Project Background.....	1
1.2 Project Statement.....	2
1.3 Research Methodology.....	2
1.4 Outline of This Thesis	3
Chapter 2 : Literature Review.....	5
2.1 Review of Previous Works.....	5
2.2 Mathematical Modelling of a Physical Structure.....	7
2.3 Vibration Control Technique	7
2.3.1 Active and Passive Control.....	7
2.3.2 Feedback and Feedforward Control	10
2.3.3 Positive Position Feedback (PPF) Control	11
Chapter 3 : Physical System Setup	13
3.1 Laboratory Plate Structure Model.....	13
3.1.1 Sensor and Actuator.....	13
3.2 Interface Board.....	15
3.3 NI DAQ Module.....	17
3.4 DSPACE Module	18
Chapter 4 : Modelling the Plate Structure.....	22
4.1 Plant Characteristics	22

4.2 Analytical Derivation of Transfer Function	24
4.3 Verify Performance of ModalVIEW Software	28
4.3.1 Measure FRF Curve Manually	28
4.3.2 Measure FRF Curve Using ModalVIEW Software.....	30
4.3.3 Compare FRF	32
4.4 Experimental Modelling in ModalVIEW Software	33
4.4.1 Draw Plate Structure in ModalVIEW	33
4.4.2 FRF Measurement in ModalVIEW	34
4.4.3 Modal Analysis in ModalVIEW	40
4.5 Simulate Plant Model in MATLAB	45
4.6 Model Truncation.....	51
4.7 Model Correction	53
Chapter 5 : Controller Design	57
5.1 PPF Controller Characteristics	57
5.2 Stability of PPF Controlled System	58
5.2.1 Single-Input Single-Output Case.....	58
5.2.2 Multi-Input Multi-Output Case	59
5.3 PPF Controller Parameters Selection	61
5.3.1 Frequency Selection	61
5.3.2 Damping and Control Gain Selection.....	63
5.4 SISO-PPF Controller Design and Validation.....	64
5.4.1 First Mode Control	64
5.4.2 Second Mode Control.....	65
5.4.3 Third Mode Control.....	67
5.4.4 Three Modes Control.....	68
5.5 MIMO-PPF Controller Design and Validation	69
5.5.1 First Mode Control	70

5.5.2 Second Mode Control.....	72
5.5.3 Third Mode Control.....	74
5.5.4 Three Modes Control.....	77
Chapter 6 : PPF Control Experiment	80
6.1 Experiment Setup	80
6.2 Open-Loop System Measurement.....	81
6.3 SISO-PPF Control Experiment	83
6.4 MIMO-PPF Control Experiment.....	87
6.5 Experiment Summary.....	90
Chapter 7 : Conclusion.....	91
7.1 Project Conclusion	91
7.2 Recommendations	93
Appendix A: Interface Board.....	94
Appendix B: Modal Analysis Procedure in ModalVIEW Software.....	96
Appendix C: MATLAB Code.....	105
Bibliography	110

Chapter 1 : Introduction

In this chapter, project background is briefly introduced, statement of the control problem, control goal and research methodology implemented in this project are described. At last, outline of this thesis is provided.

1.1 Project Background

It has been proved that every physical structure has certain natural frequencies, which are mainly determined by material properties and geometry properties of the structure. When external periodic force matched structure's natural frequencies, the structure will oscillate or vibrate fiercely, this phenomenon called resonance. Like other natural phenomenon, resonance is welcomed in some activities, such as musical instruments, resonance phenomenon is utilized to produce beautiful music. However, in mechanical area, resonance often causes mechanical distortion and dynamic stress to the structure, consequently, result in disturbance, damage or even totally destruction to the mechanical system. The most famous accident caused by resonance is the collapse of Tacoma Narrows Bridge in the year of 1940 [1]. Tacoma Narrows Bridge was a suspension bridge in Washington, the bridge was opened to traffic on 1 July 1940, and dramatically collapsed on 7 November of the same year, the reason of this accident is the wind provide an external periodic force that matched the bridge's natural frequency. In other words, resonance destroyed this bridge. This accident attracts people's attention on mechanical vibration, for many years.

In recent years, with the rapid development of material technology and economic considerations, more and more mechanical systems tend to be lighter and individuation [21], however, this makes the mechanical structure becomes more flexible, consequently much more easily be affected by external vibrations, especially when the frequency of external vibration is close to the natural frequency of the mechanical system. Therefore, vibration control, especially resonance control becomes increasingly important in the design process of mechanical systems.

Based on above information, this project mainly focuses on controlling the vibration of a plate structure while the external periodic force persistently exists.

1.2 Project Statement

In this project, a multi-input multi-output (MIMO) vibration control problem was demonstrated using a laboratory model, as shown in Figure 1.1.

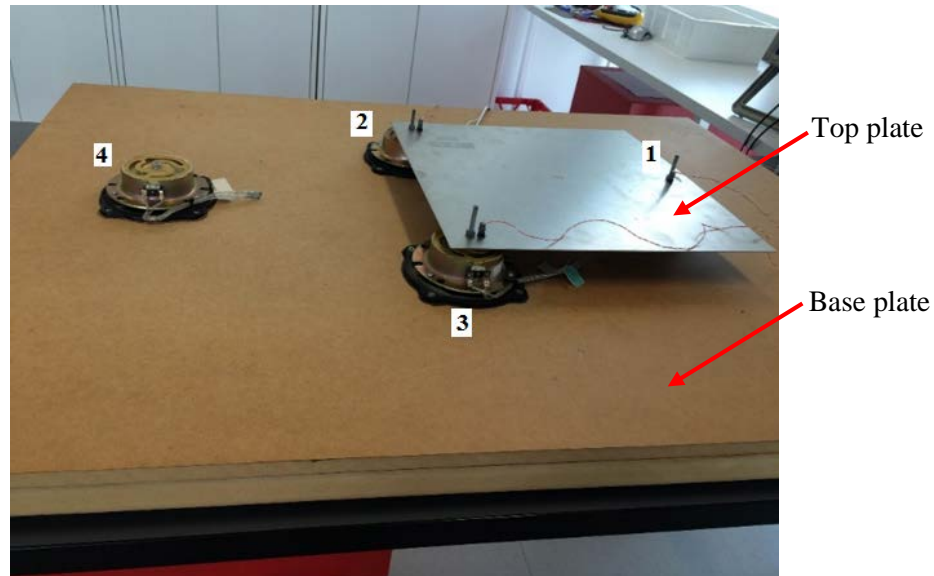


Figure 1.1 Laboratory model used in this vibration cancellation project

As shown in Figure 1.1, laboratory model is constructed by a base plate, a top plate, 4 transducers and 4 support feet. Four transducers mounted on the base plate at specified positions, transducer 1, 2 and 3 also fastened with the top plate by screws. Transducer 4 is used to simulate external disturbance, the other three transducers are used as sensors and actuators. By applying a continuous periodic force to base plate through transducer 4, the whole structure including the top plate will vibrate.

The goal of this project is to control the first three modes of resonance vibration on the top plate while the external disturbance persistently exists.

1.3 Research Methodology

With the purpose of control vibration at the resonance frequency, procedures of dealing with a typical control problem were followed.

In the first step, different modelling methods for dynamic systems were searched and compared. Various vibration control techniques as well as their advantages, drawbacks and applications were studied. Based on above information, positive position feedback control technique was selected for this project.

Chapter 1: Introduction

The second step was to build a mathematical model for the plate structure, based on the modelling knowledge and considering the complexity of the structure. Theoretical analysis method was used to obtain the mathematical expression of transfer functions. Physical experiment method was implemented to get parameters of transfer functions by using modal analysis software, ModalVIEW. After that, modal truncation and model correction techniques were applied to obtain an accurate mathematical model that suitable for controller design purpose. Numerical modelling method was not used because it is difficult to build a precise model for the whole plate structure in ANSYS software. Consequently, it is hard to get an accurate mathematical model.

The third step was to design appreciate controller and validate its control effect. Different positive position feedback (PPF) controllers were designed for single-input single-output (SISO) model and multiple-input multiple-output (MIMO) model of the plate structure. Control effects were evaluated by implementing corresponding controller into the corrected mathematical model and further into the simulated true plant model in MATLAB.

The last step was to further validate control effect in physical experiment through dSPACE. Based on the PPF controllers designed in the last step, physical control experiment was done to further evaluate control effects. SISO PPF controller and MIMO PPF controller were evaluated separately, and corresponding control results were analyzed and compared.

1.4 Outline of This Thesis

In this thesis, vibration cancellation of a square aluminum plate structure by using positive position feedback control technique is presented. Thesis outline is as follows:

In chapter 2, an overall literature review is given. Main previous works were summarized chronologically. Different modelling ways and various control techniques, as well as their applications were analyzed and compared.

In chapter 3, the physical equipment setup used in modeling stage and experimental stage are described. Main properties of each individual module, as well as its application in this project are provided.

In chapter 4, procedures of modelling the plate structure are detailed described. Two modelling methods were used. Theoretical analysis was adopted to obtain the structure of transfer function matrix. Physical experimental method was implemented to obtain parameters of transfer function by using modal analysis software, ModalVIEW. Then modal

Chapter 1: Introduction

truncation and model correction techniques were used to derive a proper mathematical model which is suitable for controller design purpose.

In chapter 5, principles of PPF controller and steps to develop PPF controller are presented. Firstly, basic PPF structure and its working principles were introduced, then detailed described how to select each PPF parameter. After that, SISO PPF controller and MIMO PPF controller for single mode control and multi-mode control were designed and evaluate respectively in MATLAB.

In chapter 6, physical vibration control experiments were performed to control vibration on the laboratory plate structure through dSPACE. SIMUINK models for SISO system control and MIMO system control were designed separately, corresponding PPF controllers were imposed on physical plant and their control effects were further validated and analyzed.

In chapter 7, the conclusion from all above experiments was drawn. Based on this project conclusion and problems encountered during the project, future works were suggested.

Chapter 2 : Literature Review

In this chapter, firstly main previous works are summarized, and then based on the need of this project, three different kinds of mathematical modelling techniques are compared and different types of vibration control methods are analyzed and compared.

2.1 Review of Previous Works

The initial work of this project was done by Groothuis and Roesthuis [2], where a multi-input multi-output (MIMO) vibration control problem was demonstrated using a laboratory model, which forms the prototype of this project. This laboratory physical model is made up of one base plate, four transducers, one top plate, and four support feet. The four transducers mounted on the base plate at specified positions, three of them also connected to the top plate, as shown in Figure 2.1. Transducer 4 used as disturbance to provide external vibration to the whole system, the other three transducers used as sensors and actuators.

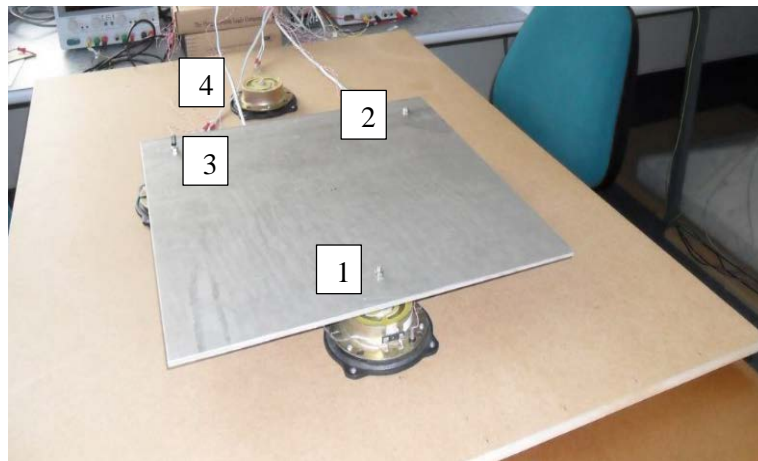


Figure 2.1 Initial laboratory model of this project

The authors modeled above laboratory physical model in ANSYS and got transfer function from the results of ANSYS modal analysis. They designed an electromagnetic shunt controller in dSPACE to reduce the current flow through the transducer by series a synthetic impedance to the transducer, so that the vibration will be suppressed.

Gusnawan [3] did the second stage of work, where theoretical method was used to derive the characteristics of the plate structure. Using classical theory of vibration of a plate structure, the classical differential equation of transverse vibration of a plate is given by:

$$D\nabla^4 w + \rho \frac{\partial^2 w}{\partial t^2} = 0 \quad (2.1)$$

Chapter 2: Literature Review

where ρ indicate mass density per unit area of the plate, t indicate time, and D indicate flexural rigidity of the plate, which is defined by

$$D = \frac{Eh^3}{12(1-\nu^2)} \quad (2.2)$$

where E is Young's modulus, h is the thickness of the plate and ν is Poisson's ratio.

By solving this vibration differential equation, natural frequency equations can be expressed as:

$$\omega_{mn} = \pi^2 \left[\left(\frac{2n-1}{2x} \right)^2 + \left(\frac{m}{y} \right)^2 \right] \sqrt{\frac{D}{\rho}} \quad (2.3)$$

$$\omega_{mn} = \pi^2 \left[\left(\frac{n}{x} \right)^2 + \left(\frac{m}{y} \right)^2 \right] \sqrt{\frac{D}{\rho}} \quad (2.4)$$

where x and y indicate dimension of the pate.

Equation (2.3) is used for mode 1, and equation (2.4) used for other modes to calculate natural frequency.

Yu [4], who explained how to obtain the transfer function of the plate structure from ANSYS analysis result, did the third phase of work.

Begin from the typical partial derivative equation (PDE) of two-dimensional structures:

$$\mathcal{L}[y(x, y, t)] + \mathcal{C} \left[\frac{\partial y(x, y, t)}{\partial t} \right] + \mathcal{M} \left[\frac{\partial^2 y(x, y, t)}{\partial t^2} \right] = f(x, y, t) \quad (2.5)$$

The transfer function of equation (2.5) is derived as:

$$T_{mn}(s) = \sum_{k=1}^{\infty} \frac{y_m y_n}{s^2 + 2\zeta_{mn} \omega_k s + \omega_k^2} \quad (2.6)$$

where: m and n are the position in two-dimensional space; y_m, y_n are the mode shape of the position on transducer m or n on the top plate; ω_k is natural frequency of K^{th} mode; ζ_k is damping ratio of K^{th} mode.

Using ANSYS software, natural frequencies and mode shape can be obtained from Modal Analysis directly, damping ratio can be calculated by using equation (2.7):

$$\zeta_{mn} = \frac{y_m y_n U_n}{2\omega_k^2 Y_m} \quad (2.7)$$

Based on the numerical model that derived in [4], Nguyen [5] introduced positive position feedback (PPF) control method and designed a single-input single-output (SISO) PPF controller. This controller was applied to experiment through dSPACE software.

2.2 Mathematical Modelling of a Physical Structure

Mathematical modelling is an essential and very important step in any control project since a reasonable mathematical model can mathematically represent behaviors and dynamics of a physical structure and is the fundamental of the following steps [23]. There are usually three ways to build a model for a given structure, which are theoretical analysis, numerical analysis and physical experiment [6][7].

Theoretical analysis must base on the basic physical principles and laws. This is the way to derive a very precise mathematical model. In most cases, unfortunately, due to the complexity of the physical structure, it is difficult or time-consuming to conduct theoretical analysis.

Numerical analysis plays an important role in terms of mathematical modeling. With the rapid development of computer techniques, numerical analysis often conducted with the help of specific software, such as ANSYS, MATLAB, Category, etc. The precision of modeling results depends on how precise the model built in the software is [8].

Physical experiment is the most reliable way to derive the mathematical model. All data comes from real experiment or real measurement, which can maximally reflect system's dynamics.

2.3 Vibration Control Technique

Vibration control techniques can be classified as active and passive control, feedback and feedforward control, open-loop and closed loop control, collocated control and un-collocated control [11].

2.3.1 Active and Passive Control

Most vibration control methods can be classified as either active control or passive control, the others combined features of both active control and passive control, called hybrid [10].

Passive vibration control

Passive vibration control methods usually using additional simple mechanical structures, rely on passive damping by using viscoelastic materials such as traditional vibration damper, shock absorber and base isolation. Therefore, successful usage of passive vibration control

requires a totally understanding of the vibration problem and properly selection of the damping material.

Main properties of passive vibration control technique are listed below [9] [10]:

- a) Almost all passive control methods have low-frequency resonance problems, which means when frequency is very low, instead of damping the vibration, the passive control system will increase the vibration. This phenomenon may cause unwanted problems.
- b) Passive control systems have high performance once they are started, substantially suppressing vibration effectively within a few Hz.
- c) The weight, size, structure and gravity center of the instrument can affect the performance of the vibration control system.
- d) The majority of passive control systems is only focused on Z-axis of vibration and are not able to cancel out horizontal vibrations, which means additional mechanisms need to be applied if X-axis or Y-axis of vibration required to be attenuated.
- e) Due to the softness property, passive control systems often have a relatively long settling time, typically several seconds.
- f) Passive vibration control systems often have relatively large size and huge weight for the purpose of better control effect.
- g) Passive control systems are much cheaper than active control systems since no precise component is used.

Figure 2.2 shows an example of passive vibration control system. The vibration elimination mainly relies on the use of Tuned Mass Absorbers. This tuned mass absorber can absorb the vibration energy at the resonance frequency of the main structure.

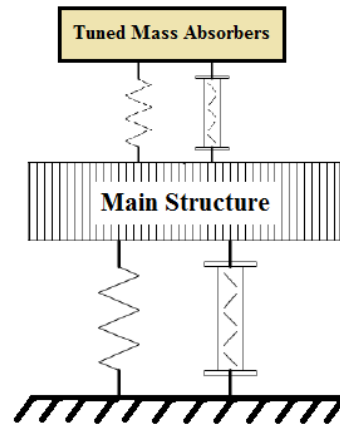


Figure 2.2 An example of passive vibration control

Active vibration control

Active vibration control systems are realized by using a set of sensors and actuators [22] [28], often with the help of specific software, which are active application of the vibration signal. Analog or digital controller needs to be designed to compose a closed feedback loop. The sensors collect real time data from the vibration and feedback to controller, the controller then generate an equal magnitude but opposite phase signal and imposed on actuator to cancel out vibration. This way can attenuate vibration effectively.

Main properties of active vibration control technique are listed below [9] [10]:

- a) Active vibration control can eliminate vibration at any frequencies, because of the use of real time closed control loop.
- b) In active control system, because the vibrations are cancelled by the closed control loop, it has a relatively smooth roll-off moving from the target frequency to higher frequency.
- c) The performance of the active vibration system is mainly decided by the controller rather than surrounding mechanical structures.
- d) By properly selection of positions and directions of the sensors and actuators, active control system can eliminate vibration almost on every direction.
- e) Active vibration control systems have relatively shorter settling time, usually in order of milliseconds.
- f) Due to usage of precise and expensive electrical components, active control systems are expensive.

Figure 2.3 shows a simple example of active vibration control. A sensor/actuator pair and a controller is used. The controller is to compute a suitable control signal by using data obtained from sensors. Then the control signal is fed to the main structure through actuators to cancel vibration [24].

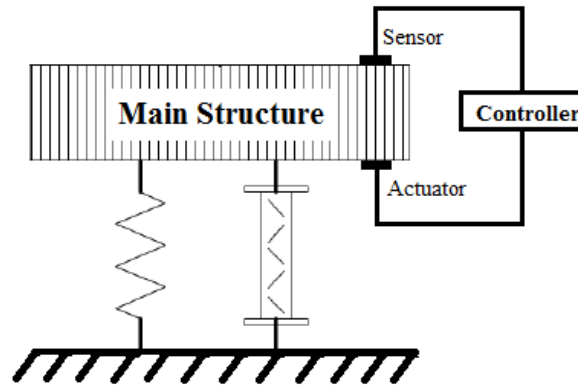


Figure 2.3 An example of active vibration control

2.3.2 Feedback and Feedforward Control

Feedback control

Feedback theory was first developed by Black and Nyquist in the 1930's at Bell Labs [12]. The general block diagram of a feedback control system is shown in Figure 2.4. It can be seen that the output of a feedback control system is controlled by using its measurement as feedback signal, this feedback signal compared with reference signal (desired value) to produce an error signal, this error signal filtered by the feedback controller to generate the input signal of the plant. Main aim of feedback control system is to make sure the interested variable (output signal) either following reference trajectories (servo) or maintained close to the set point (regulation). Feedback control usually used to adjust variables in a control system which include time varying disturbances [23].

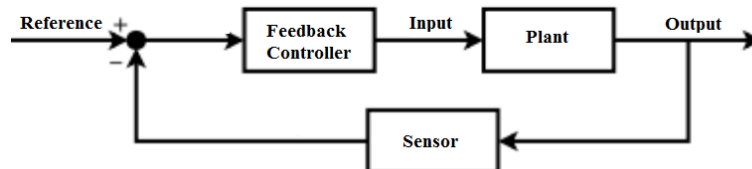


Figure 2.4 Block diagram of feedback control

Feedback control systems have many useful properties [12]. First, it can precisely control a system without a precise plant model, this is very useful since in practice, most of the systems

or structures are complex or complicated, it is difficult to understand the control problem well. Second, by using a proper feedback controller, an unstable system may become stable. Third, feedback control systems are relatively less sensitive to disturbances, therefore the effects of disturbances could be reduced. Fourth, feedback control can be used on linearize systems. Fifth, with the high performance, feedback control can reach the desired point quickly.

Feedforward Control

Feedforward control is a kind of open loop control. In a feedforward control system, the output signal is not regulated based on using the error signal, instead it is relying on knowledge about the system and external disturbances, therefore, it is usually used to well understand process or system. A simplified block diagram of feedforward control system is shown in Figure 2.5 [11].

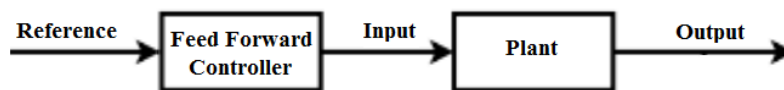


Figure 2.5 Block diagram of feedforward control

In the feedforward control system, the disturbances must be measured or calculated accurately before they affect the plant [25], and must not have unmeasured disturbances. With sufficient precision of the plant's mathematical model and proper implementation of the feedforward controller, the control accuracy can be improved significantly. Energy consumption of a feedforward control system is often lower than other control systems. Feedforward control technique often combined with feedback control technique for the purpose of optimizing control performance.

2.3.3 Positive Position Feedback (PPF) Control

It is proved that several properties of PPF control are suitable for position feedback control and resonance feedback control. For example, PPF control only works on the target frequency and roll-off quickly at higher frequencies since PPF controller is actually a second order low pass filter [13]. It is also known to be insensitive to spillover effect, which comes from the truncated modes affecting the control of interest modes. Because of above outstanding advantages, PPF control method was selected for this project.

Chapter 2: Literature Review

PPF control was firstly introduced by Chuen Jin Goh in 1983. The equations of PPF controller are [14]:

$$\text{Structure: } \ddot{\xi} + 2\zeta\omega\dot{\xi} + \omega^2\xi = g\omega^2\eta \quad (2.8)$$

$$\text{Compensator: } \ddot{\eta} + 2\zeta_c\omega_c\dot{\eta} + \omega_c^2\eta = \omega_c^2\xi \quad (2.9)$$

where ξ indicate structure coordinate, η indicate compensator coordinate, ζ indicate damping ratio of structure, ζ_c indicate damping ratio of compensator, ω indicate natural frequency of structure, ω_c indicate natural frequency of compensator, and g indicate control gain with $g > 0$ [13].

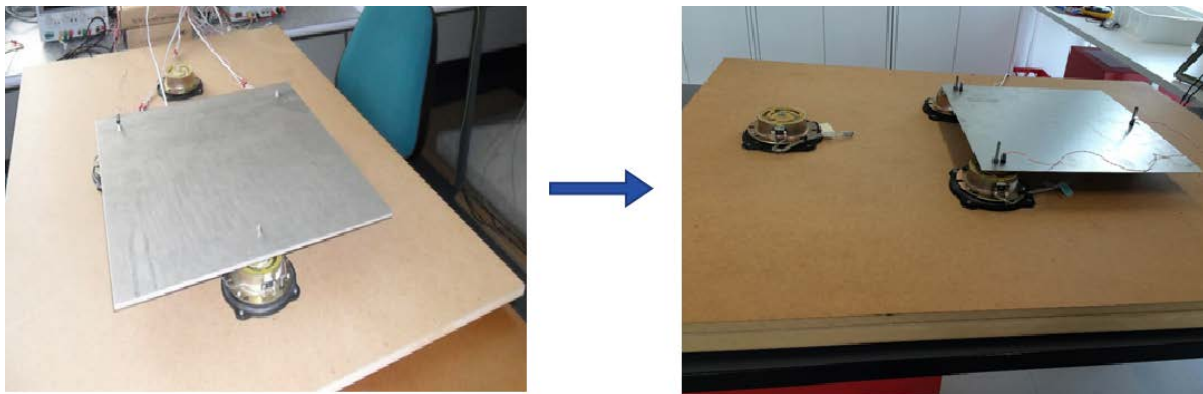
From equation (2.8) and (2.9), it is clear that the structure position is positively feedback to the compensator, and the compensator position is positively feedback to structure, that is why this control technique called positive position feedback [13]. More details about PPF controller will be discussed in chapter 5.

Chapter 3 : Physical System Setup

In this chapter, physical setup used in this project are introduced. The entire physical setup utilized in this “vibration cancellation in plate structure” project can be divided into four parts. The plate system itself, used to simulate a MIMO vibration problem; Interface board, used to communication with transducer and dSPACE; NI DAQ 9234, used for data acquisition for ModalVIEW software; And dSPACE module, used to compute and generate control signals. Main properties of above physical equipment and applications in this project are described in the following sections.

3.1 Laboratory Plate Structure Model

The laboratory plate structure model used in this project followed ideas of the initial proto model constructed by Groothuis and Roesthuis [2], with dimensions of base plate and top plate were slightly changed for the purpose of move the natural frequency of the first mode into transducer’s frequency range (20Hz-200Hz) so that it can be detected. Comparison of previous setup and current setup is shown below in Figure 3.1.



Previous setup:

Base plate: 1200mmx900mmx16mm

Top plate: 500mmx500mmx6.55mm

First mode: 12Hz

Current setup:

Base plate: 1200mmx900mmx47mm

Top plate: 400mmx400mmx1.5mm

First mode: 22Hz

Figure 3.1 Comparison of previous and current plate structure

3.1.1 Sensor and Actuator

As described before, the electromagnetic transducers, as shown in Figure 3.2, were selected as sensors and actuators, the reason for this selection is due to the fact that electromagnetic transducer is a perfect energy converter, which can convert mechanical energy (vibration

energy, in this project) into electrical energy as well as convert electrical energy into mechanical energy.



Figure 3.2 Electromagnetic transducer used as sensor and actuator

The electromagnetic transducer used in this project is actually a bass speaker, which has significant vibration effect when the frequency is low. Figure 3.3 shows cross section of the electromagnetic transducer [2], it can be seen that there is a large magnet as well as coil inside the transducer, according to Faraday Law of Electromagnetic Induction, the magnetic and coil are the core and necessary parts to realize energy conversion.

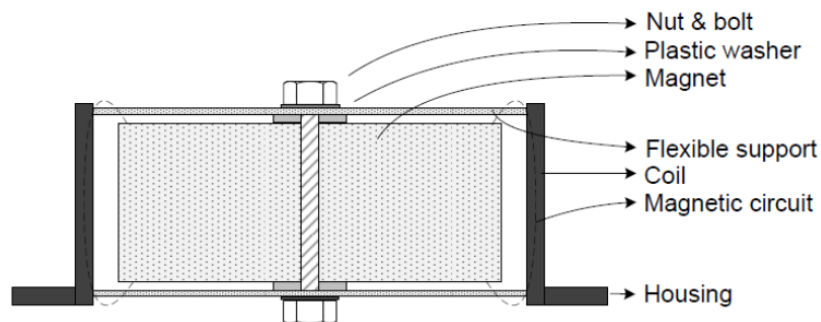


Figure 3.3 Cross section of the electromagnetic transducer

When transducer works as sensor, it collects magnitude signal of the vibration imposed on it, and convert this mechanical vibration signal into electrical signal for further use in dSPACE.

When transducer works as actuator, it receives control signal comes from dSPACE through interface board (introduced in section 3.2), which is electrical signal, and this control signal used to cancel out the vibration.

3.2 Interface Board

The interface board is an interface circuit between transducer and A/D, D/A modules of dSPACE.

For the purpose of generating correct control signal used for actuating, the induced voltage on the transducer due to mechanical vibration must be isolated and measured first. In this project, electromagnetic transducer works as both sensor and actuator concurrently, which means the induced voltage from the transducer and the control voltage into transducer both appear at two terminals of the same transducer. To solve this problem, “self-sensing” technique was introduced to the interface board to isolate the induced voltage before measuring [2]. The printed circuit board (PCB) was designed as shown in Figure 3.4. Detail information about this interface board can be found in appendix A.

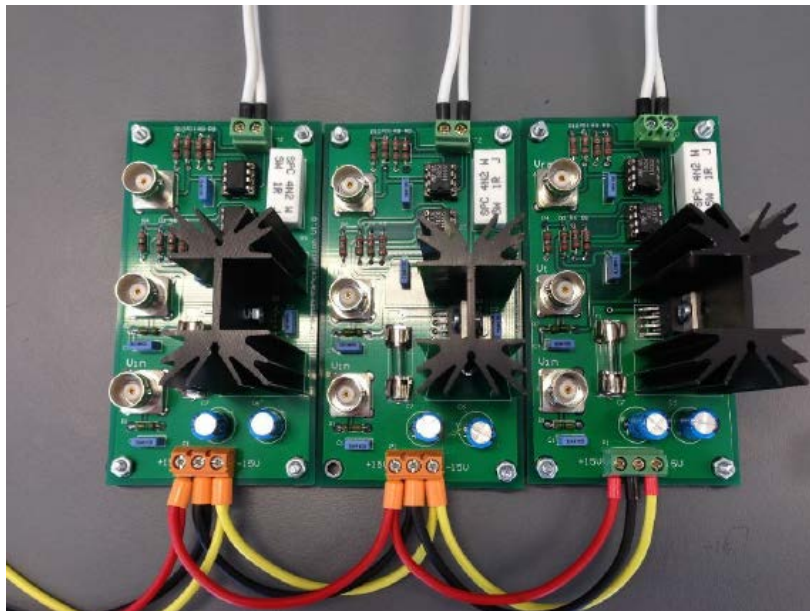


Figure 3.4 PCB of interface board

Principle of the self-sensing technique is shown in Figure 3.5.

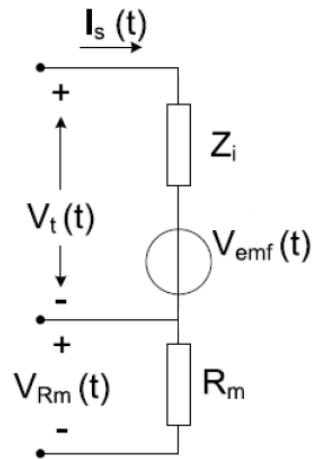


Figure 3.5 Working principle of self-sensing technique

where $I_s(t)$ indicate current flow through this circuit.

Z_i indicate impedance of the transducer.

R_m indicate an external resistor used to calculate current.

V_{emf} indicate the induce voltage, need to be computed.

$V_t(t)$ and $V_{Rm}(t)$ are voltage on the transducer and voltage on resistor R_m respectively, which can be measured directly.

By applying Kirchhoff's Voltage Law (KVL) and Kirchhoff's Current Law (KCL), it is easy to derive following equations.

$$V_t(t) = V_{emf}(t) + I_s(t) * Z_i \quad (3.1)$$

$$I_s(t) = \frac{V_{Rm}(t)}{R_m} \quad (3.2)$$

Substitute equation (3.2) into equation (3.1), the induce voltage V_{emf} can be calculated by:

$$V_{emf}(t) = V_t(t) - \frac{V_{Rm}(t)}{R_m} * Z_i \quad (3.3)$$

Impedance of the transducer is 4Ω according to the datasheet, and R_m used in this interface circuitry is 1Ω . Therefore, the block diagram representation of equation (3.3) used to implement in SIMULINK is as follow:

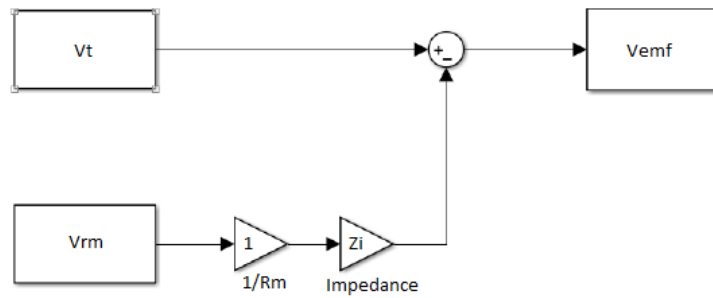


Figure 3.6 Block diagram to compute induced voltage

3.3 NI DAQ Module

NI DAQ 9234 is a 4-channel dynamic signal acquisition module (see Figure 3.7), used for high-accuracy audio frequency data acquisition from electronic piezoelectric and other types of sensors. NI DAQ9234 provides four BNC connectors that used for connecting to analog signal source, the center pin of the BNC connector is AI+ and the shell is AI- as shown in figure 3.7.

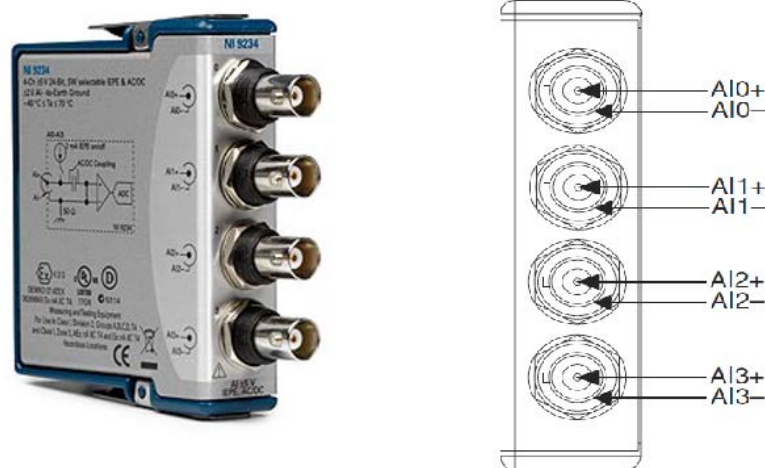


Figure 3.7 NI DAQ 9234 module and BNC connector assignments

Figure 3.8 shows the build-in circuitry in each input channel of DAQ9234. It can be seen that input analogue signal is referenced to ground through a 50Ω resistor, for the purpose of minimizing the ground noise, this ground should be connected to earth ground. NI DAQ9234 introduced a common-mode bias current in the circuitry to bias the current limiting diodes when piezoelectric current is turned off. A combination of analogue filters and digital filters

were used inside NI DAQ9234 in order to provide an accurate representation of in-band signals meanwhile reject out-band signals. Each input analogue signal is buffered, conditioned then sampled by a 24-bit A/D converter.

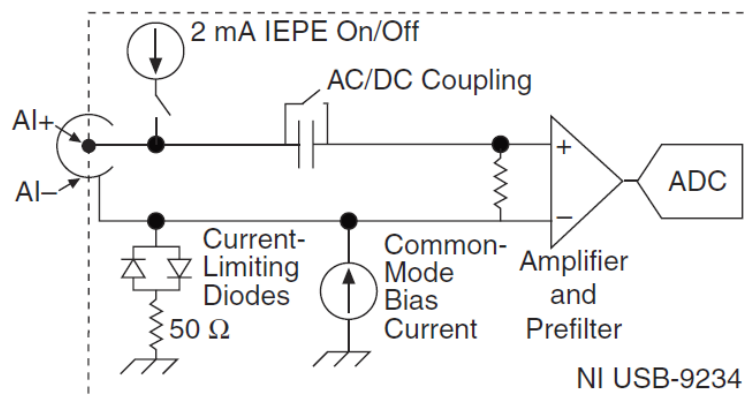


Figure 3.8 Input circuitry for each channel

In this project, DAQ 9234 module used to collect vibration signals on the plate structure, where channel 0 is connected to input exciting signal and channel 1 to channel 3 are connected to 3 response signals come from three transducers respectively through accelerometers (model number: 353B17). These four channel signals then used by ModalVIEW software to generate frequency response function (FRF) curve of the three transducers.

3.4 DSPACE Module

The term DSPACE stands for “Digital Signal Processing and Control Engineering”. DSPACE module is a combination of series of software and hardware, which is a widely used engineering tool for developing and testing solutions in mechatronic control systems.

In this project, DS1103 PPC controller board was used to implement the vibration cancellation process. The DS1103 is a single board system based on the PowerPC 604e processor (PPC), which is the main processing unit. A set of build-in peripherals frequently used in digital control systems has been added to this PPC, as well as analog/digital (A/D) and digital/analog (D/A) converters, digital I/O ports, and a serial interface.

As induced voltage is analog signal and control voltage also need to be an analog signal, whereas dSPACE is a digital signal processor, A/D, D/A converter was utilized to link the interface board (analog signal) and dSPACE processor (digital signal).

There are two different types of A/D converter provided by DS1103 PPC controller Board.

Chapter 3: Physical System Setup

- (1) ADC1-ADC4 are 4 parallel A/D converters with 4 channels each, input signals of this four converters can be selected by a 4:1 input multiplexers respectively. This four ADC have 16-bit resolution, 4us sampling time and integrated sample/holds.
- (2) ADC5-ADC8 are 4 parallel A/D converters with only 1 channel each. 12-bit resolution, 800ns sampling time and integrated sample/holds.

Input signal range of all above A/D converters is $\pm 10V$.

Mapping of A/D converters and channels to related I/O pins of DS1103 is listed below in Table 3.1.

Table 3.1 Mapping of A/D converters to DS1103 I/O pins

A/D converter	Channel number	Signal	I/O pin number
ADC1	1	ADCH1	P1-3
	2	ADCH2	P1-4
	3	ADCH3	P1-7
	4	ADCH4	P1-8
ADC2	5	ADCH5	P1-11
	6	ADCH6	P1-12
	7	ADCH7	P1-15
	8	ADCH8	P1-16
ADC3	9	ADCH9	P1-19
	10	ADCH10	P1-20
	11	ADCH11	P1-23
	12	ADCH12	P1-24
ADC4	13	ADCH13	P1-27
	14	ADCH14	P1-28
	15	ADCH15	P1-31
	16	ADCH16	P1-32
ADC5	17	ADCH17	P1-35
ADC6	18	ADCH18	P1-36
ADC7	19	ADCH19	P1-39
ADC8	20	ADCH20	P1-40

Chapter 3: Physical System Setup

There are two quad D/A converters with 4 channels each, each quad converter could be considered as 4 parallel converters. DAC1-DAC4 are on the first quad, DAC5-DAC8 are on the second quad. 14-bit resolutions, 6 μ s settling time.

Output signal range of all above D/A converters is $\pm 10V$ with single ended.

Mapping of D/A converters and channels to related I/O pins of DS1103 is listed below in Table 3.2.

Table 3.2 Mapping of D/A converters to DS1103 I/O pins

D/A converter	Channel number	Signal	I/O pin number
DAC1	1	DACH1	P1-47
DAC2	2	DACH2	P1-48
DAC3	3	DACH3	P1-51
DAC4	4	DACH4	P1-52
DAC5	5	DACH5	P1-55
DAC6	6	DACH6	P1-56
DAC7	7	DACH7	P1-59
DAC8	8	DACH8	P1-60

In this project, A/D converter ADC1-ADC4 and the first quad of D/A converter were used. The mapping of A/D, D/A channels to each interface board is listed in Table 3.3.

Table 3.3 A/D and D/A channels used in dSPACE

Type of connection	Symbol on interface board	Transducer 1	Transducer 2	Transducer 3
Control voltage	V _{in}	DACH1	DACH3	DACH5
Voltage on transducer	V _t	ADCH1	ADCH7	ADCH13
Voltage on resistor R _m	V _{rm}	ADCH3	ADCH9	ADCH15

When using A/D and D/A converter, one issue needs to pay attention is that there is a build-in gain, 0.1 for ADC and 10 for DAC respectively. Hence, when programming in SIMULINK,

Chapter 3: Physical System Setup

the signal after ADC should multiply by 10 and signal before DAC should multiply by 0.1 to counteract the effect of the build-in gain, as shown in Figure 3.9.

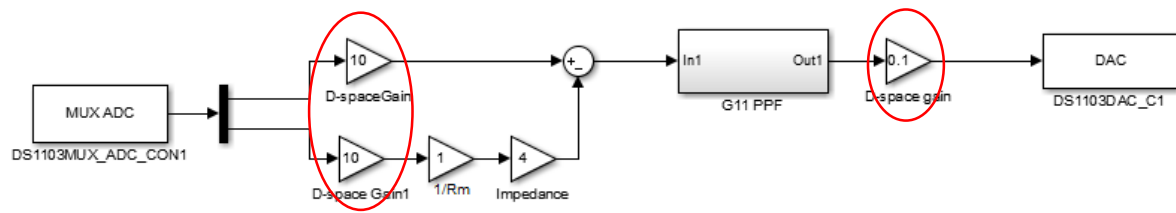


Figure 3.9 Effect of build-in gain in dSPACE

Chapter 4 : Modelling the Plate Structure

In this project, instead of numerical modelling technique that conducted in ANSYS by previous students, theoretical analysis and physical experiment modelling methods are utilized to obtain the mathematical model of the structure. In this chapter, procedures of mathematically modeling the plate structure are described. Firstly, characteristics of the plate structure is analyzed, then theoretical analysis method is used to derive the mathematical expression of the transfer function. Modal analysis software, ModalVIEW, is then used to obtain the frequency response function (FRF) of the plate as well as the parameters of the transfer functions including natural frequencies, damping ratios, and mode shapes. For the purpose of the controller design, the measured model of the plate is truncated to the first three modes and a model correction technique based on spatial H_2 norm is applied to the truncated model to minimize the truncation error in order to achieve the accurate transfer function used for controller design in the next chapter.

4.1 Plant Characteristics

As described in Chapter 1, the disturbance signal in this plate structure is introduced by the disturbance transducer (Transducer 4). This disturbance signal then travels through the base board to the other three transducers and finally onto the top plate. Because transducer 1 to transducer 3 are used as sensors and meanwhile actuators, from control point of view, this system can be considered as a multi-input multi-output system with three-input three-output. Where the three input signals are the vibration force into three transducers (transducer1, 2, 3), three output signals are the vibration amplitude of the point right above corresponding transducer on the top plate.

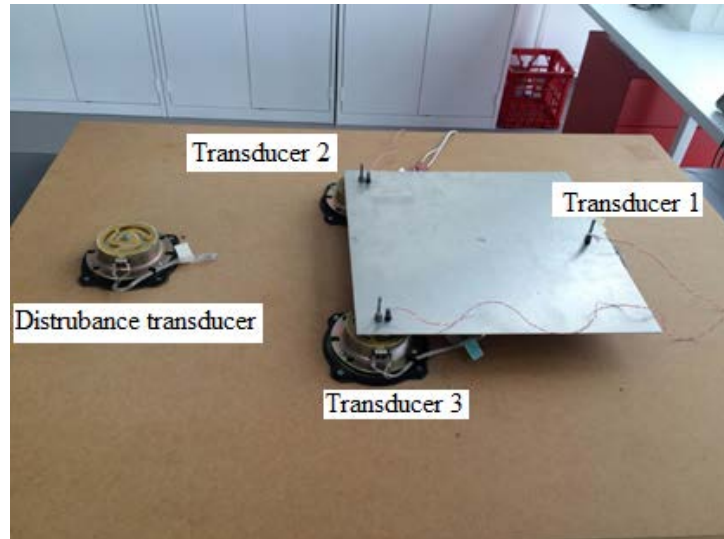


Figure 4.1 Input and output in plate structure

The general control system equation:

$$Y(s) = G(s) * U(s) \quad (4.1)$$

where $Y(s)$ is output signal, $U(s)$ is input signal and $G(s)$ is plant dynamics (transfer function). then can be written as

$$\begin{bmatrix} Y_1(s) \\ Y_2(s) \\ Y_3(s) \end{bmatrix} = \begin{bmatrix} G_{11}(s) & G_{12}(s) & G_{13}(s) \\ G_{21}(s) & G_{22}(s) & G_{23}(s) \\ G_{31}(s) & G_{32}(s) & G_{33}(s) \end{bmatrix} * \begin{bmatrix} U_1(s) \\ U_2(s) \\ U_3(s) \end{bmatrix} \quad (4.2)$$

where $Y_i(s)$ ($i = 1, 2, 3$) represents three output signals, $U_i(s)$ ($i = 1, 2, 3$) represent three input signals, $G_{mn}(s)$ ($m = 1, 2, 3$ and $n = 1, 2, 3$) represent transfer function related to m^{th} output (output of transducer m) and n^{th} input (input of transducer n). It can be observed that the transfer function G of the simulated plant model should be a 3×3 matrix, each element (G_{mn}) of this matrix represent the dynamics between transducer m and transducer n .

Block diagram representation of equation 4.2 can be found in Figure 4.2.

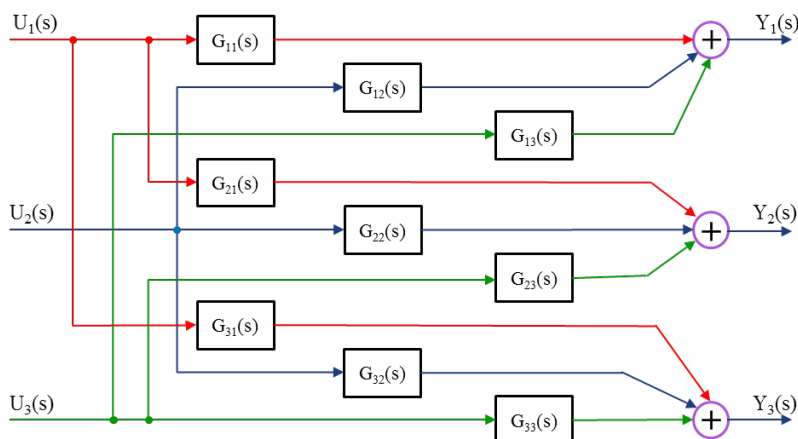


Figure 4.2 Block diagram of 3-input 3-output system

From above analysis, it can be concluded that each input signal has effect on three output signals simultaneously, and each output signal is determined by three input signals simultaneously [26].

After clearly analysis of the characteristics of the plate structure, analytical derivation for the transfer function matrix is performed in the next section.

4.2 Analytical Derivation of Transfer Function

In this section, the transfer function is derived from theoretical analysis point of view. Mathematical equations presented in this section are from thesis of G.Pratama [3]. Modal analysis technique was utilized to get transfer function.

For a 2-dimensional flexible mechanical structure, the typical partial differential equation (PDE) is presented as:

$$L[W(x, y, t)] + C \left[\frac{\partial W(x, y, t)}{\partial t} \right] + M \left[\frac{\partial^2 W(x, y, t)}{\partial t^2} \right] = f(x, y, t) \quad (4.3)$$

where L is linear homogeneous differential stiffness operator of order $2p$.

M is linear homogeneous differential mass operator of order $2q$, $q \leq p$.

C is linear homogeneous differential damping operator.

(x, y) is the spatial coordinates, which is defined on plane D .

$W(x, y, t)$ is eigenvector (mode shape) of point (x, y) .

$f(x, y, t)$ is the general arbitrary input force on the point (x, y) .

Boundary condition of equation 4.3 can be written as:

$$B_i[W(x, y, t)] = 0, \quad \text{where } i = 1, 2, 3 \dots p \quad (4.4)$$

where B_i in above equation is a linear homogeneous differential operator with order $\leq 2p-1$.

In practice, the proportional damping, which is proportional to mass and stiffness, is usually used to estimate natural frequencies and mode shapes of a structure, the reason is due to the fact that by using proportional damping, the mode shape (eigenvectors) of both damped and un-damped systems are the same and the natural frequencies (eigenvalues) are also very similar. By assuming proportional damping, damping C can be expressed as:

$$C = c_1L + c_2M \quad (4.5)$$

where c_1 and c_2 are constants great or equal than 0.

Thus, for un-damped cases of equation (4.3), the mode shape (eigenvector) and natural frequencies (eigenvalues) can be obtained by solving the eigen function problem:

$$L[W_{mn}(x, y)] = \lambda_{mn}M[W_{mn}(x, y)], \quad m = n = 1, 2, 3, \dots \quad (4.6)$$

Associate equation (4.6) with boundary conditions (equation (4.4)), the natural frequencies can be determined from eigenvalues:

$$\lambda_{mn} = \omega_{mn}^2 \quad (4.7)$$

The eigen functions need to be orthogonal before used as a basic function to solve the solution of equation (4.3). To develop the general principle of orthogonality, self-joint eigenvalue problem is introduced. For any two arbitrary eigen functions $W_{mn}(x, y)$ and $W_{nm}(x, y)$, the eigenvalue problem is self-joint if:

$$\int_D W_{mn}(x, y)L[W_{nm}(x, y)]dD(x, y) = \int_D W_{nm}(x, y)L[W_{mn}(x, y)]dD(x, y) \quad (4.8)$$

and

$$\int_D W_{mn}(x, y)M[W_{nm}(x, y)]dD(x, y) = \int_D W_{nm}(x, y)M[W_{mn}(x, y)]dD(x, y) \quad (4.9)$$

Let ω_{mn}^2 and ω_{nm}^2 be two different eigenvalues corresponding to eigenvector $W_{mn}(x, y)$ and $W_{nm}(x, y)$ respectively. General conditions of orthogonality equation can be expressed as:

$$\int_D W_{mn}(x, y)M[W_{nm}(x, y)]dD(x, y) = 0, \quad \text{for } \omega_{mn}^2 \neq \omega_{nm}^2 \quad (4.10)$$

$$\int_D W_{mn}(x, y)L[W_{nm}(x, y)]dD(x, y) = 0, \quad \text{for } \omega_{mn}^2 \neq \omega_{nm}^2 \quad (4.11)$$

For simplicity, the eigen functions are usually normalized to M such that

$$\int_D W_{mn}(x, y)M[W_{nm}(x, y)]dD(x, y) = \delta_{mn} \quad (4.12)$$

Chapter 4: Modelling the Plate Structure

where δ_{mn} is the Kronecker delta function with:

$$\delta_{mn} = \begin{cases} 1, & m = n \\ 0, & m \neq n \end{cases} \quad (4.13)$$

Therefore, equation (4.11) can be written as

$$\int_D W_{mn}(x, y) L[W_{nm}(x, y)] dD(x, y) = \delta_{mn} \omega_{mn}^2 \quad (4.14)$$

Since damping C is assumed to be proportional damping,

$$\int_D W_{mn}(x, y) C[W_{nm}(x, y)] dD(x, y) = c_1 \delta_{mn} \omega_{mn}^2 + c_2 \delta_{mn} \quad (4.15)$$

which can be represented as:

$$\int_D W_{mn}(x, y) C[W_{nm}(x, y)] dD(x, y) = \delta_{mn} 2\zeta_{mn} \omega_{mn} \quad (4.16)$$

with

$$\zeta_{mn} = \frac{1}{2\omega_{mn}} (c_1 \omega_{mn}^2 + c_2) \quad (4.17)$$

where ζ_{mn} is damping ratio of mode m and mode n ($m=n$). Equation (4.12), (4.14) and (4.16) are orthonormal eigen functions that can be used as basic functions. Therefore, the response of any arbitrary point in the system can be calculated as superposition of these basic functions as shown in equation (4.18).

$$W(x, y, t) = \sum_{m=1}^{\infty} \sum_{n=1}^{\infty} W_{mn}(x, y) q_{mn}(t) \quad (4.18)$$

where $q_{mn}(t)$ indicates generalized coordinates.

To use modal analysis technique, substituting equation (4.18) into equation (4.3),

$$\begin{aligned} & L\left[\sum_{m=1}^{\infty} \sum_{n=1}^{\infty} W_{mn}(x, y) q_{mn}(t)\right] + C\left[\frac{\partial}{\partial t} \sum_{m=1}^{\infty} \sum_{n=1}^{\infty} W_{mn}(x, y) q_{mn}(t)\right] \\ & + M\left[\frac{\partial^2}{\partial t^2} \sum_{m=1}^{\infty} \sum_{n=1}^{\infty} W_{mn}(x, y) q_{mn}(t)\right] = f(x, y, t) \end{aligned} \quad (4.19)$$

Multiply equation (4.19) with $W_{nm}(x, y)$ and integrate over plane D , the result is:

$$\begin{aligned} & \sum_{m=1}^{\infty} \sum_{n=1}^{\infty} q_{mn}(t) \delta_{mn} \omega_{mn}^2 + \sum_{m=1}^{\infty} \sum_{n=1}^{\infty} \dot{q}_{mn}(t) \delta_{mn} 2\zeta_{mn} \omega_{mn} \\ & + \sum_{m=1}^{\infty} \sum_{n=1}^{\infty} \ddot{q}_{mn}(t) \delta_{mn} = Q_{mn}(t) \end{aligned} \quad (4.20)$$

where

$$Q_{mn}(t) = \int_D W_{mn}(x, y) f(x, y, t) dD(x, y) \quad (4.21)$$

An infinite set of ordinary differential equation can be written as:

$$\ddot{q}_{mn}(t) + 2\zeta_{mn}\omega_{mn}\dot{q}_{mn}(t) + q_{mn}(t)\omega_{mn}^2 = Q_{mn}(t), m = n = 1,2,3 \quad (4.22)$$

From equation (4.22), it can be observed that the system can be described as sum of infinity number of second-order differential equations that can be solved independently.

From control point of view, time domain differential equation (4.22) need to be changed to frequency domain by using Laplace Transform. Usually, the generalized force $Q_{mn}(t)$ can be expressed as a decomposition of the spatial and temporal components:

$$Q_{mn}(t) = P_{mn}u(t) \quad (4.23)$$

where $u(t)$ is the input force to the system, P_{mn} is the time-independent forcing term.

Take Laplace Transform of equation (4.22), transfer function of this system can be found as:

$$G(x, y, s) = \sum_{m=1}^{\infty} \sum_{n=1}^{\infty} \frac{W_{mn}(x,y)P_{mn}}{s^2 + 2\zeta_{mn}\omega_{mn}s + \omega_{mn}^2} \quad (4.24)$$

Equation (4.24) is infinity dimensional transfer function, which means infinite number of modes are existing in this system.

Equation (4.24) is general solution for partial differential equation (4.3). For a particular structure, after finding eigenvectors (W_{mn}), natural frequencies (ω_{mn}) and damping ratio (ζ_{mn}), the transfer function can be obtained.

Furthermore, transfer function (4.24) can be expressed as:

$$\frac{W(x,y,s)}{U(s)} = \sum_{m=1}^{\infty} \sum_{n=1}^{\infty} \frac{W_{mn}(x,y)W_{mn}(x1,y1)}{s^2 + 2\zeta_{mn}\omega_{mn}s + \omega_{mn}^2} \quad (4.25)$$

where $W_{mn}(x,y)$ is eigenvector of m^{th} and n^{th} mode at position (x,y) , $W_{mn}(x1,y1)$ is eigenvector of m^{th} and n^{th} mode at position $(x1,y1)$, ω_{mn} is natural frequency of m^{th} and n^{th} mode, ζ_{mn} is damping ratio of m^{th} and n^{th} mode.

Considering $\omega = 0$, substitute $s = j\omega = j0 = 0$ into equation 4.25, the result is:

$$\frac{W(x,y,s)}{U(s)} = \sum_{m=1}^{\infty} \sum_{n=1}^{\infty} \frac{W_{mn}(x,y)W_{mn}(x1,y1)}{\omega_{mn}^2} \quad (4.26)$$

Equation (4.25) and equation (4.26) shows that each transfer function is superposition of single degree of freedom systems with DC gain determined by product of eigenvectors divided by square of eigenvalues.

As mathematical expression of transfer function is found, next step of work is to obtain parameters of transfer function by using modal analysis software, ModalVIEW.

4.3 Verify Performance of ModalVIEW Software

ModalVIEW is a LabVIEW based modal analysis software used in physical experiment to extract modal parameters and simulate mode shape for mechanical structure.

Since this is the first time to use ModalVIEW software, before formal measurement, a verification experiment was designed to confirm the performance of this software.

The basic principle of this verification experiment is: compare the frequency response function (FRF) curve of each transducer measured by ModalVIEW software with the manually measured FRF curve of each transducer to check if the former curve can match the latter curve. To do this, FRF curves need to be measured manually first, then measure FRF curve by using ModalVIEW software, after that, these two sets of FRF curves can be compared with each other.

4.3.1 Measure FRF Curve Manually

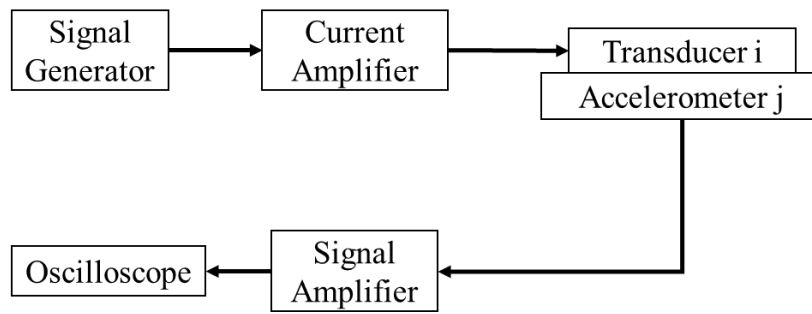
In this step, FRF curves from 20 Hz to 60 Hz associated with different input transducer and different output transducer were measured and plotted manually. To do this, the plate structure itself as well as other equipment, which include: signal generator, oscilloscope, accelerometer and signal amplifier were used to implement the measurement. The block diagram of hardware connection for this manual measurement and physical setup are shown in Figure 4.3.

Standard sine wave signal with $V_{p-p} = 250\text{mV}$ was generated by signal generator and amplified by current amplifier then flow into transducer i ($i = 1, 2, 3$) as input signal. Output signal was captured by accelerometer mounted right above each transducer, this output signal then be amplified by signal amplifier and appeared on oscilloscope screen finally.

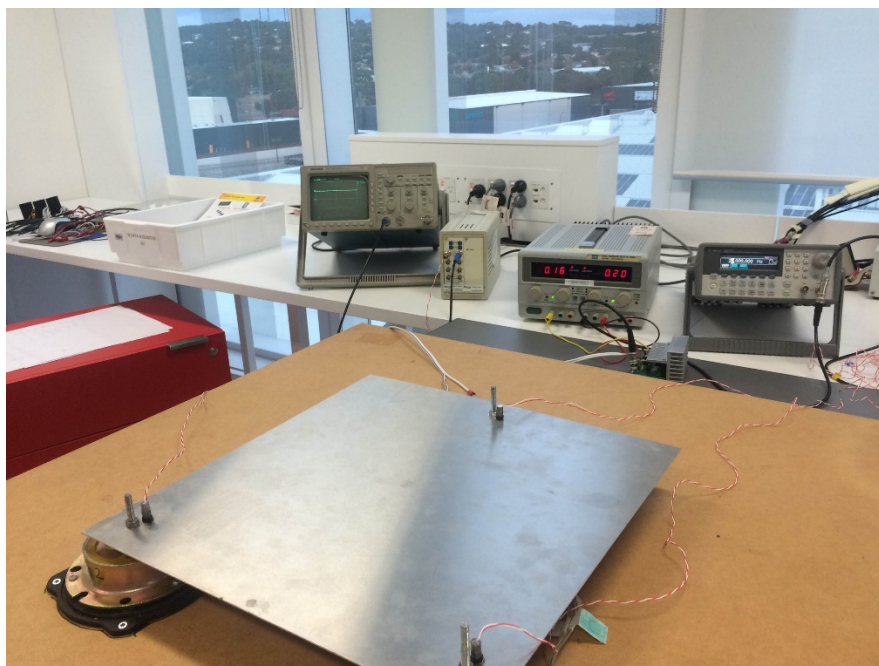
Change frequency of the sine wave signal from 20 Hz to 60 Hz by increase 0.1 Hz each time. For each frequency, write down the output voltage amplitude (peak-peak value) shown on the oscilloscope screen. The ratio of output voltage and input voltage is known as absolute magnitude, then dB value of each frequency can be calculated by:

$$dB = 20 * \log_{10} A \quad (4.27)$$

where, A is the absolute magnitude. Therefore, a data list associated to frequencies and corresponding dB values can be obtained, furthermore FRF curves can be plotted from this list of data.



(a) Block diagram of hardware connection



(b) Physical setup

Figure 4.3 Hardware connection for manual measurement

Nine combinations related to 3 inputs and 3 outputs were measured to get 9 FRF curves, as shown in Table 4.1.

Table 4.1 Input and output combinations for FRF measurement

Output \ Input	Transducer 1	Transducer 2	Transducer 3
Transducer 1	G11	G12	G13
Transducer 2	G21	G22	G23
Transducer 3	G31	G32	G33

Manually measured FRF curve are shown below.

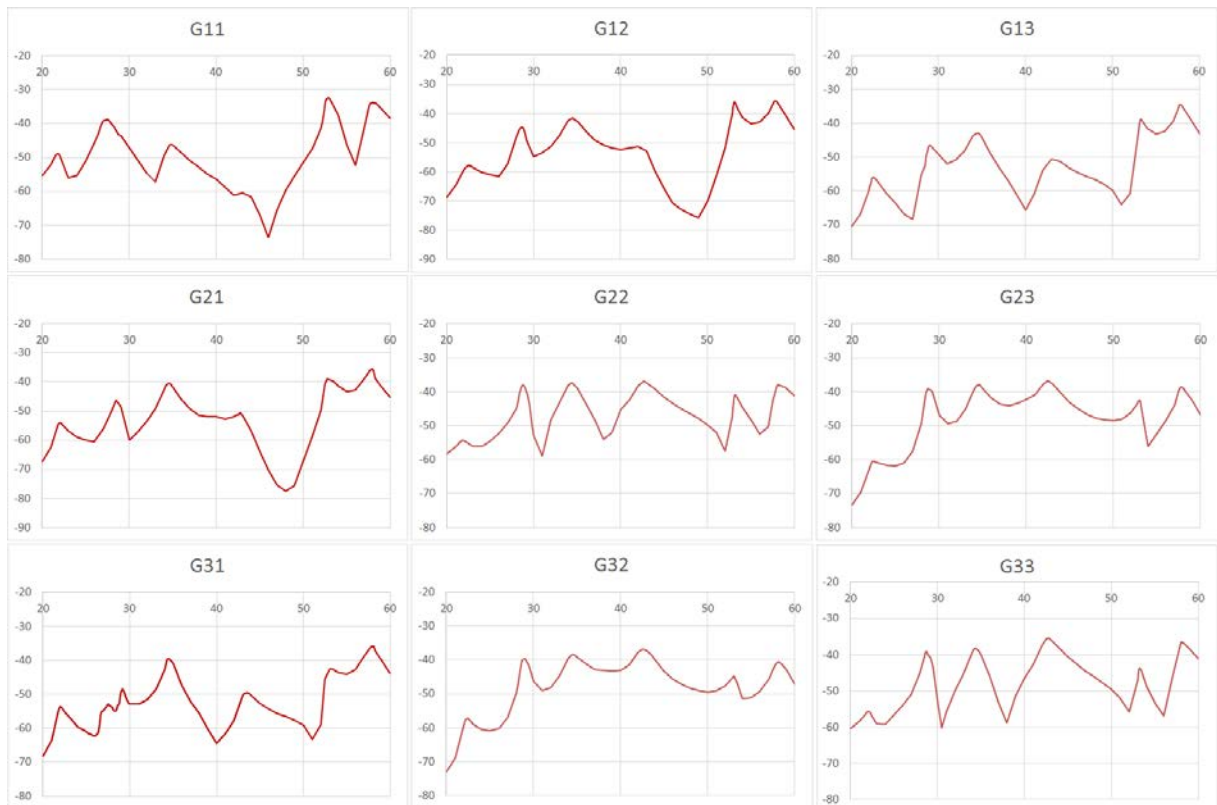


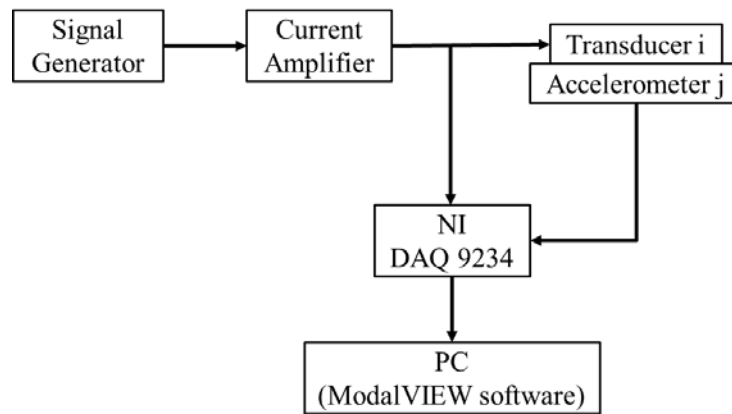
Figure 4.4 Manually measured FRF curves

4.3.2 Measure FRF Curve Using ModalVIEW Software

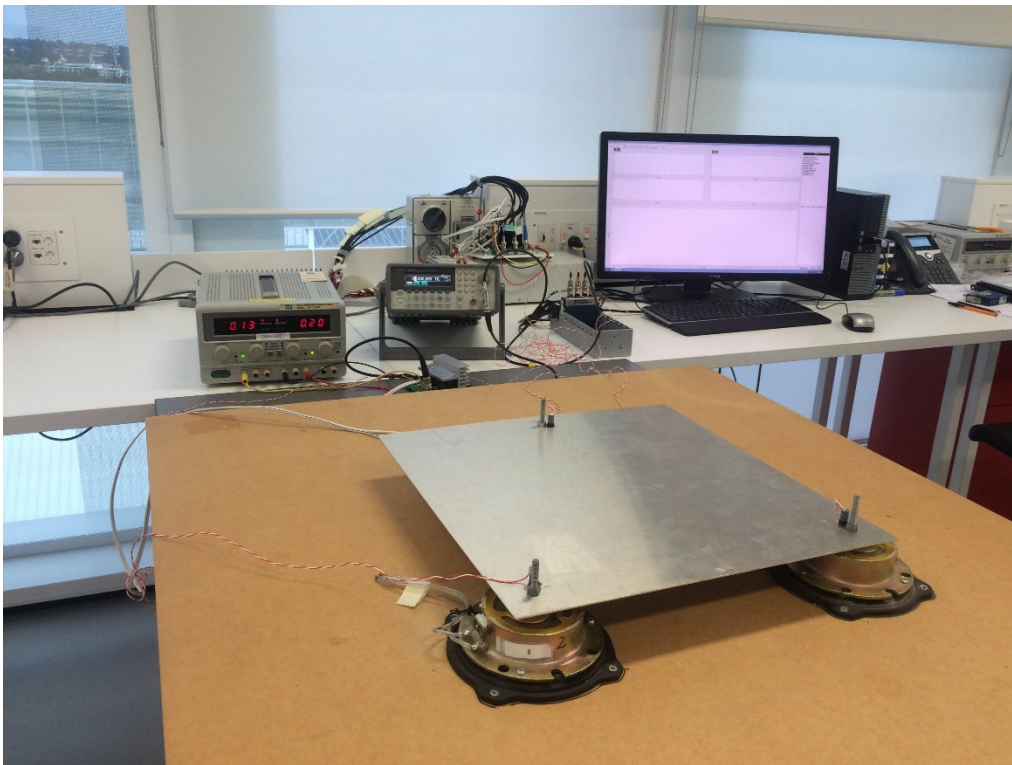
In this step, each FRF curve mentioned in Section 4.3.1 was measured by using ModalVIEW software. Signal generator, current amplifier, accelerometer, NI DAQ 9234 and ModalVIEW software were used to perform this measurement.

The block diagram of implement measurement in ModalVIEW software, as well as physical setup is shown in Figure 4.5.

Chapter 4: Modelling the Plate Structure



(a) Block diagram of physical setup



(b) Physical setup

Figure 4.5 Block diagram and physical setup for performing measurement in ModalVIEW. Amplified standard sine wave sweep signal (20Hz-60Hz) as input signal flew into transducer 1 to 3 one by one. The accelerometer voltages from each transducer are the output signals. Both input signal and output signal are collected by NI DAQ9234 concurrently and sent to ModalVIEW software and then FRF curves were generated automatically.

FRF curves generated by using ModalVIEW software are shown in Figure 4.6.

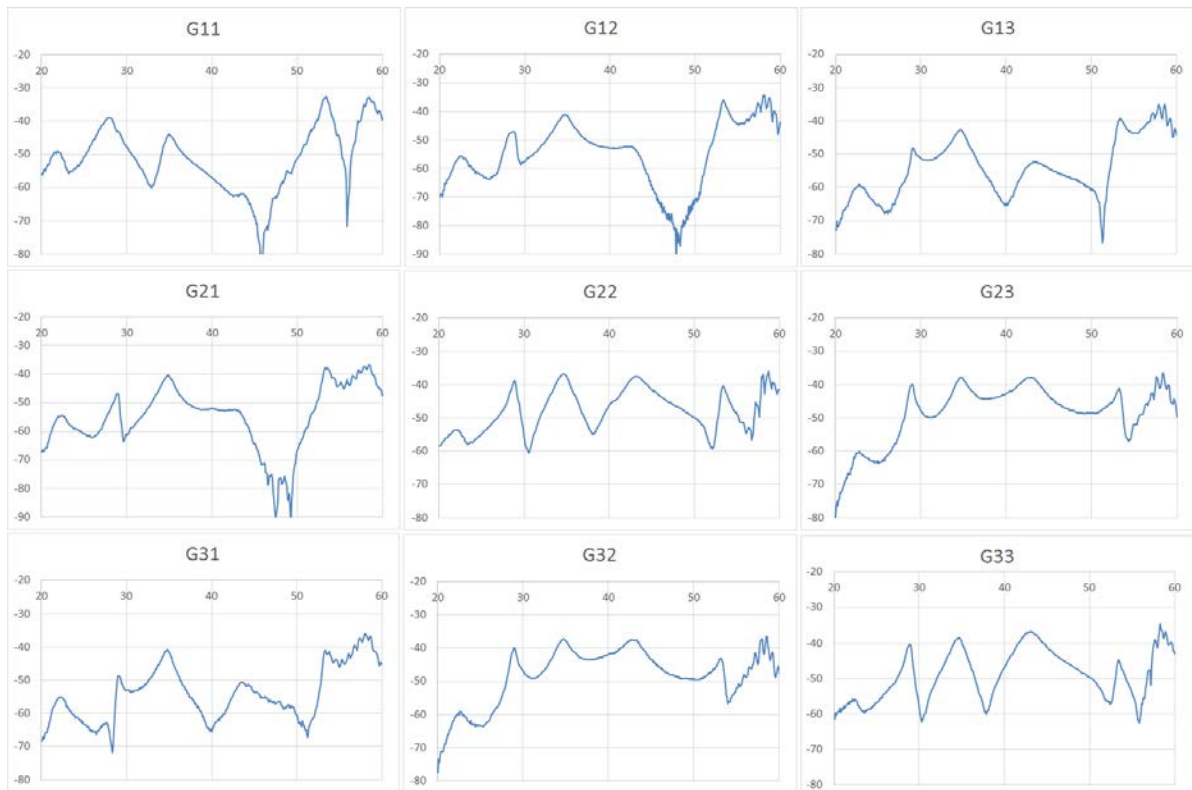


Figure 4.6 ModalVIEW software measured FRF curves

4.3.3 Compare FRF

The last step to check the performance of ModalVIEW software is to compare previous FRF curves generated by ModalVIEW with corresponding FRF curves measured manually.

Comparison results of above two sets of FRF curves is shown in Figure 4.7.

From Figure 4.7, it can be observed that for each input and output combination, the FRF curve generated by ModalVIEW software can match the manually measured FRF curve almost perfectly. Therefore, it can be concluded that the ModalVIEW software can measure the dynamics of this plate structure with high accuracy, in other words, it can be trusted to perform modal analysis to get modal parameters include natural frequencies, damping ratios and mode shape that used for controller designing purpose.

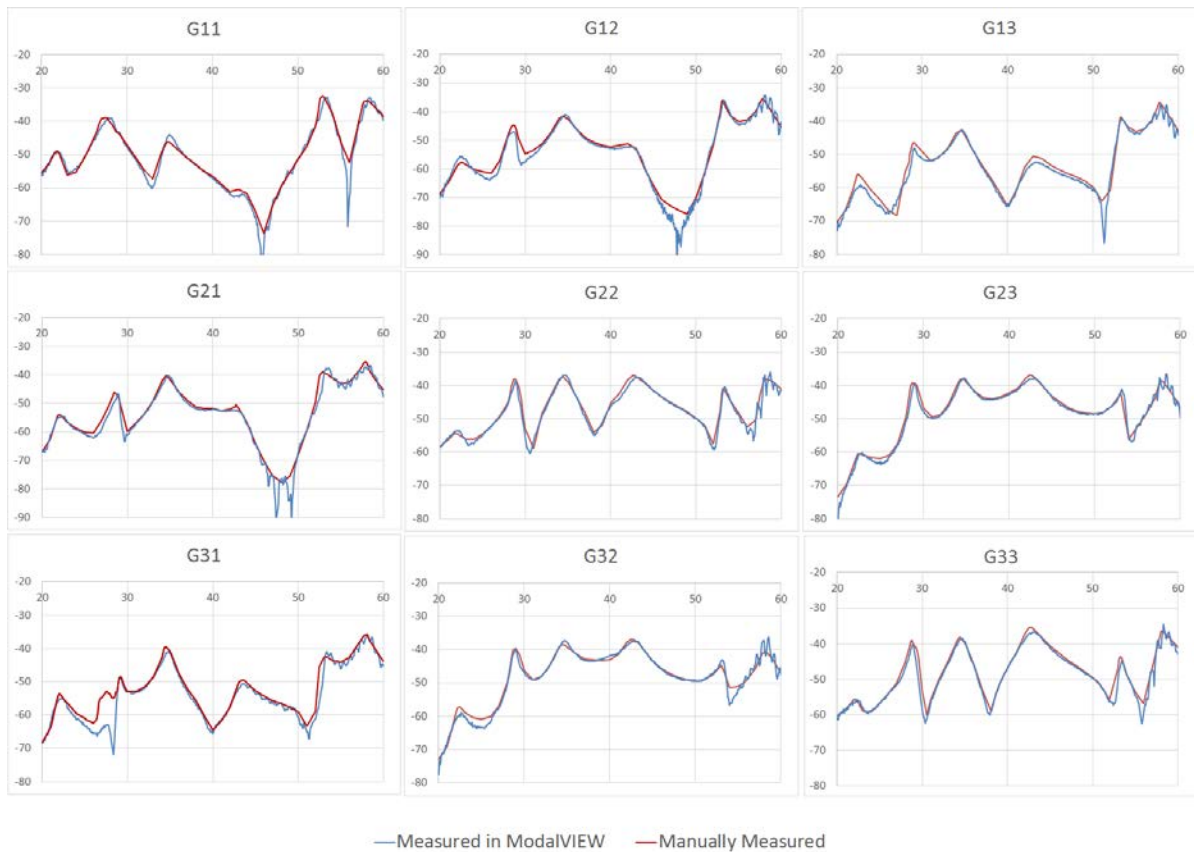


Figure 4.7 Comparison of manually measured and ModalVIEW measured FRF curves

4.4 Experimental Modelling in ModalVIEW Software

To obtain the transfer function, natural frequencies, damping ratios and mode shape need to be found first through modal analysis according to previous explanation in section 4.2. In this section, procedures of modal analysis by using ModalVIEW software is provided.

There are usually four steps to perform modal analysis in ModalVIEW software:

- 1) Draw a simplified structure
- 2) Perform FRF measurement
- 3) Estimate model parameters
- 4) Animate mode shape

Above steps are described in the following sections.

4.4.1 Draw Plate Structure in ModalVIEW

In ModalVIEW software, the top plate was defined by a plate structure on the X-Y plane with the same dimension of the physical top aluminum plate, as shown in Figure 4.8.

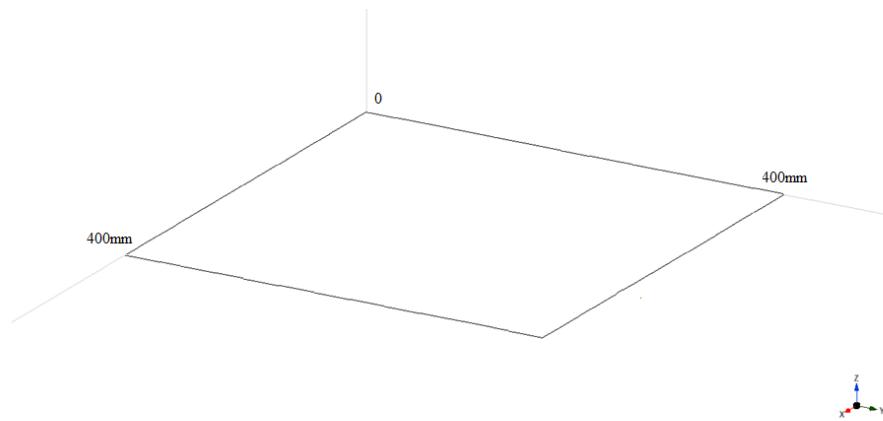


Figure 4.8 Plate structure in ModalVIEW software

Then for the purpose of simulating the locations of the transducers on the real plate, the plate structure in ModalVIEW was divided into 6×6 grids, therefore, 49 points were appeared on the plate as shown in Figure 4.9, and displacement direction of each point was defined in Z-axis. Refer to real positions of each transducer on the top plate, point 11, 37 and 41 were selected to simulate the transducer positions.

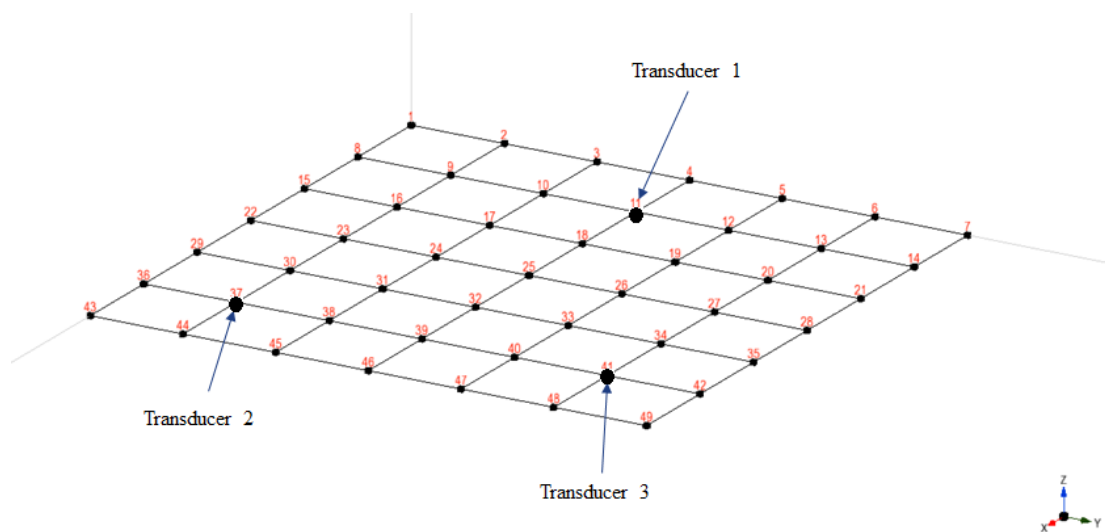


Figure 4.9 Simulated transducer positions in ModalVIEW software

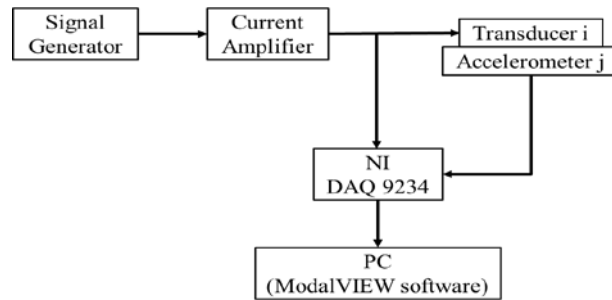
More detailed information about modal analysis procedures can be found in Appendix B.

4.4.2 FRF Measurement in ModalVIEW

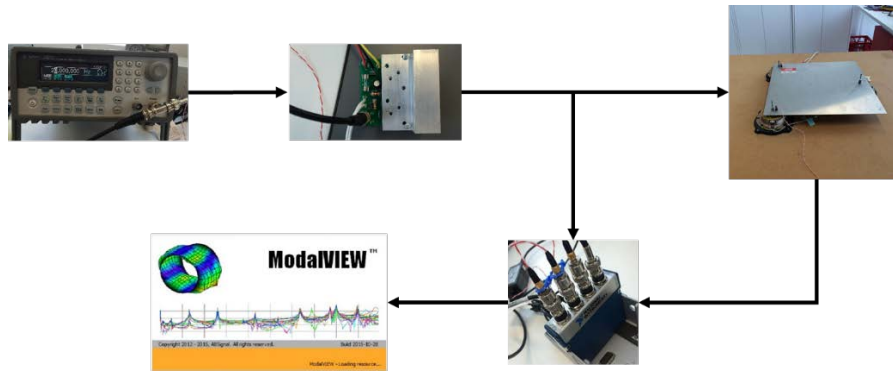
When performing FRF measurement in ModalVIEW software, four channels of NI DAQ9234 were used concurrently. Channel 0 was connected to input signal, which is the amplified standard sine wave signal from 20Hz to 200Hz generated by function generator. This amplified signal also flew into one of the three transducers as exciting signal. Channel 1,

Chapter 4: Modelling the Plate Structure

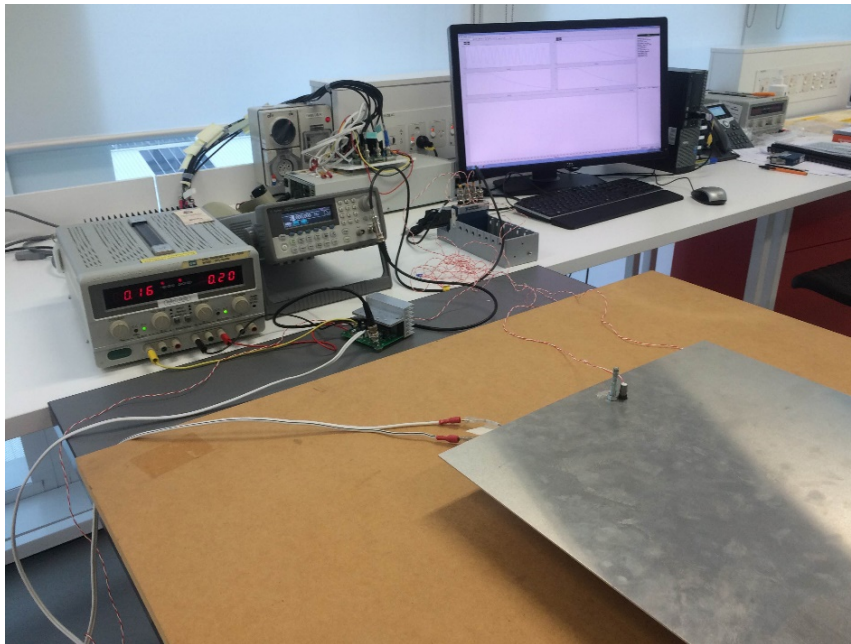
2, 3 were connected to output signal of accelerometers 1, 2, 3, which reflect corresponding vibration on transducer 1, 2, 3 respectively. Block diagram of hardware connections is shown in Figure 4.10.



(a) Block diagram of hardware connection for modelling



(b) Physical hardware connection for modelling



(c) Physical setup

Figure 4.10 Hardware connection for modelling

Chapter 4: Modelling the Plate Structure

In the measurement, “sweep” function on the signal generator was used to generate a standard sine wave signal from 20 Hz to 200Hz with 250 mV peak-peak value and 10 seconds period time. Amplified sweep sine wave signal flow into transducer 1 first, then this input signal as well as three output signals from each accelerometer (transducer) were recorded by NI DAQ9234 and sent to ModalVIEW software simultaneously (Figure 4.11) for further development of FRF curves.

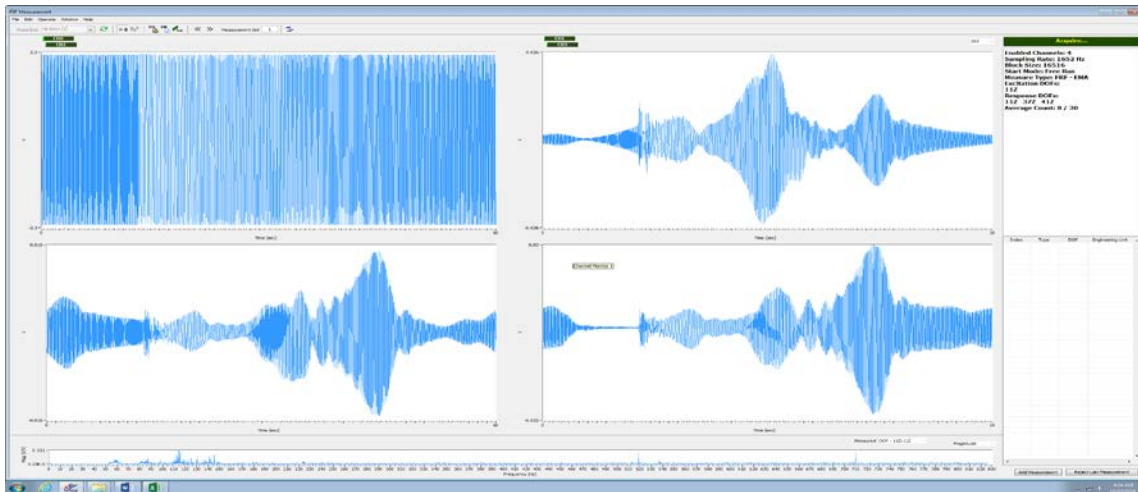


Figure 4.11 Input and output signals

In Figure 4.11, the left top curve is the input sweep sine wave signal and the other three are output signals from each accelerometer. Based on these signals, ModalVIEW software generated FRF curves (G11, G21 and G31 as shown in Table 4.1) with input from transducer 1 are illustrated in Figure 4.12.

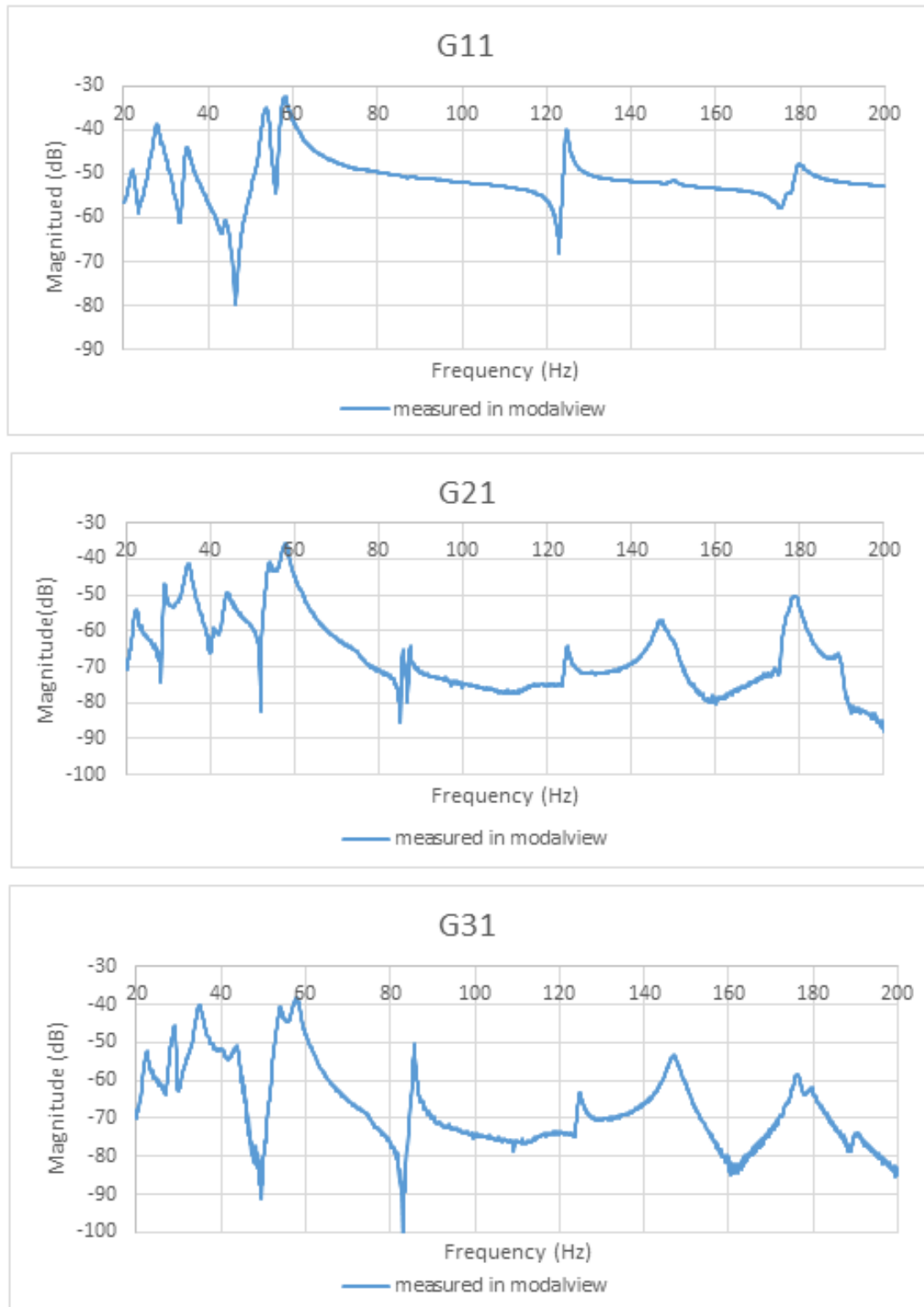


Figure 4.12 FRF curve of G11, G21, G31 generated in ModalVIEW

ModalVIEW software generated FRF curves (G12, G22 and G32 as shown in Table 4.1) with input from transducer 2 are illustrated in Figure 4.13.

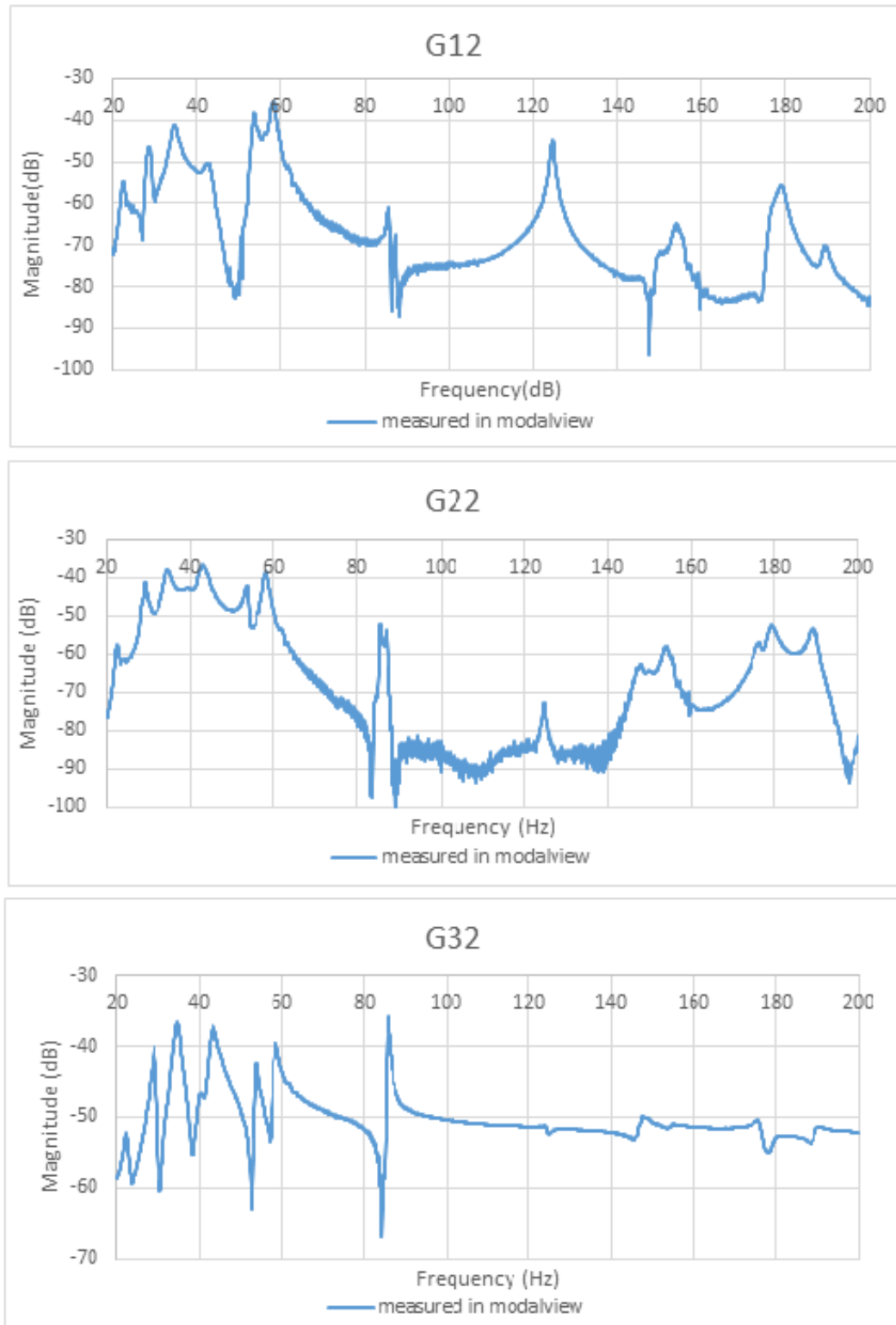


Figure 4.13 FRF curve of G12, G22, G32 generated in ModalVIEW

ModalVIEW software generated FRF curves (G13, G23 and G33 as shown in Table 4.1) with input from transducer 3 are illustrated in Figure 4.14.

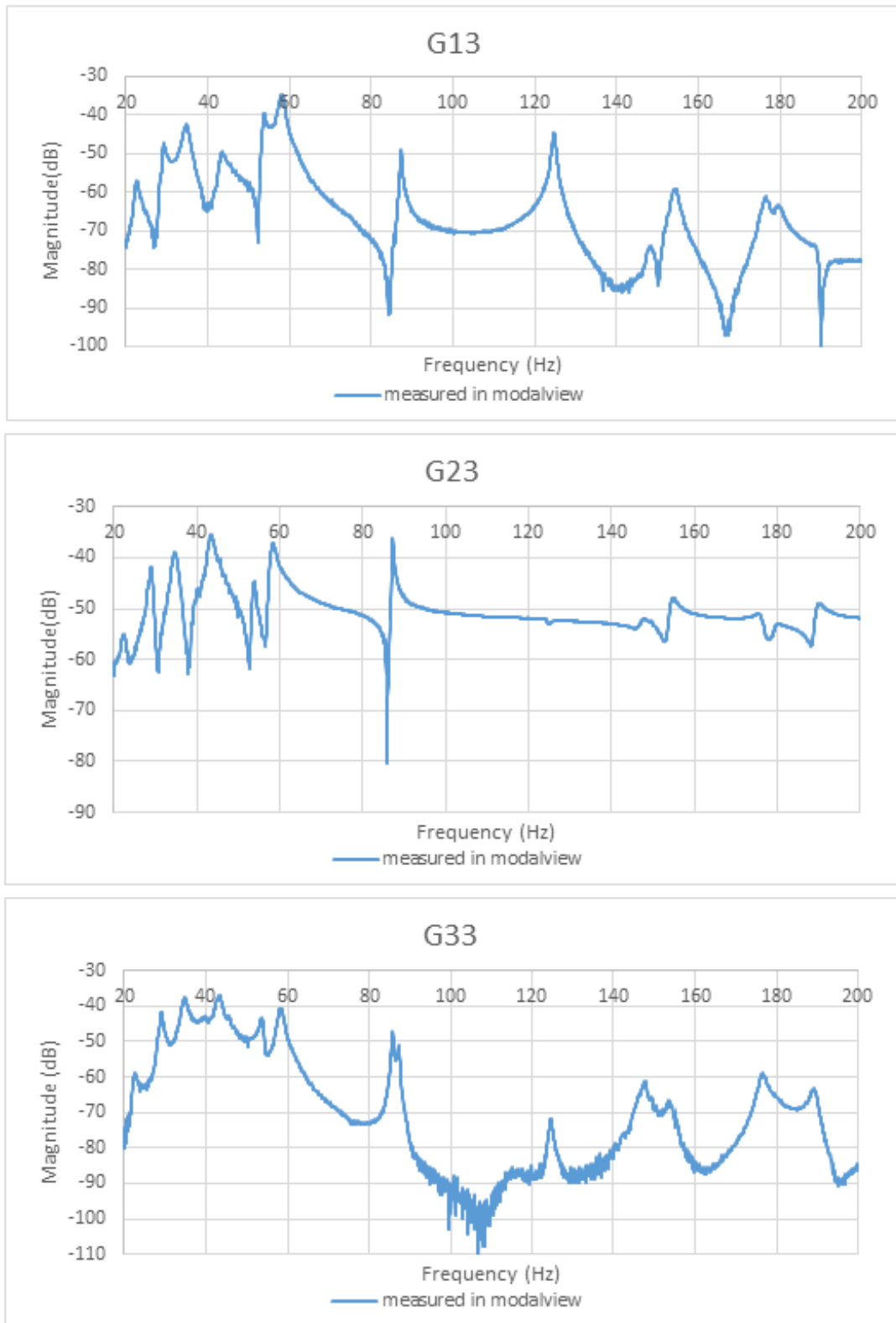


Figure 4.14 FRF curve of G13, G23, G33 generated in ModalVIEW

4.4.3 Modal Analysis in ModalVIEW

After all the FRF curves are successfully obtained from ModalVIEW software, next step is to perform modal analysis within this software.

There are many different modal analysis methods to derive vibration characteristics in time domain and frequency domain respectively [15]. “In time domain, there are Least-squares time domain method, Ibrahim time domain method, Random decrement method, ARMA time series method, Least-squares complex exponential method, etc. In frequency domain, there are Peak-picking method, Circle fit method, Inverse FRF method, Least-squares method, Dobson’s method” [5], and so on.

In ModalVIEW software, MDOF polynomial curve fitting method was utilized to estimate modal parameters, which provide a quick insight into the natural frequency, damping ratio and mode shape with minimum interaction.

In ModalVIEW software, modal analysis window is shown in Figure 4.15.

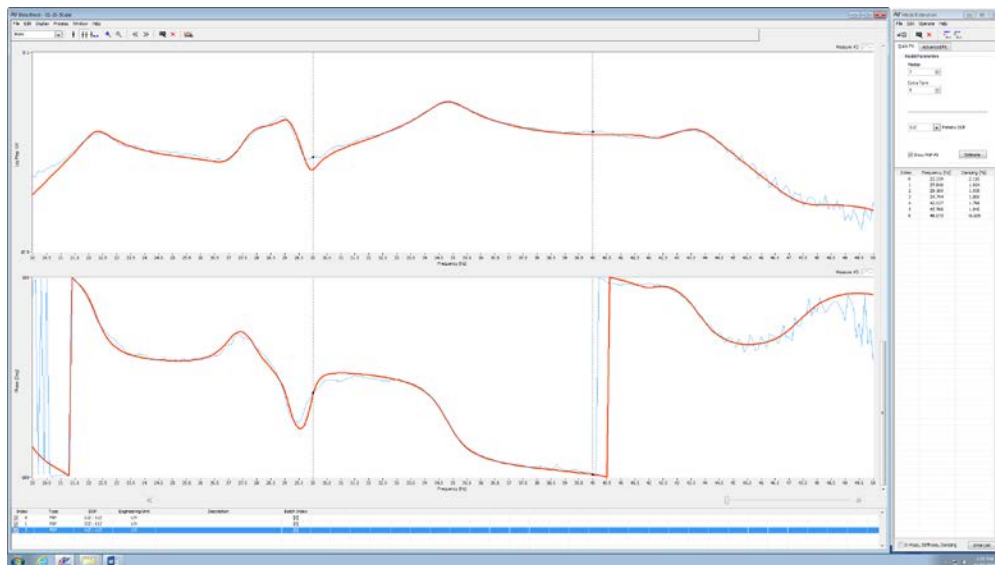


Figure 4.15 Modal analysis window in ModalVIEW software

After setting mode estimate parameters, which include mode numbers and extra term number, and check the “show FRF fit” option, as shown in Figure 4.16. Click “estimate” button, the mode information will appear in the result area, only frequencies and damping ratio can be seen in the result area, all mode information can be found in the “xxx.mod” file after save the estimation result in a file, which include natural frequencies, damping ratios, magnitude and phase of each mode.

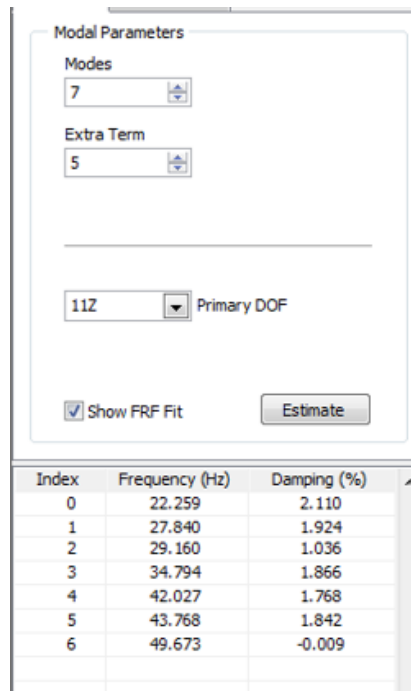


Figure 4.16 Modal estimate parameter setting window

Modal analysis result by using ModalVIEW software are listed in Table 4.2. In Table 4.2, 11Z, 37Z and 41Z stand for transducer 1, 2, 3 respectively as defined in section 4.4.1, Z means the measured displacements are in Z-axis, 37Z:11Z means input from 11Z (transducer 1) output from 37Z (transducer 2), others defined in the same way.

Table 4.2 Modal analysis result

Input from transducer 1				11Z : 11Z	37Z : 11Z	41Z : 11Z
Index	Frequency (Hz)	Damping (%)	Shape Type	magnitude	magnitude	magnitude
0	22.26	2.11	Residue Shape	0.00734121	0.00623846	0.00790573
1	27.84	1.924	Residue Shape	0.0404406	0.00213116	0.00704695
2	29.16	1.036	Residue Shape	0.00695505	0.00779947	0.0079244
3	34.79	1.866	Residue Shape	0.0228629	0.0361383	0.0426454
4	42.03	1.768	Residue Shape	0.000872615	0.003148	0.00337096
5	43.77	1.842	Residue Shape	0.00246116	0.0161142	0.0141889
6	49.67	-0.00854	Residue Shape	3.83E-05	9.20E-06	2.15E-07
7	53.7	1.047	Residue Shape	0.0675787	0.0291909	0.0328873
8	58.06	1.458	Residue Shape	0.124132	0.0871378	0.0645218
9	85.62	0.2173	Residue Shape	0.00012324	0.00069505	0.00364918
10	124.7	0.3444	Residue Shape	0.0252533	0.00122437	0.0013487
11	147.2	0.5374	Residue Shape	0.00195614	0.00427431	0.00830553
12	148.2	1.534	Residue Shape	0.0053848	0.0114359	0.013082
13	176.3	0.5288	Residue Shape	0.00478862	0.00650253	0.00648526

Chapter 4: Modelling the Plate Structure

14	179.1	0.5678	Residue Shape	0.0160113	0.0207087	0.00316221
15	189.7	0.5049	Residue Shape	5.55E-05	0.00206845	0.0006544
Input from transducer 2				11Z : 37Z	37Z : 37Z	41Z : 37Z
Index	Frequency (Hz)	Damping (%)	Shape Type	magnitude	magnitude	magnitude
0	22.36	2.33	Residue Shape	0.00511256	0.0047365	0.00491893
1	27.68	1.559	Residue Shape	0.00727462	0.00142457	0.00247211
2	29.01	1.489	Residue Shape	0.0116428	0.0231798	0.0251961
3	32.95	-0.4644	Residue Shape	3.98E-05	0.000137	0.00011119
4	34.72	2.612	Residue Shape	0.0513296	0.0747005	0.0868091
5	40.36	2.708	Residue Shape	0.00308732	0.022949	0.0292004
6	43.01	2.635	Residue Shape	0.0210864	0.111906	0.0995804
7	47.26	-1.242	Residue Shape	0.00028949	0.0008129	0.00025496
8	49.85	0.01635	Residue Shape	1.11E-05	1.20E-05	2.85E-05
9	53.55	0.7323	Residue Shape	0.0314204	0.0167561	0.0173905
10	58.23	1.117	Residue Shape	0.0688694	0.0474745	0.0338544
11	85.69	0.243	Residue Shape	0.00101917	0.00365656	0.0214477
12	87.77	0.2926	Residue Shape	0.000391137	0.00142646	0.00067802
13	111.3	1.717	Residue Shape	0.000378693	0.00042752	0.00060699
14	124.6	0.3087	Residue Shape	0.014731	0.00063531	0.000791779
15	147.4	0.763	Residue Shape	0.000872607	0.00461431	0.00708143
16	154.3	0.6028	Residue Shape	0.00381132	0.00780258	0.00122142
17	176.3	0.5722	Residue Shape	0.0048449	0.00643959	0.00663882
18	179.2	0.596	Residue Shape	0.0114811	0.0147498	0.00239068
19	189.3	0.4941	Residue Shape	0.00107498	0.0123975	0.00362142
Input from transducer 3				11Z : 41Z	37Z : 41Z	41Z : 41Z
Index	Frequency (Hz)	Damping (%)	Shape Type	magnitude	magnitude	magnitude
0	22.68	2.443	Residue Shape	0.00505895	0.00367955	0.00404956
1	29.04	1.336	Residue Shape	0.0097148	0.0191741	0.0208998
2	34.74	2.105	Residue Shape	0.0369463	0.0529193	0.0610965
3	40.05	2.784	Residue Shape	0.00242215	0.0179184	0.0215443
4	43.31	2.368	Residue Shape	0.019318	0.0981001	0.0874305
5	49.62	0.8021	Residue Shape	0.000749112	0.00222257	0.00218348
6	50.29	2.162	Residue Shape	0.00307012	0.0152884	0.0132733
7	45.78	-4.392	Residue Shape	0.0345218	0.106962	0.0508661
8	53.56	1.157	Residue Shape	0.0333832	0.0188864	0.0195637
9	58.2	1.331	Residue Shape	0.0906203	0.0617275	0.0450441
10	85.79	0.2307	Residue Shape	0.0001737	0.00150597	0.0054208
11	87.28	0.3554	Residue Shape	0.00584494	0.0242989	0.00429695
12	105.9	1.114	Residue Shape	0.000199115	0.0002198	0.0001596

Chapter 4: Modelling the Plate Structure

13	124.7	0.3561	Residue Shape	0.0155728	0.00076488	0.0007754
14	130.8	-0.4139	Residue Shape	2.11E-06	3.45E-05	2.53E-05
15	147.6	0.6466	Residue Shape	0.000534169	0.00364881	0.0049906
16	154.3	0.5684	Residue Shape	0.00610854	0.013879	0.00212628
17	176.4	0.862	Residue Shape	0.00670819	0.0163996	0.0115843
18	179.2	0.3049	Residue Shape	0.00154019	0.00169844	0.0004933
19	189.4	0.5215	Residue Shape	0.00124655	0.0135343	0.00387029

One issue need to pay attention is: the magnitudes given in above Table 4.2 cannot be used directly to form the transfer function because of the following reason:

In ModalVIEW software, the relationship of individual mode and the final FRF curve follow below equation:

$$h_{ij}(s) = \sum_{k=1}^N \left(\frac{r_{ijk}}{s-\lambda_k} + \frac{r_{ijk}^*}{s-\lambda_k^*} \right) \quad (4.28)$$

where $h(s)$ is the FRF curve, r_{ijk} is the magnitude of one mode, $\lambda_k = -\zeta\omega + j\omega\sqrt{1-\zeta^2}$ and $\lambda_k^* = -\zeta\omega - j\omega\sqrt{1-\zeta^2}$. The magnitude given in Table 4.2 is the magnitude of r_{ijk} .

To compute the 'a' value, change transfer function as:

$$\begin{aligned} T(s) &= \frac{a}{s^2+2\zeta\omega+s\omega^2} \\ &= \frac{a}{(s+\zeta\omega+j\omega\sqrt{1-\zeta^2})(s+\zeta\omega-j\omega\sqrt{1-\zeta^2})} = \frac{-j\frac{a}{2\omega\sqrt{1-\zeta^2}}}{(s+\zeta\omega+j\omega\sqrt{1-\zeta^2})} + \frac{j\frac{a}{2\omega\sqrt{1-\zeta^2}}}{(s+\zeta\omega-j\omega\sqrt{1-\zeta^2})} \end{aligned} \quad (4.29)$$

It can be observed that:

$$|r| = \left| \frac{a}{2\omega\sqrt{1-\zeta^2}} \right| \quad (4.30)$$

Therefore, the mode shape can be obtained by using equation 4.31.

$$a = r * 2\omega\sqrt{1-\zeta^2} \quad (4.31)$$

Applying equation 4.31 to all the magnitude value in Table 4.2, the results shown in Table 4.3. Data in Table 4.3 is the modal parameters that can be used to form transfer functions.

Table 4.3 Modal parameters

Input from transducer 1			11Z : 11Z	37Z : 11Z	41Z : 11Z
Index	Frequency (Hz)	Damping (%)	a	a	a
0	22.26	2.11	2.0531	1.7447	2.2110
1	27.84	1.924	14.1454	0.7454	2.4649
2	29.16	1.036	2.5484	2.8578	2.9036
3	34.79	1.866	9.9935	15.7963	18.6406
4	42.03	1.768	0.4608	1.6624	1.7801
5	43.77	1.842	1.3535	8.8618	7.8030
6	49.67	-0.008539	0.0239	0.0057	0.0001
7	53.7	1.047	45.6005	19.6973	22.1916
8	58.06	1.458	90.5574	63.5692	47.0703
9	85.62	0.2173	0.1326	0.7478	3.9263
10	124.7	0.3444	39.5723	1.9186	2.1134
11	147.2	0.5374	3.6184	7.9064	15.3631
12	148.2	1.534	10.0271	21.2950	24.3602
13	176.3	0.5288	10.6088	14.4058	14.3676
14	179.1	0.5678	36.0350	46.6070	7.1169
15	189.7	0.5049	0.1323	4.9308	1.5600
Input from transducer 2			11Z : 37Z	37Z : 37Z	41Z : 37Z
Index	Frequency (Hz)	Damping (%)	a	a	a
0	22.36	2.33	1.4362	1.3305	1.3818
1	27.68	1.559	2.5301	0.4955	0.8598
2	29.01	1.489	4.2439	8.4493	9.1842
3	32.95	-0.4644	0.0165	0.0568	0.0460
4	34.72	2.612	22.3877	32.5810	37.8622
5	40.36	2.708	1.5652	11.6350	14.8044
6	43.01	2.635	11.3928	60.4619	53.8024
7	47.26	-1.242	0.1719	0.4827	0.1514
8	49.85	0.01635	0.0069	0.0075	0.0179
9	53.55	0.7323	21.1431	11.2754	11.7023
10	58.23	1.117	50.3913	34.7368	24.7710
11	85.69	0.243	1.0975	3.9374	23.0951
12	87.77	0.2926	0.4314	1.5733	0.7478
13	111.3	1.717	0.5296	0.5979	0.8488
14	124.6	0.3087	23.0652	0.9947	1.2397
15	147.4	0.763	1.6163	8.5468	13.1164
16	154.3	0.6028	7.3900	15.1288	2.3683
17	176.3	0.5722	10.7335	14.2664	14.7077
18	179.2	0.596	25.8537	33.2144	5.3835

19	189.3	0.4941	2.5571	29.4910	8.6146
Input from transducer 3			11Z : 41Z	37Z : 41Z	41Z : 41Z
Index	Frequency (Hz)	Damping (%)	a	a	a
0	22.68	2.443	1.4414	1.0484	1.1538
1	29.04	1.336	3.5449	6.9965	7.6262
2	34.74	2.105	16.1255	23.0971	26.6661
3	40.05	2.784	1.2186	9.0145	10.8387
4	43.31	2.368	10.5109	53.3759	47.5706
5	49.62	0.8021	0.4671	1.3858	1.3614
6	50.29	2.162	1.9397	9.6594	8.3863
7	45.78	-4.392	19.8408	61.4746	29.2344
8	53.56	1.157	22.4672	12.7107	13.1665
9	58.2	1.331	66.2704	45.1412	32.9406
10	85.79	0.2307	0.1873	1.6235	5.8440
11	87.28	0.3554	6.4106	26.6507	4.7128
12	105.9	1.114	0.2650	0.2925	0.2124
13	124.7	0.3561	24.4028	1.1986	1.2152
14	130.8	-0.4139	0.0035	0.0566	0.0416
15	147.6	0.6466	0.9908	6.7677	9.2563
16	154.3	0.5684	11.8442	26.9108	4.1228
17	176.4	0.862	14.8695	36.3517	25.6780
18	179.2	0.3049	3.4683	3.8247	1.1109
19	189.4	0.5215	2.9668	32.2121	9.2114

As all model parameters are obtained, the modal analysis step is completed, next stage is to simulate plant model in MATLAB.

4.5 Simulate Plant Model in MATLAB

From control point of view, modes with negative damping ratio are unreasonable in practice [32], so those modes should be omitted when building the plant model. Furthermore, modes with very small mode shape ('a' value) have very few effect on controller design compared to those significant modes. Therefore, for controller design purpose, these modes can be ignored when building the simulated plant model. Figure 4.17, 4.18 and 4.19 illustrate the comparison of MATLAB simulated FRF curves of all the modes found in ModalVIEW software and those significant modes.

Chapter 4: Modelling the Plate Structure



Figure 4.17 Comparison of FRF curves of all modes and significant modes-input from transducer 1

Chapter 4: Modelling the Plate Structure



Figure 4.18 Comparison of FRF curves of all modes and significant modes-input from transducer 2

Chapter 4: Modelling the Plate Structure



Figure 4.19 Comparison of FRF curves of all modes and significant modes-input from transducer 3

Chapter 4: Modelling the Plate Structure

From the comparison in Figure 4.17, 4.18 and 4.19, it can be observed that the omit of negative damped modes and insignificant modes do not distort the FRF curves too much, so that this simplicity can be accepted.

Since this is a 3-input 3-output system, simulated plant model in MATLAB should be like:

$$\begin{bmatrix} Y_1(s) \\ Y_2(s) \\ Y_3(s) \end{bmatrix} = \begin{bmatrix} G_{11}(s) & G_{12}(s) & G_{13}(s) \\ G_{21}(s) & G_{22}(s) & G_{23}(s) \\ G_{31}(s) & G_{32}(s) & G_{33}(s) \end{bmatrix} * \begin{bmatrix} U_1(s) \\ U_2(s) \\ U_3(s) \end{bmatrix} \quad (4.32)$$

Each component of the transfer matrix is:

$$G_{ij}(s) = \sum_{k=1}^N \frac{a_{ijk}}{s^2 + 2\zeta_{ijk}\omega_{ijk}s + \omega_{ijk}^2} \quad (4.33)$$

Substitute parameters of significant modes, which can be found in Table 4.3, into above equation (4.33), each element of transfer matrix can be obtained as:

$$\begin{aligned} G_{11}(s) = & \frac{2.0531}{s^2+5.9022s+19561.8} + \frac{14.1454}{s^2+6.7311s+30598.3} + \frac{9.9935}{s^2+8.1578s+47782.4} + \frac{1.3535}{s^2+10.1315s+75633.1} + \\ & \frac{45.6005}{s^2+7.0653s+113843} + \frac{90.5574}{s^2+10.6376s+133080} + \frac{39.5723}{s^2+5.3968s+613892} + \frac{3.6184}{s^2+9.9407s+855411} + \\ & \frac{10.6088}{s^2+11.7153s+1227054} + \frac{36.035}{s^2+12.7791s+1266340} \end{aligned} \quad (4.34)$$

$$\begin{aligned} G_{21}(s) = & \frac{1.7447}{s^2+5.9022s+19561.8} + \frac{2.8578}{s^2+3.7963s+33568.7} + \frac{15.7963}{s^2+8.1578s+47782.4} + \frac{8.8618}{s^2+10.1315s+75633.1} + \\ & \frac{19.6973}{s^2+7.0653s+113843} + \frac{63.5692}{s^2+10.6376s+133080} + \frac{0.7478}{s^2+2.3380s+289407} + \frac{1.9186}{s^2+5.3968s+613892} + \\ & \frac{7.9064}{s^2+9.9407s+855411} + \frac{14.4058}{s^2+11.7153s+1227054} + \frac{46.6070}{s^2+12.7791s+1266340} + \frac{4.9308}{s^2+12.0360s+1420671} \end{aligned} \quad (4.35)$$

$$\begin{aligned} G_{31}(s) = & \frac{2.2110}{s^2+5.9022s+19561.8} + \frac{2.9036}{s^2+3.7963s+33568.7} + \frac{18.6406}{s^2+8.1578s+47782.4} + \frac{7.8030}{s^2+10.1315s+75633.1} + \\ & \frac{22.1916}{s^2+7.0653s+113843} + \frac{47.0703}{s^2+10.6376s+133080} + \frac{3.9263}{s^2+2.3380s+289407} + \frac{2.1134}{s^2+5.3968s+613892} + \frac{15.3631}{s^2+9.9407s+855411} + \\ & \frac{14.3676}{s^2+11.7153s+1227054} + \frac{7.1169}{s^2+12.7791s+1266340} + \frac{1.5600}{s^2+12.0360s+1420671} \end{aligned} \quad (4.36)$$

$$\begin{aligned} G_{12}(s) = & \frac{1.4362}{s^2+6.5469s+19738} + \frac{4.2439}{s^2+5.4282s+33224.2} + \frac{22.3877}{s^2+11.3963s+47590.3} + \frac{11.3928}{s^2+14.2416s+73029.4} + \\ & \frac{21.1431}{s^2+4.9279s+113208} + \frac{50.3913}{s^2+8.1735s+133861} + \frac{1.0975}{s^2+2.6167s+289881} + \frac{0.4314}{s^2+3.2272s+304124} + \frac{23.0652}{s^2+4.8325s+612908} + \end{aligned}$$

Chapter 4: Modelling the Plate Structure

$$\frac{1.6163}{s^2+14.1329s+857737} + \frac{7.3900}{s^2+11.6882s+939920} + \frac{10.7335}{s^2+12.6768s+1227054} + \frac{25.8537}{s^2+13.4213s+1267754} + \frac{2.5571}{s^2+11.7537s+1414687} \quad (4.37)$$

$$G_{22}(s) = \frac{1.3305}{s^2+6.5469s+19738} + \frac{8.4493}{s^2+5.4282s+33224.2} + \frac{32.5810}{s^2+11.3963s+47590.3} + \frac{60.4619}{s^2+14.2416s+73029.4} + \frac{11.2754}{s^2+4.9279s+113208} + \frac{34.7368}{s^2+8.1735s+133861} + \frac{3.9374}{s^2+2.6167s+289881} + \frac{1.5733}{s^2+3.2272s+304124} + \frac{0.9947}{s^2+4.8325s+612908} + \frac{8.5468}{s^2+14.1329s+857737} + \frac{15.1288}{s^2+11.6882s+939920} + \frac{14.2664}{s^2+12.6768s+1227054} + \frac{33.2144}{s^2+13.4213s+1267754} + \frac{29.4910}{s^2+11.7537s+1414687} \quad (4.38)$$

$$G_{32}(s) = \frac{1.3818}{s^2+6.5469s+19738} + \frac{9.1842}{s^2+5.4282s+33224.2} + \frac{37.8622}{s^2+11.3963s+47590.3} + \frac{14.8044}{s^2+13.7344s+64307.5} + \frac{53.8024}{s^2+14.2416s+73029.4} + \frac{11.7023}{s^2+4.9279s+113208} + \frac{24.7710}{s^2+8.1735s+133861} + \frac{23.0951}{s^2+2.6167s+289881} + \frac{0.7478}{s^2+3.2272s+304124} + \frac{1.2397}{s^2+4.8325s+612908} + \frac{13.1164}{s^2+14.1329s+857737} + \frac{2.3683}{s^2+11.6882s+939920} + \frac{14.7077}{s^2+12.6768s+1227054} + \frac{5.3835}{s^2+13.4213s+1267754} + \frac{8.6164}{s^2+11.7537s+1414687} \quad (4.39)$$

$$G_{13}(s) = \frac{1.4414}{s^2+6.9627s+20307} + \frac{3.5449}{s^2+4.8754s+33292.9} + \frac{16.1255}{s^2+9.1895s+47645.1} + \frac{1.2186}{s^2+14.0114s+63323.4} + \frac{10.5109}{s^2+12.8878s+74051.8} + \frac{22.4672}{s^2+7.7872s+113251} + \frac{66.2704}{s^2+9.7344s+133723} + \frac{0.1873}{s^2+2.4871s+290558} + \frac{6.4106}{s^2+3.8980s+300738} + \frac{24.4028}{s^2+5.5802s+613892} + \frac{0.9908}{s^2+11.9931s+860066} + \frac{11.8442}{s^2+11.0212s+939920} + \frac{14.8695}{s^2+19.1080s+1228446} + \frac{2.9668}{s^2+12.4121s+1416182} \quad (4.40)$$

$$G_{23}(s) = \frac{1.0484}{s^2+6.9627s+20307} + \frac{6.9965}{s^2+4.8754s+33292.9} + \frac{23.0971}{s^2+9.1895s+47645.1} + \frac{9.0145}{s^2+14.0114s+63323.4} + \frac{53.3759}{s^2+12.8878s+74051.8} + \frac{12.7107}{s^2+7.7872s+113251} + \frac{45.1412}{s^2+9.7344s+133723} + \frac{1.6235}{s^2+2.4871s+290558} + \frac{26.6507}{s^2+3.8980s+300738} + \frac{1.1986}{s^2+5.5802s+613892} + \frac{6.7677}{s^2+11.9931s+860066} + \frac{26.9108}{s^2+11.0212s+939920} + \frac{36.3517}{s^2+19.1080s+1228446} + \frac{32.2121}{s^2+12.4121s+1416182} \quad (4.41)$$

$$G_{33}(s) = \frac{1.1538}{s^2+6.9627s+20307} + \frac{7.6262}{s^2+4.8754s+33292.9} + \frac{26.6661}{s^2+9.1895s+47645.1} + \frac{10.8387}{s^2+14.0114s+63323.4} + \frac{47.5706}{s^2+12.8878s+74051.8} + \frac{13.1665}{s^2+7.7872s+113251} + \frac{32.9406}{s^2+9.7344s+133723} + \frac{5.8440}{s^2+2.4871s+290558} +$$

$$\begin{aligned} & \frac{4.7128}{s^2+3.8980s+300738} + \frac{1.2152}{s^2+5.5802s+613892} + \frac{9.2563}{s^2+11.9931s+860066} + \\ & \frac{4.1228}{s^2+11.0212s+939920} + \frac{25.6780}{s^2+19.1080s+1228446} + \frac{9.2114}{s^2+12.4121s+1416182} \end{aligned} \quad (4.42)$$

Above equations are considered as components of the true plant model of the plate structure, in the following sections, model truncation and model correction technique are applied to derive the mathematical model that suitable for controller design purpose.

4.6 Model Truncation

In this project, only low frequency vibration (first three modes) are targeted to be canceled out because high frequency vibration can be easily controlled by passive vibration control techniques [29]. Therefore, model truncation technique was utilized to truncate the true plant model obtained in section 4.5 to first three modes only, the truncated model is shown in equation (4.43) to equation (4.51).

$$G_{11}(s) = \frac{2.0531}{s^2+5.9022s+19561.8} + \frac{14.1454}{s^2+6.7311s+30598.3} + \frac{9.9935}{s^2+8.1578s+47782.4} \quad (4.43)$$

$$G_{21}(s) = \frac{1.7447}{s^2+5.9022s+19561.8} + \frac{2.8578}{s^2+3.7963s+33568.7} + \frac{15.7963}{s^2+8.1578s+47782.4} \quad (4.44)$$

$$G_{31}(s) = \frac{2.2110}{s^2+5.9022s+19561.8} + \frac{2.9036}{s^2+3.7963s+33568.7} + \frac{18.6406}{s^2+8.1578s+47782.4} \quad (4.45)$$

$$G_{12}(s) = \frac{1.4362}{s^2+6.5469s+19738} + \frac{4.2439}{s^2+5.4282s+33224.2} + \frac{22.3877}{s^2+11.3963s+47590.3} \quad (4.46)$$

$$G_{22}(s) = \frac{1.3305}{s^2+6.5469s+19738} + \frac{8.4493}{s^2+5.4282s+33224.2} + \frac{32.5810}{s^2+11.3963s+47590.3} \quad (4.47)$$

$$G_{32}(s) = \frac{1.3818}{s^2+6.5469s+19738} + \frac{9.1842}{s^2+5.4282s+33224.2} + \frac{37.8622}{s^2+11.3963s+47590.3} \quad (4.48)$$

$$G_{13}(s) = \frac{1.4414}{s^2+6.9627s+20307} + \frac{3.5449}{s^2+4.8754s+33292.9} + \frac{16.1255}{s^2+9.1895s+47645.1} \quad (4.49)$$

$$G_{23}(s) = \frac{1.0484}{s^2+6.9627s+20307} + \frac{6.9965}{s^2+4.8754s+33292.9} + \frac{23.0971}{s^2+9.1895s+47645.1} \quad (4.50)$$

$$G_{33}(s) = \frac{1.1538}{s^2+6.9627s+20307} + \frac{7.6262}{s^2+4.8754s+33292.9} + \frac{26.6661}{s^2+9.1895s+47645.1} \quad (4.51)$$

Figure 4.20 illustrate comparison of FRF curves of true plant model and the truncated model.

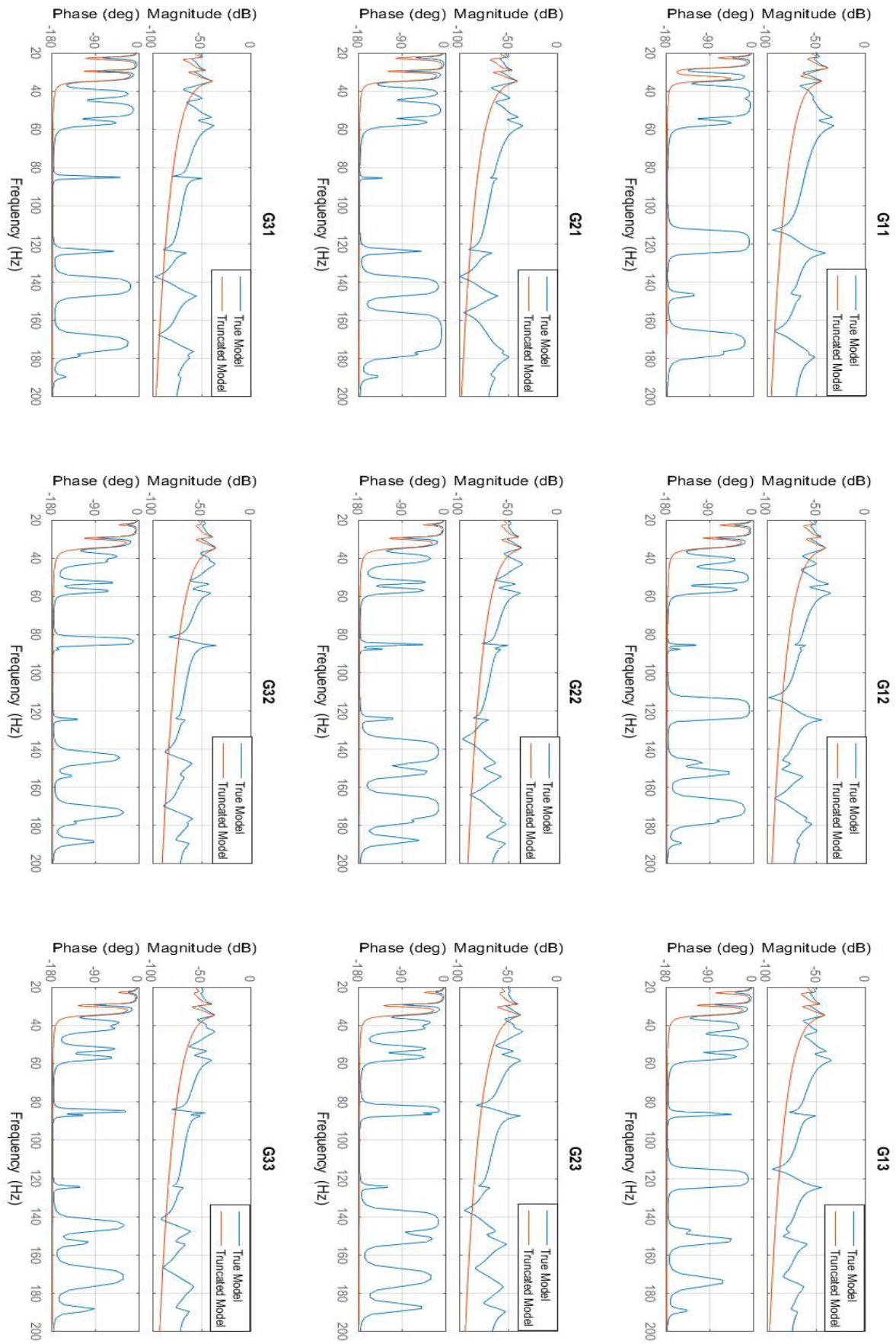


Figure 4.20 Comparison of FRF of true model and truncated model

From Figure 4.20, it can be seen that the truncated model has similar trend with the true model, but significant different phase and magnitude on the first three modes, which is because the truncated higher order modes have an effect on the frequency response of the first three modes.

This truncation error should be minimized by using model correction technique before controller design as described in next section.

4.7 Model Correction

Dynamics of flexible structure often consist of infinity number of modes, for controller design purpose, these infinite modes are often approximated by a finite modes transfer function by using truncation method. It is obvious that direct truncation of higher order modes can result in errors in the frequency response function [31], model correction is a way to control this error. In this section, spatial H_2 norm is introduced to generate a spatially distributed DC term that is used to minimize the truncation error [16].

For a multi-input multi-output system with transfer function of the form:

$$G(s) = \sum_{i=1}^{\infty} \frac{\Phi_i}{s^2 + 2\zeta_i \omega_i s + \omega_i^2} \quad (4.52)$$

where $\Phi_i \in R^{m \times n}$, m is the number of sensors and n is number of actuators.

Approximate equation (4.52) with

$$\hat{G}(s) = \sum_{i=1}^N \frac{\Phi_i}{s^2 + 2\zeta_i \omega_i s + \omega_i^2} + K \quad (4.53)$$

Since spatial H_2 norm is used, the value of the DC term K should be determined such that the spatial cost function shown in equation (4.54) is minimized.

$$J = \ll W(s)[G(s) - \hat{G}(s)] \gg_2^2 \quad (4.54)$$

where $|W(s)| = |W(j\omega)| = \begin{cases} 1 & -\omega_c \leq \omega \leq \omega_c \\ 0 & \text{elsewhere} \end{cases}$.

Above cost function can be expressed as:

$$J = \ll W(s)[\tilde{G}(s) - K] \gg_2^2 \quad (4.55)$$

where $\tilde{G}(s) = \sum_{i=N+1}^{\infty} \frac{\Phi_i}{s^2 + 2\zeta_i \omega_i s + \omega_i^2}$

Chapter 4: Modelling the Plate Structure

So that

$$J = \ll W(s)\tilde{G}(s) \gg_2^2 + \ll W(s)K \gg_2^2 - (\langle W(s)\tilde{G}(s), W(s)K \rangle + \langle W(s)K, W(s)\tilde{G}(s) \rangle) \quad (4.56)$$

where $\langle F, G \rangle = \frac{1}{2\pi} \int_{-\infty}^{\infty} \text{tr}\{F^*(j\omega)G(j\omega)\}d\omega$.

Then the spatial cost function (4.55) can be rewritten as:

$$J = \ll W(s)\tilde{G}(s) \gg_2^2 + \frac{1}{2\pi} \int_{-\infty}^{\infty} \text{tr}\{K'W^*(j\omega)W(j\omega)K\}d\omega - \frac{1}{2\pi} \int_{-\infty}^{\infty} \left[\begin{array}{c} \text{tr}\{\tilde{G}^*(j\omega)W^*(j\omega)W(j\omega)K\} \\ K'W^*(j\omega)W(j\omega)\tilde{G}(j\omega) \end{array} \right] d\omega \quad (4.57)$$

Differentiating equation (4.57) with respect to K , the optimum value of K can be obtained.

$$\begin{aligned} K_{opt} &= \left(\int_{-\infty}^{\infty} W^*(j\omega)W(j\omega)d\omega \right)^{-1} \times \left(\int_{-\infty}^{\infty} W^*(j\omega)W(j\omega)\text{Re}\{\tilde{G}(j\omega)\}d\omega \right) \\ &= \frac{1}{2\omega_c} \int_{-\omega_c}^{\omega_c} \text{Re}\{\tilde{G}(j\omega)\}d\omega \\ &= \frac{1}{2\omega_c} \int_{-\omega_c}^{\omega_c} \sum_{i=N+1}^{\infty} \frac{\Phi_i}{\omega_i^2 - \omega^2} d\omega \\ &= \frac{1}{2\omega_c} \sum_{i=N+1}^{\infty} \frac{1}{\omega_i} \ln \frac{\omega_i + \omega_c}{\omega_i - \omega_c} \Phi_i \end{aligned} \quad (4.58)$$

Therefore, the spatial DC term is written as

$$K = \sum_{i=N+1}^{\infty} \frac{1}{2\omega_c\omega_i} \ln \frac{\omega_i + \omega_c}{\omega_i - \omega_c} \Phi_i \quad (4.59)$$

Apply equation (4.59) in MATLAB (associated MATLAB code can be found in Appendix C: MATLAB code), the truncation error of each transfer function for the first three modes can be obtained as:

$$\text{Truncation Error} = \begin{bmatrix} 0.0015 & 0.001 & 0.0012 \\ 0.0011 & 0.0019 & 0.0021 \\ 0.0009 & 0.002 & 0.0018 \end{bmatrix} \quad (4.60)$$

Finally, the transfer matrix used for controller design can be expressed as:

$$G(s) = \begin{bmatrix} G_{11}(s) & G_{12}(s) & G_{13}(s) \\ G_{21}(s) & G_{22}(s) & G_{23}(s) \\ G_{31}(s) & G_{32}(s) & G_{33}(s) \end{bmatrix} + \begin{bmatrix} E_{11} & E_{12} & E_{13} \\ E_{21} & E_{22} & E_{23} \\ E_{31} & E_{32} & E_{33} \end{bmatrix} \quad (4.61)$$

where E_{ij} is the truncation error listed in equation (4.60).

Chapter 4: Modelling the Plate Structure

Substitute the truncated model that found in section 4.6 and truncation error in equation (4.60) into equation (4.61), components of the transfer matrix are shown below.

$$G_{11}(s) = \frac{2.0531}{s^2+5.9022s+19561.8} + \frac{14.1454}{s^2+6.7311s+30598.3} + \frac{9.9935}{s^2+8.1578s+47782.4} + 0.0015 \quad (4.62)$$

$$G_{21}(s) = \frac{1.7447}{s^2+5.9022s+19561.8} + \frac{2.8578}{s^2+3.7963s+33568.7} + \frac{15.7963}{s^2+8.1578s+47782.4} + 0.0011 \quad (4.63)$$

$$G_{31}(s) = \frac{2.2110}{s^2+5.9022s+19561.8} + \frac{2.9036}{s^2+3.7963s+33568.7} + \frac{18.6406}{s^2+8.1578s+47782.4} + 0.0009 \quad (4.64)$$

$$G_{12}(s) = \frac{1.4362}{s^2+6.5469s+19738} + \frac{4.2439}{s^2+5.4282s+33224.2} + \frac{22.3877}{s^2+11.3963s+47590.3} + 0.001 \quad (4.65)$$

$$G_{22}(s) = \frac{1.3305}{s^2+6.5469s+19738} + \frac{8.4493}{s^2+5.4282s+33224.2} + \frac{32.5810}{s^2+11.3963s+47590.3} + 0.0019 \quad (4.66)$$

$$G_{32}(s) = \frac{1.3818}{s^2+6.5469s+19738} + \frac{9.1842}{s^2+5.4282s+33224.2} + \frac{37.8622}{s^2+11.3963s+47590.3} + 0.002 \quad (4.67)$$

$$G_{13}(s) = \frac{1.4414}{s^2+6.9627s+20307} + \frac{3.5449}{s^2+4.8754s+33292.9} + \frac{16.1255}{s^2+9.1895s+47645.1} + 0.0012 \quad (4.68)$$

$$G_{23}(s) = \frac{1.0484}{s^2+6.9627s+20307} + \frac{6.9965}{s^2+4.8754s+33292.9} + \frac{23.0971}{s^2+9.1895s+47645.1} + 0.0021 \quad (4.69)$$

$$G_{33}(s) = \frac{1.1538}{s^2+6.9627s+20307} + \frac{7.6262}{s^2+4.8754s+33292.9} + \frac{26.6661}{s^2+9.1895s+47645.1} + 0.0018 \quad (4.70)$$

Above equation (4.62) to (4.70) are the final equations that used to design the controller.

Figure 4.21 illustrate comparison of FRF curves of true plant model and the corrected model.

Comparing Figure 4.20 and Figure 4.21, it can be easily concluded that after performing model correction, the corrected model matched the first three modes of the true model almost perfectly, which is the desired result.

Now the modelling stage is completed. Based on the mathematical model built in this chapter, controllers will be designed in the next chapter.

Chapter 4: Modelling the Plate Structure

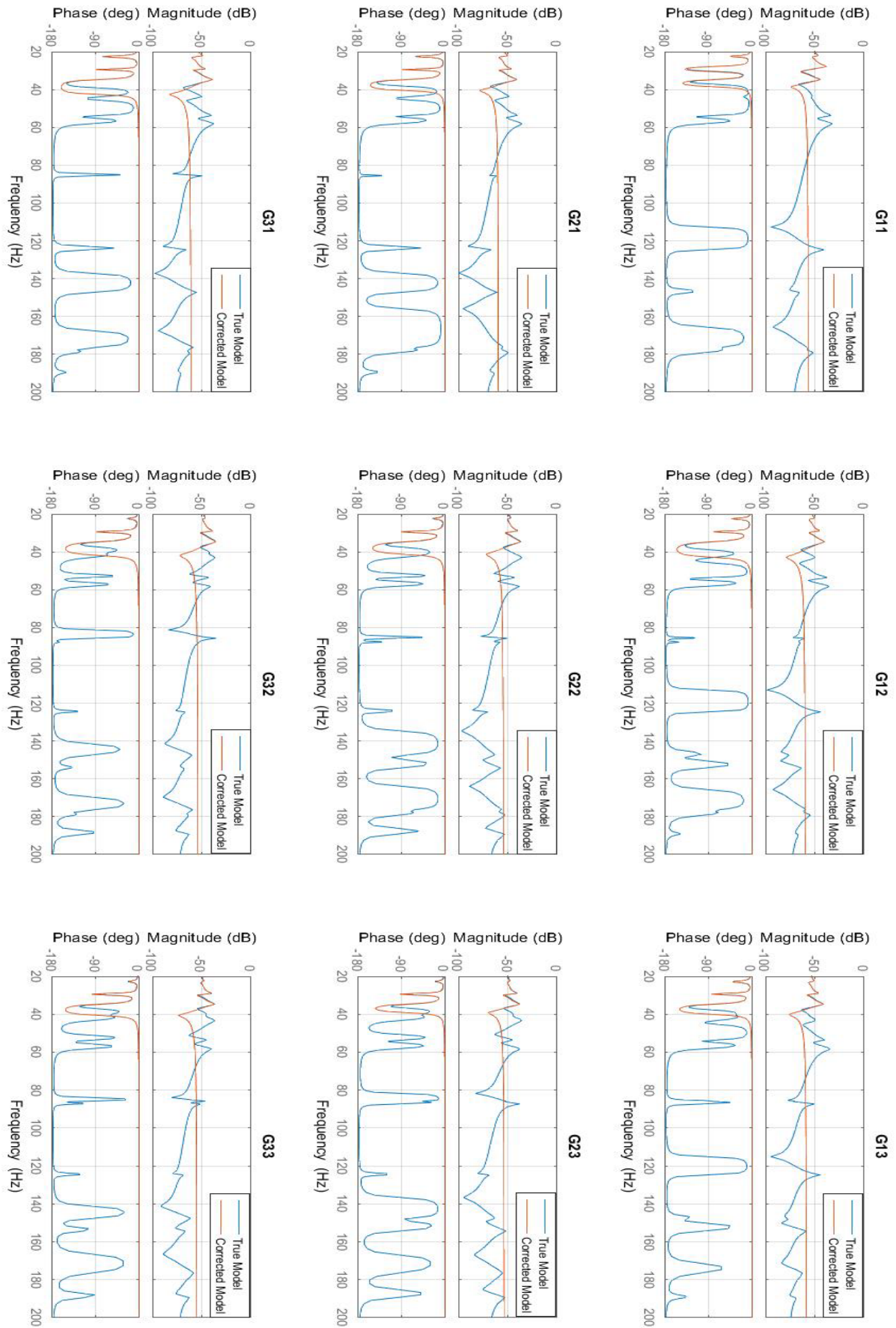


Figure 4.21 Comparison of FRF of true model and corrected model

Chapter 5 : Controller Design

Based on the mathematical model derived in chapter 4, positive position feedback (PPF) controllers are designed and applied to the simulated mathematical model in this chapter. Firstly, PPF properties and basic characteristics are described in section 5.1. Then in section 5.2, PPF controlled closed-loop system are analyzed to obtain the stability boundary. In section 5.3 PPF parameters selection methods are provided. Then in section 5.4 and 5.5, based on the parameters selection methods, PPF controllers are designed for single-input single-output (SISO) model and multi-input multi-output (MIMO) model of the plate structure respectively and applied to the simulated mathematical model to validate the vibration control effect.

5.1 PPF Controller Characteristics

The basic principle of positive position feedback (PPF) controller is to add extra damping to the target modes of the structure so that the effect of the disturbance can be reduced [17] [30].

PPF control system can be expressed by two equations:

$$\text{Structure: } \ddot{\xi} + 2\zeta\omega\dot{\xi} + \omega^2\xi = g\omega^2\eta \quad (5.1)$$

$$\text{Compensator: } \ddot{\eta} + 2\zeta_c\omega_c\dot{\eta} + \omega_c^2\eta = \omega_c^2\xi \quad (5.2)$$

where ξ indicate structure coordinate (displacement).

ζ indicate damping ratio of structure.

ω indicate natural frequency of structure.

η indicate compensator coordinate (displacement).

ζ_c indicate damping ratio of compensator.

ω_c indicate natural frequency of compensator.

g indicate control gain with $g > 0$.

From equation (5.1) and (5.2), it is easy to find that the structure position feedback to compensator equation positively, and compensator position feedback to structure equation positively, that is the essence of PPF controller.

Take Laplace transform to equation (5.1) and (5.2), the PPF controlled system could be rewritten as:

$$\frac{\xi(s)}{\eta(s)} = \frac{g\omega^2}{s^2 + 2\zeta\omega s + \omega^2} \quad (5.3)$$

$$\frac{\eta(s)}{\xi(s)} = \frac{\omega_c^2}{s^2 + 2\zeta_c\omega_c s + \omega_c^2} \quad (5.4)$$

And corresponding block diagram is shown in below Figure 5.1.

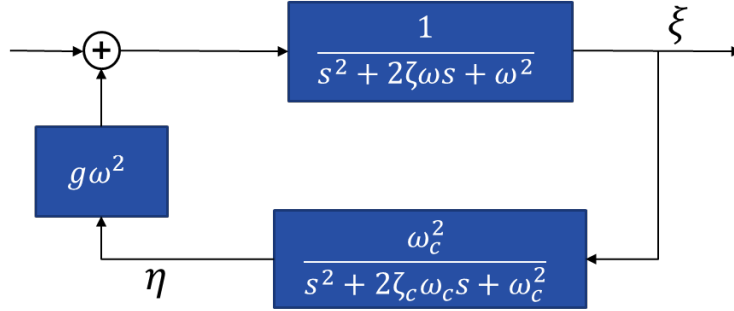


Figure 5.1 Block diagram of PPF control system

From above block diagram and equation (5.4), it can be observed that the PPF controller is actually a standard second order low pass filter and the actual control gain is $g\omega^2$.

5.2 Stability of PPF Controlled System

Before implement PPF control, it is necessary to study the stability boundary of the PPF compensated system in order to achieve a stable closed-loop system. In this section, Routh-Hurwitz Stability Criterion and Lyapunov stability theorem are used respectively to derive the stability boundary for SISO system and MIMO system.

5.2.1 Single-Input Single-Output Case

For single-input single-output system, Routh-Hurwitz Stability Criterion was utilized to derive the stability boundary [23].

From above block diagram of PPF controlled system, the closed-loop transfer function is:

$$CLTF = \frac{\frac{1}{s^2 + 2\zeta\omega s + \omega^2}}{1 - \frac{1}{s^2 + 2\zeta\omega s + \omega^2} * \frac{g\omega^2\omega_c^2}{s^2 + 2\zeta_c\omega_c s + \omega_c^2}} = \frac{s^2 + 2\zeta_c\omega_c s + \omega_c^2}{(s^2 + 2\zeta\omega s + \omega^2)(s^2 + 2\zeta_c\omega_c s + \omega_c^2) - g\omega^2\omega_c^2} \quad (5.5)$$

Closed-loop characteristic equation of equation (5.5) is:

$$\begin{aligned} CLCE &= (s^2 + 2\zeta\omega s + \omega^2)(s^2 + 2\zeta_c\omega_c s + \omega_c^2) - g\omega^2\omega_c^2 \\ &= s^4 + (2\zeta\omega + 2\zeta_c\omega_c)s^3 + (\omega^2 + \omega_c^2 + 4\zeta\omega\zeta_c\omega_c)s^2 + (2\zeta\omega\omega_c^2 + 2\zeta_c\omega_c\omega^2)s + \\ &\quad (1 - g)\omega^2\omega_c^2 = 0 \end{aligned} \quad (5.6)$$

Routh- Hurwitz array of the system is constructed as:

Table 5.1 Routh- Hurwitz array of PPF control system

s^4	$M1=1$	$\omega^2 + \omega_c^2 + 4\zeta\omega\zeta_c\omega_c$	$(1 - g)\omega^2\omega_c^2$
s^3	$M2=2\zeta\omega + 2\zeta_c\omega_c$	$2\zeta\omega\omega_c^2 + 2\zeta_c\omega_c\omega^2$	0
s^2	$M3=-\frac{1}{2\zeta\omega+2\zeta_c\omega_c} \left \begin{array}{cc} 1 & \omega^2 + \omega_c^2 + 4\zeta\omega\zeta_c\omega_c \\ 2\zeta\omega + 2\zeta_c\omega_c & 2\zeta\omega\omega_c^2 + 2\zeta_c\omega_c\omega^2 \end{array} \right $	$(1 - g)\omega^2\omega_c^2$	0
s^1	$M4=-\frac{1}{M3} \left \begin{array}{cc} 2\zeta\omega + 2\zeta_c\omega_c & 2\zeta\omega\omega_c^2 + 2\zeta_c\omega_c\omega^2 \\ M3 & (1 - g)\omega^2\omega_c^2 \end{array} \right $	0	0
s^0	$M5=(1 - g)\omega^2\omega_c^2$	0	0

According to Routh-Hurwitz Stability Criterion, all the principal minors ($M1$ to $M5$) in Routh-Hurwitz array have to be greater than zero if the system is desired to be stable, which is the sufficient and necessary condition for stability.

For the SISO-PPF controlled system, the principal minors are found to be:

$$M1 = 1$$

$$M2 = 2\zeta\omega + 2\zeta_c\omega_c$$

$$M3 = \frac{(2\zeta\omega+2\zeta_c\omega_c)(\omega^2+\omega_c^2+4\zeta\omega\zeta_c\omega_c)-(2\zeta_c\omega_c\omega^2+2\zeta\omega\omega_c^2)}{2\zeta\omega+2\zeta_c\omega_c}$$

$$M4 = \frac{4\zeta\omega\zeta_c\omega_c[(\omega^2-\omega_c^2)^2+(2\zeta\omega+2\zeta_c\omega_c)(2\zeta\omega\omega_c^2+2\zeta_c\omega_c\omega^2)]+g(2\zeta\omega+2\zeta_c\omega_c)^2\omega^2\omega_c^2}{2\zeta\omega\omega^2+2\zeta_c\omega_c\omega_c^2+4\zeta\omega\zeta_c\omega_c(2\zeta\omega+2\zeta_c\omega_c)}$$

$$M5 = (1 - g)\omega^2\omega_c^2$$

For positive control gain g , $M1$, $M2$, $M3$ and $M4$ are unconditionally greater than zero, $M5$ is greater than zero if $g < 1$.

Therefore, to be a stable PPF controlled system, the control gain must be: $0 < g < 1$.

5.2.2 Multi-Input Multi-Output Case

For multi-input multi-output system, Lyapunov stability theorem was utilized to derive the stability boundary [14] [18].

General system equations for MIMO-PPF controlled system are:

$$\text{Structure: } \ddot{\xi} + D\dot{\xi} + \Omega\xi = a_1 C^T G \eta \quad (5.7)$$

$$\text{Compensator: } \ddot{\eta} + D_c\dot{\eta} + \Omega_c\eta = a_2 \Omega_c C \xi \quad (5.8)$$

where ξ indicate state vector of the physical structure.

Chapter 5: Controller Design

η indicate state vector of the PPF compensator.

G indicate diagonal gain matrix.

C indicate transfer matrix of the structure.

Ω indicate frequency matrix of the structure.

Ω_c indicate frequency matrix of the PPF compensators.

D indicate damping matrix of structure.

D_c indicate damping matrix of PPF compensators.

For the purpose of symmetrize the equations, substitute equation (5.9)

$$\eta = \sqrt{\frac{a_2}{a_1}} G^{-1/2} \Omega_c^{1/2} \psi \quad (5.9)$$

into equation (5.7) and (5.8), and multiply equation (5.8) with $\sqrt{a_1/a_2} \Omega_c^{1T/2} G^{T/2}$, the result is:

$$\ddot{\xi} + D\dot{\xi} + \Omega\xi = \sqrt{a_1 a_2} C^T G^{1/2} \Omega_c^{1/2} \psi \quad (5.10)$$

$$\ddot{\psi} + D_c \dot{\psi} + \Omega_c \psi = \sqrt{a_1 a_2} \Omega_c^{1/2} G^{1/2} C \xi \quad (5.11)$$

Further define

$$E^{1/2} = \sqrt{a_1 a_2} G^{1/2} C \quad (5.12)$$

So that the state space representation of the MIMO system is:

$$\begin{bmatrix} \ddot{\xi} \\ \ddot{\psi} \end{bmatrix} + \begin{bmatrix} D & 0 \\ 0 & D_c \end{bmatrix} \begin{bmatrix} \dot{\xi} \\ \dot{\psi} \end{bmatrix} + \begin{bmatrix} \Omega & -E^{T/2} \Omega_c^{T/2} \\ -\Omega_c^{1/2} E^{1/2} & \Omega_c \end{bmatrix} \begin{bmatrix} \xi \\ \psi \end{bmatrix} = 0 \quad (5.13)$$

Define Lyapunov Function V as:

$$V = \frac{1}{2} [\dot{\xi}^T \quad \dot{\psi}^T] \begin{bmatrix} \dot{\xi} \\ \dot{\psi} \end{bmatrix} + \frac{1}{2} [\xi^T \quad \psi^T] \begin{bmatrix} \Omega & -E^{T/2} \Omega_c^{T/2} \\ -\Omega_c^{1/2} E^{1/2} & \Omega_c \end{bmatrix} \begin{bmatrix} \xi \\ \psi \end{bmatrix} \quad (5.14)$$

Equation (5.14) can be rewrite as:

$$V = \frac{1}{2} [\dot{\xi}^T \dot{\xi} + \dot{\psi}^T \dot{\psi}] + \frac{1}{2} [\xi^T \Omega \xi + \psi^T \Omega_c \psi] - \xi^T E^{T/2} \Omega_c^{T/2} \psi \quad (5.15)$$

It is easy to observe that:

$$V \geq \frac{1}{2} [\dot{\xi}^T \dot{\xi} + \dot{\psi}^T \dot{\psi}] + \frac{1}{2} [\xi^T \Omega \xi + \psi^T \Omega_c \psi] - |\xi^T E^{T/2} \Omega_c^{T/2} \psi| \quad (5.16)$$

Perform Cauchy-Schwartz inequality to the last component:

$$V \geq \frac{1}{2}[\dot{\xi}^T \dot{\xi} + \dot{\psi}^T \dot{\psi}] + \frac{1}{2}[\xi^T \Omega \xi + \psi^T \Omega_c \psi] - \frac{1}{2}\xi^T E^{T/2} E^{1/2} \xi - \frac{1}{2}\psi^T \Omega_c \psi \quad (5.17)$$

Simplify equation (5.17), the result is:

$$V \geq \frac{1}{2}[\dot{\xi}^T \dot{\xi} + \dot{\psi}^T \dot{\psi}] + \frac{1}{2}\xi^T (\Omega - E) \xi \quad (5.18)$$

From equation (5.18), it can be seen that if $\Omega - E > 0$, then $V > 0$ for all non-regular $\xi, \psi, \dot{\xi}, \dot{\psi}$.

Differentiating equation (5.14) with respect to t, the result is:

$$\dot{V} = [\dot{\xi}^T \quad \dot{\psi}^T] \begin{bmatrix} \ddot{\xi} \\ \ddot{\psi} \end{bmatrix} + [\xi^T \quad \psi^T] \begin{bmatrix} \Omega & -E^{T/2} \Omega_c^{T/2} \\ -\Omega_c^{1/2} E^{1/2} & \Omega_c \end{bmatrix} \begin{bmatrix} \dot{\xi} \\ \dot{\psi} \end{bmatrix} \quad (5.19)$$

Substituting equation (5.13),

$$\dot{V} = -\dot{\xi}^T D \dot{\xi} - \dot{\psi}^T D_c \dot{\psi} \leq 0 \quad (5.20)$$

According to the Second Lyapunov Theorem, the MIMO PPF control system is Lyapunov Asymptotically Stable if and only if [26] [27]:

$$\Omega - E = \Omega - a_1 a_2 C^T G C > 0 \quad (5.21)$$

Therefore, the stable condition for the MIMO-PPF controlled system is: $\Omega - a_1 a_2 C^T G C > 0$.

Above stability boundaries were followed in the next controller design stage in order to achieve a stable system.

5.3 PPF Controller Parameters Selection

To perform PPF control, each parameter (frequency, damping ratio and control gain) of the PPF controller need to be designed properly for the best control performance purpose.

5.3.1 Frequency Selection

To illustrate PPF controller's frequency selection clearly, assume a single degree of freedom vibration in the form of:

$$\xi(t) = a * e^{j\omega t} \quad (5.22)$$

The output of compensator will be:

$$\eta(t) = b * e^{j(\omega t - \phi)} \quad (5.23)$$

Phase angle of equation (5.23) is:

$$\phi = \tan^{-1} \left[\frac{2\zeta_c(\omega/\omega_c)}{1-(\omega^2/\omega_c^2)} \right] \quad (5.24)$$

When natural frequency of the structure much lower than frequency of the compensator, the phase angle shown in equation (5.24) approaches 0, substitute equation (5.23) with $\phi = 0$ into equation (5.1), the result is:

$$\ddot{\xi} + 2\zeta\omega\dot{\xi} + (\omega^2 - gb\omega^2)\xi = 0 \quad (5.25)$$

From equation (5.25), it can be observed that in this case, the PPF compensator reduced the stiffness term of the structure, which is called active flexibility [19].

When the structure and PPF compensator have the same frequency, the phase angle shown in equation (5.24) approaches $\pi/2$, substitute equation (5.23) with $\phi = \pi/2$ into equation (5.1), the result is:

$$\ddot{\xi} + (2\zeta\omega + gb\omega)\dot{\xi} + \omega^2\xi = 0 \quad (5.26)$$

From equation (5.26), it can be observed that in this case, the PPF compensator increased the damping ratio term of the structure, which is called active damping [19].

When natural frequency of the structure much higher than frequency of the compensator, the phase angle shown in equation (5.24) approaches π , substitute equation (5.23) with $\phi = \pi$ into equation (5.1), the result is:

$$\ddot{\xi} + 2\zeta\omega\dot{\xi} + (\omega^2 + gb\omega^2)\xi = 0 \quad (5.27)$$

From equation (5.27), it can be observed that in this case, the PPF compensator increased the stiffness term of the structure, which is called active stiffness [19].

According to above analysis, since the essence of the PPF controller is to add extra damping to the structure, the frequency of the compensator should be set equal to the natural frequency of the structure.

In practice, multi-mode control need multiple PPF controllers with frequency of each PPF controller equal to corresponding natural frequency of the structure.

5.3.2 Damping and Control Gain Selection

In terms of damping ratio and control gain of the PPF compensator, H_∞ optimal technique was applied. H_∞ method has been widely used in control problems to improve performance of the controller or stability of the closed-loop system [16].

Basic principle of H_∞ method is to minimize the effect of disturbance acting on the system output. Block diagram of the standard H_∞ control problem is shown in Figure 5.2 [20].

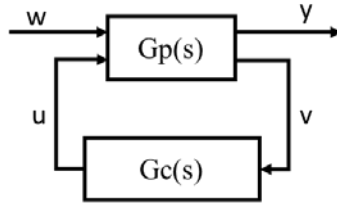


Figure 5.2 Configuration of standard H_∞ method

It can be seen that the system has two inputs and two outputs, where, w is the disturbance input, y is system output, u is the manipulated variable and v is the measured variable. Variable v is used in controller to compute the manipulated variable u .

Above diagram can be rewritten as:

$$\begin{bmatrix} y \\ v \end{bmatrix} = G_p(s) \begin{bmatrix} w \\ u \end{bmatrix} = \begin{bmatrix} G_{p_{11}}(s) & G_{p_{12}}(s) \\ G_{p_{21}}(s) & G_{p_{22}}(s) \end{bmatrix} \begin{bmatrix} w \\ u \end{bmatrix} \quad (5.28)$$

$$u = G_c(s) * v \quad (5.29)$$

From equation (5.28) and (5.29), the dependency of output y on disturbance input w can be written as:

$$y = F_l(G_p(s), G_c(s)) * w \quad (5.30)$$

where

$$F_l(G_p(s), G_c(s)) = G_{p_{11}}(s) + G_{p_{12}}(s) * G_c(s) [I(s) - G_{p_{22}}(s) G_c(s)]^{-1} G_{p_{21}}(s) \quad (5.31)$$

It can be observed that the aim of H_∞ control design is to find the controller $G_c(s)$ so that $F_l(G_p(s), G_c(s))$ can be minimized according to H_∞ norm. The H_∞ norm of $F_l(G_p(s), G_c(s))$ is defined as:

$$\|F_l(G_p(s), G_c(s))\|_\infty = \sup_w \bar{\sigma} [F_l(G_p(s), G_c(s))(j\omega)] \quad (5.32)$$

where $\bar{\sigma}$ is the maximum singular value of $F_l(G_p(s), G_c(s))(j\omega)$.

In this project, with the purpose of optimize the controller, i.e. find the minimum value of H_∞ norm, generic algorithm (GA) in MATLAB optimization toolbox was utilized.

Based on above analysis, in the following sections, PPF controllers used for SISO system and MIMO system are designed and applied to corresponding mathematical model respectively to control the first three modes of vibration.

5.4 SISO-PPF Controller Design and Validation

In this section, SISO-PPF controllers were designed based on the parameters selection method described in section 5.3, these PPF controllers aimed to minimize the effect of disturbance to system output. Effects of corresponding controller were analyzed and validated based on the below configuration.

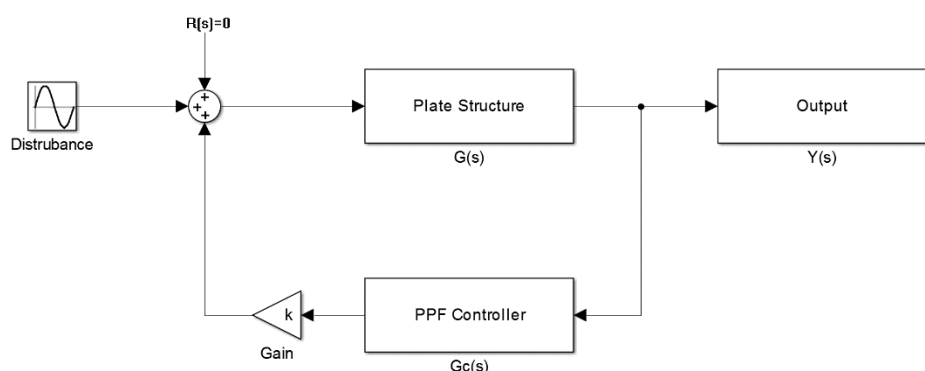


Figure 5.3 Block diagram for PPF controller evaluation

5.4.1 First Mode Control

Three PPF controllers were designed to control the first mode of transducer 1, 2 and 3 respectively. The frequencies of these controllers are equal to the frequencies of the first mode of each transducer, H_∞ optimized values of damping ratio and control gain are listed in Table 5.2.

Table 5.2 Parameters for SISO-PPF controller-Mode 1

	Frequency(Hz)	Control Gain g	Damping Ratio
PPF for G11	22.26	0.2432	0.5577
PPF for G22	22.36	0.3382	0.4500
PPF for G33	22.68	0.4366	0.5500

Bode plot of above SISO-PPF controllers are shown in Figure 5.4.

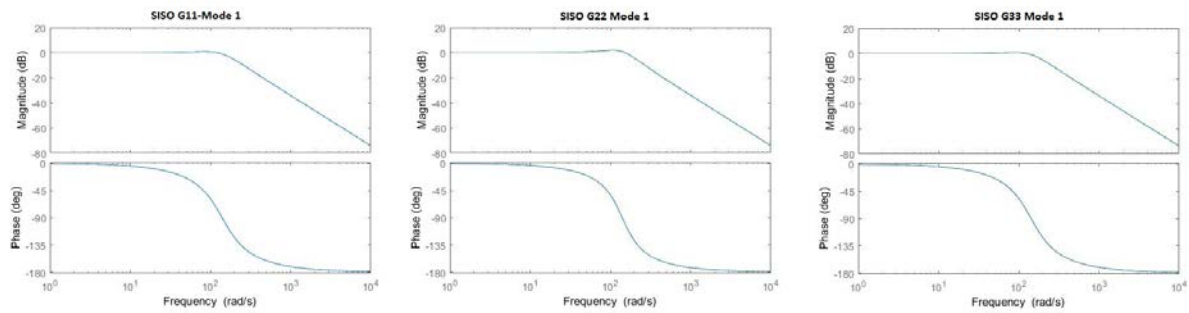


Figure 5.4 H_∞ optimized SISO-PPF controller for mode 1

Substitute each PPF controller into first mode of the simulated SISO model, the control effects on each transducer is shown in Figure 5.5.

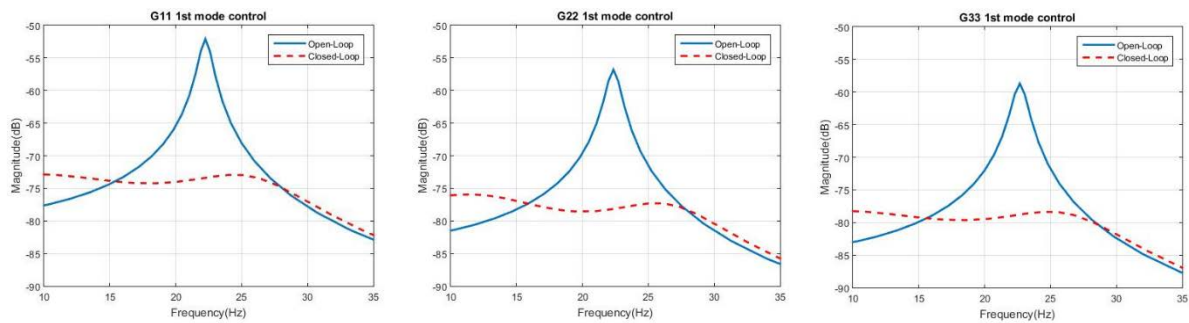


Figure 5.5 Control effects of SISO-PPF Mode 1

Corresponding dB drop values can be obtained from Figure 5.5, as shown in Table 5.3.

Table 5.3 Vibration control result for SISO-PPF mode 1

	G11(Transducer 1)	G22(Transducer 2)	G33(Transducer 3)
Open-loop (dB)	-52.08	-56.79	-58.69
Closed-loop (dB)	-73.21	-78.16	-79.06
dB drop (dB)	21.13	21.37	20.37

From Table 5.3, it can be seen that each PPF controller achieved about 21 dB vibration suppression at the first mode of the simulated SISO model.

5.4.2 Second Mode Control

Three PPF controllers were designed to control the second mode of transducer 1, 2 and 3 respectively. The frequencies of these controllers are equal to the frequencies of the second

Chapter 5: Controller Design

mode of each transducer, H_∞ optimized values of damping ratio and control gain are listed in Table 5.4.

Table 5.4 Parameters for SISO-PPF controller-Mode 2

	Frequency(Hz)	Control Gain g	Damping Ratio
PPF for G11	27.84	0.0354	0.5591
PPF for G22	29.01	0.0611	0.5682
PPF for G33	29.04	0.0668	0.5599

Bode plot of above SISO-PPF controllers are shown in Figure 5.6.

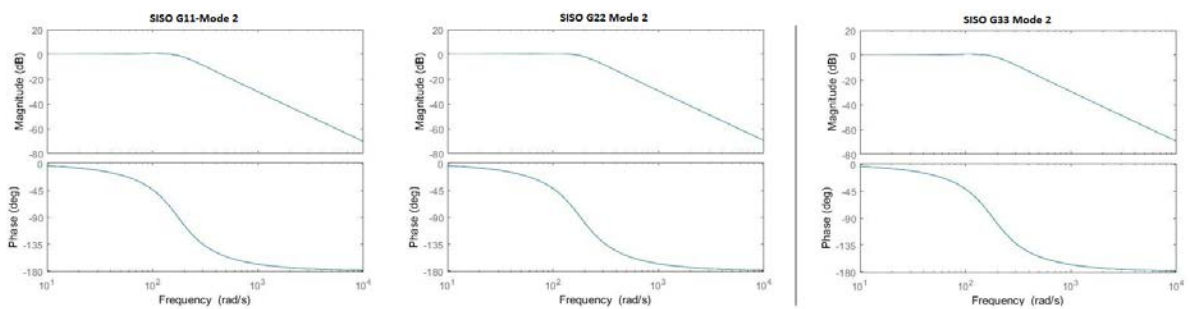


Figure 5.6 H_∞ optimized SISO-PPF controller for mode 2

Substitute each PPF controller into second mode of the simulated SISO model, the control effects on each transducer is shown in Figure 5.7.

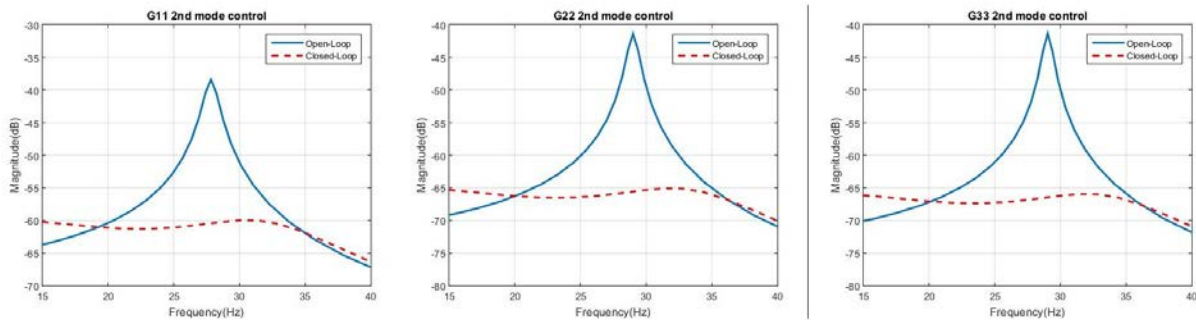


Figure 5.7 Control effects of SISO-PPF Mode 2

Corresponding dB drop values can be obtained from Figure 5.7, as shown in Table 5.5.

Table 5.5 Vibration control result for SISO-PPF mode 2

	G11(Transducer 1)	G22(Transducer 2)	G33(Transducer 3)
Open-loop (dB)	-38.4	-41.37	-41.34
Closed-loop (dB)	-60.27	-65.87	-66.26
dB drop (dB)	21.87	24.5	24.92

From Table 5.5, it can be seen that each PPF controller achieved about 23 dB vibration suppression at the second mode of the simulated SISO model.

5.4.3 Third Mode Control

Three PPF controllers were designed to control the third mode of transducer 1, 2 and 3 respectively. The frequencies of these controllers are equal to the frequencies of the third mode of each transducer, H_∞ optimized values of damping ratio and control gain are listed in Table 5.6.

Table 5.6 Parameters for SISO PPF-controller Mode 3

	Frequency(Hz)	Control Gain g	Damping Ratio
PPF for G11	34.79	0.0519	0.5779
PPF for G22	34.72	0.0154	0.5691
PPF for G33	34.74	0.0191	0.5698

Bode plot of above SISO-PPF controllers are shown in Figure 5.8.

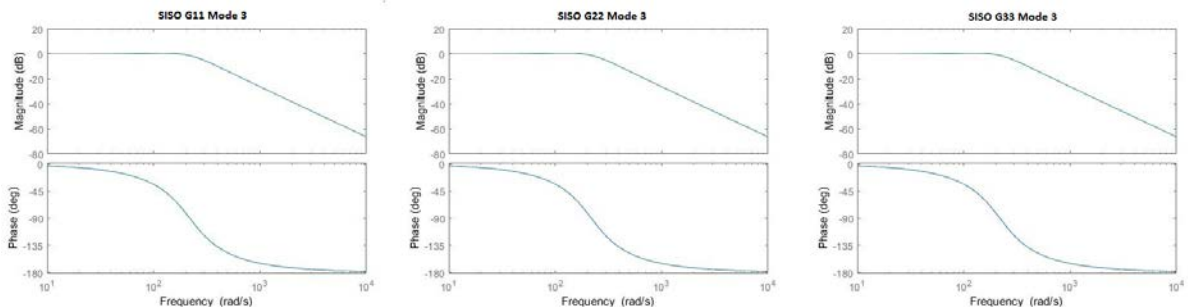


Figure 5.8 H_∞ optimized SISO-PPF controller for mode 3

Substitute each PPF controller into third mode of the simulated SISO model, the control effects on each transducer is shown in Figure 5.9.

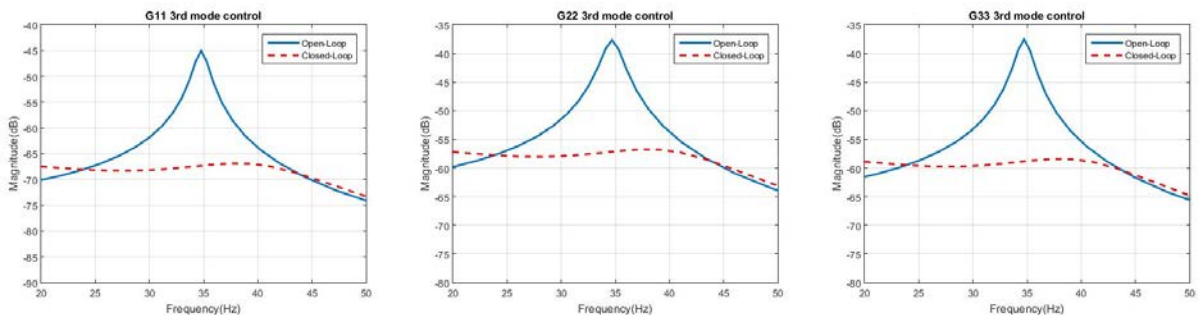


Figure 5.9 Control effects of SISO-PPF Mode 3

Corresponding dB drop values can be obtained from Figure 5.9, as shown in Table 5.7.

Table 5.7 Vibration control result for SISO-PPF mode 3

	G11(Transducer 1)	G22(Transducer 2)	G33(Transducer 3)
Open-loop (dB)	-45.03	-37.65	-37.52
Closed-loop (dB)	-67.18	-57.01	-58.68
dB drop (dB)	22.15	19.36	21.16

From Table 5.7, it can be seen that each PPF controller achieved about 20 dB vibration suppression at the third mode of the simulated SISO model.

5.4.4 Three Modes Control

After each individual mode achieved desired vibration depression, all above PPF controllers were utilized to control the first three modes simultaneously.

Firstly, PPF controller were implemented on the corrected model, corresponding vibration control effect can be found in Figure 5.10.

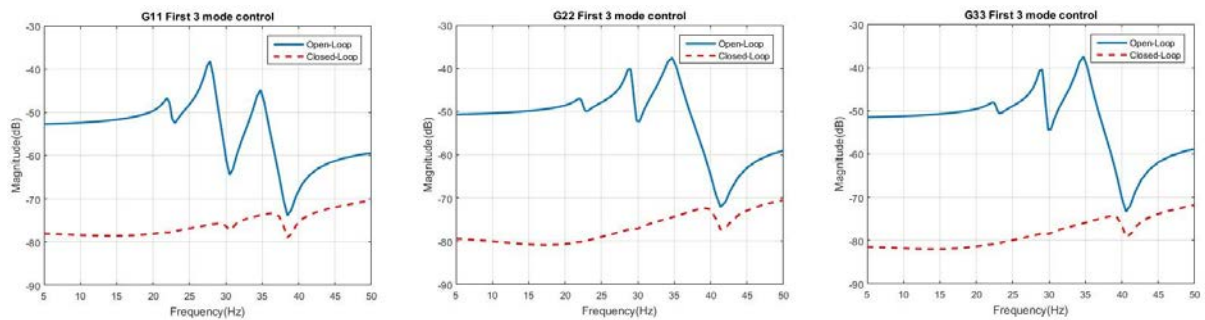


Figure 5.10 Control effects of SISO-PPF three modes control on corrected model

Corresponding dB drop values can be obtained from Figure 5.10, as shown in Table 5.8.

Table 5.8 Vibration control result for SISO-PPF first three modes control

G11	Mode 1	Mode 2	Mode3
Open-loop (dB)	-46.75	-38.23	-44.85
Closed-loop (dB)	-77.78	-76.14	-73.81
dB drop (dB)	31.03	37.91	28.96
G22	Mode 1	Mode 2	Mode3
Open-loop (dB)	-47.01	-40.18	-37.55
Closed-loop (dB)	-80.03	-77.43	-74.68
dB drop (dB)	33.02	37.25	37.13

G33	Mode 1	Mode 2	Mode3
Open-loop (dB)	-48.05	-40.42	-37.44
Closed-loop (dB)	-80.89	-78.58	-75.82
dB drop (dB)	32.84	38.16	38.38

From Table 5.8, it can be seen that PPF controlled SISO system achieved more than 30 dB vibration suppression at each mode of the simulated SISO model.

Then, three modes PPF controller were implemented on the true model that constructed in MATLAB. Control effects are illustrated in Figure 5.11.

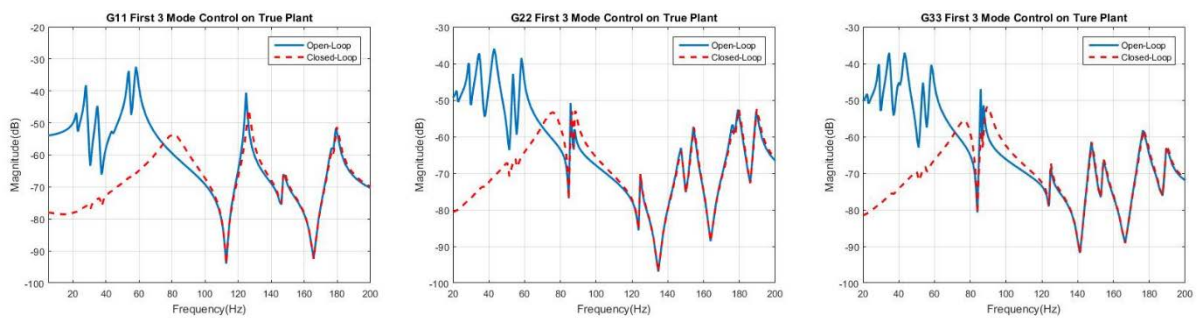


Figure 5.11 Control effects of SISO-PPF three modes control on true model

From comparison between Figure 5.11 and Figure 5.10, it can be concluded that SISO-PPF control on the true plant can also achieve about 30 dB vibration suppression at the first three modes, and there is also some effect on the fourth and fifth modes, whereas no effect on the further higher frequency mode. Theoretically, three modes PPF controller can only cancel out three modes of vibration. In this project, because modes are not well separated from each other, i.e. the natural frequency of each mode are not far away enough from the other modes, that is why the fourth and fifth modes affected by PPF controller but higher frequency modes do not.

5.5 MIMO-PPF Controller Design and Validation

In this section, three sets of PPF controllers were designed for mode one, two, three of MIMO system respectively based on the parameters selection method described in section 5.3, these PPF controllers aimed to minimize the effect of disturbance to system output. Effects of corresponding controller were analyzed and evaluated based on the configuration of Figure 5.3.

5.5.1 First Mode Control

Since this is a 3-input 3-output system, corresponding PPF controller is a 3x3 matrix. Therefore, nine PPF controllers were designed to control the first mode of the MIMO system. As analyzed before, the frequencies of these controllers are equal to the frequencies of the first mode of each transducer, H_∞ optimized values of damping ratio and control gain are listed in Table 5.9.

Table 5.9 Parameters for MIMO-PPF Controller-Mode 1

	G11	G12	G13
Control gain g	0.4652	0.4675	0.6639
Damping	0.9212	0.9884	0.7043
	G21	G22	G23
Control gain g	0.5487	0.7466	0.9085
Damping	0.9542	0.6228	0.9548
	G31	G32	G33
Control gain g	0.4432	0.7183	0.2304
Damping	0.5977	0.9855	0.9548

Bode plot of above PPF controller is shown in Figure 5.12.

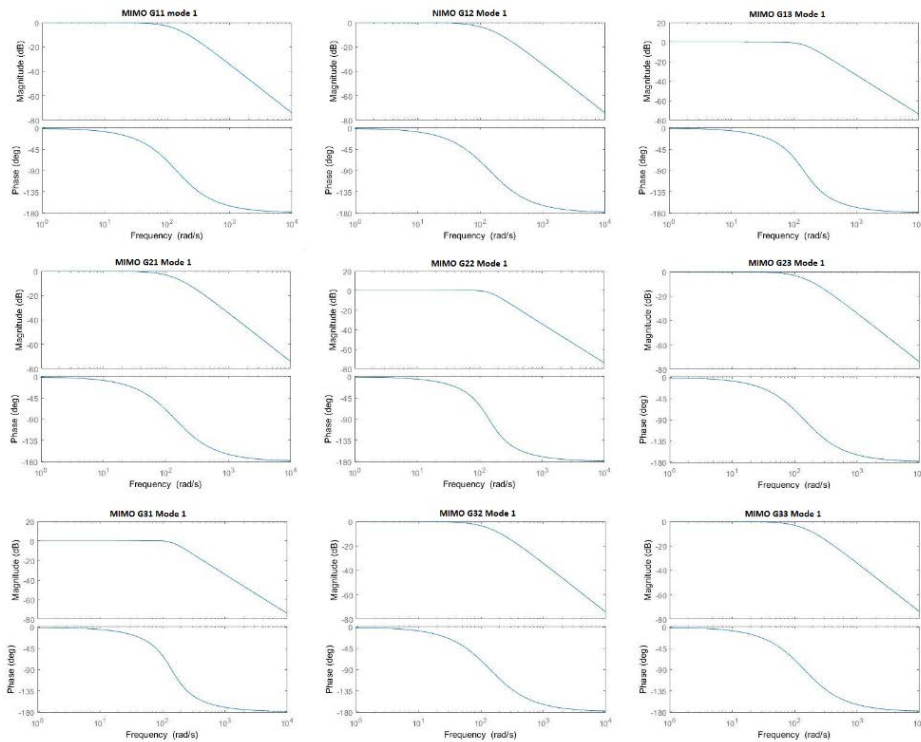


Figure 5.12 H_∞ optimized MIMO-PPF controller for mode 1

Chapter 5: Controller Design

Substitute above PPF controller into first mode of the simulated MIMO model, the simulated control effects on each transfer function is shown in Figure 5.13.

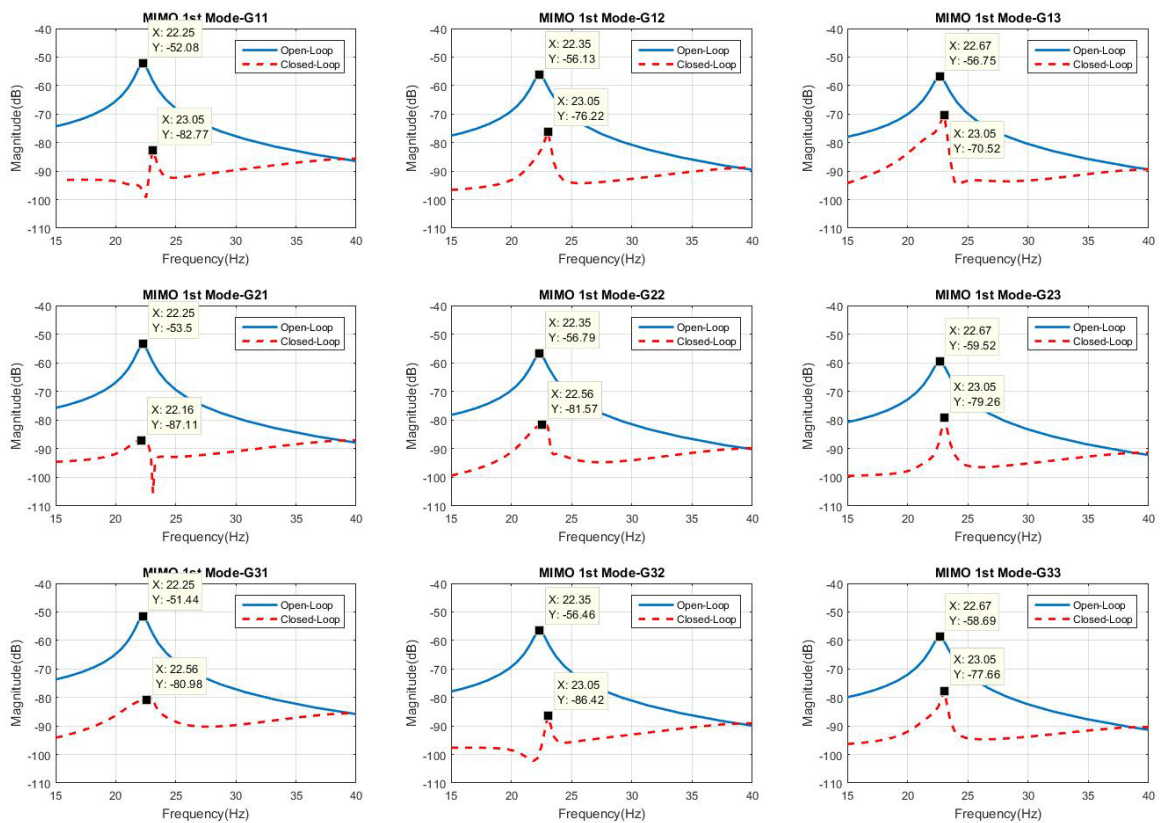


Figure 5.13 Control effects of MIMO-PPF mode 1

Corresponding dB drop values are listed in Table 5.10.

Table 5.10 Vibration control result for MIMO PPF mode 1

	G11	G12	G13
Open-loop (dB)	-52.08	-56.13	-56.75
Closed-loop (dB)	-82.77	-76.22	-70.52
dB drop (dB)	30.69	20.09	13.77
	G21	G22	G23
Open-loop (dB)	-53.5	-56.79	-59.52
Closed-loop (dB)	-87.11	-81.57	-79.26
dB drop (dB)	33.61	24.78	19.74
	G31	G32	G33
Open-loop (dB)	-51.44	-56.46	-58.69
Closed-loop (dB)	-80.98	-86.42	-77.66
dB drop (dB)	29.54	29.96	18.97

From table 5.10, it can be observed that MIMO-PPF controller for mode 1 achieved 13dB to 33dB vibration suppression on each simulated transfer function in MATLAB simulation. To achieve the minimum energy cost (H_∞ value), vibration suppression levels are not as balance as in the SISO control system.

5.5.2 Second Mode Control

For second mode vibration control of the MIMO system, also a 3 by 3 PPF matrix were designed, and as analyzed before, the frequencies of these controllers are equal to the frequencies of the second mode of each transducer, H_∞ optimized values of damping ratio and control gain are listed in Table 5.11.

Table 5.11 Parameters for MIMO-PPF controller-Mode 2

	G11	G12	G13
Control gain g	0.0561	0.1543	0.1244
Damping	0.5912	0.2337	0.5519
	G21	G22	G23
Control gain g	0.2168	0.0120	0.0510
Damping	0.3372	0.5296	0.7413
	G31	G32	G33
Control gain g	0.1988	0.0920	0.1087
Damping	0.2193	0.5798	0.8097

Bode plot of above PPF controllers are illustrated in Figure 5.14.

Substitute above PPF controller into the second mode of the simulated MIMO model, the simulated control effects on each transducer is shown in Figure 5.15.

Chapter 5: Controller Design

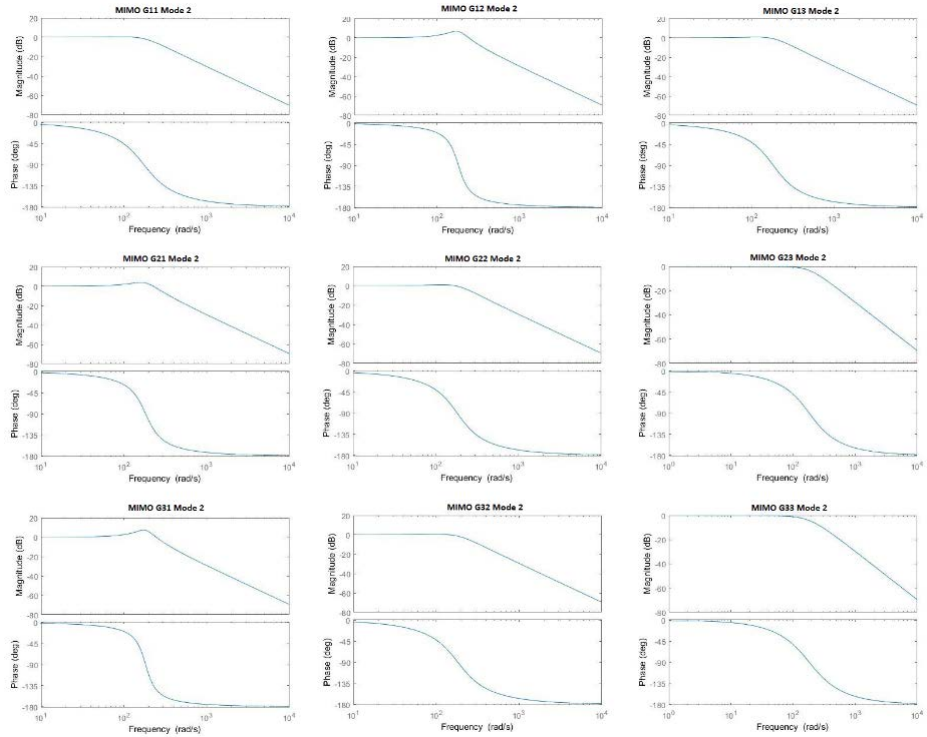


Figure 5.14 H_∞ optimized MIMO PPF controller for mode 2

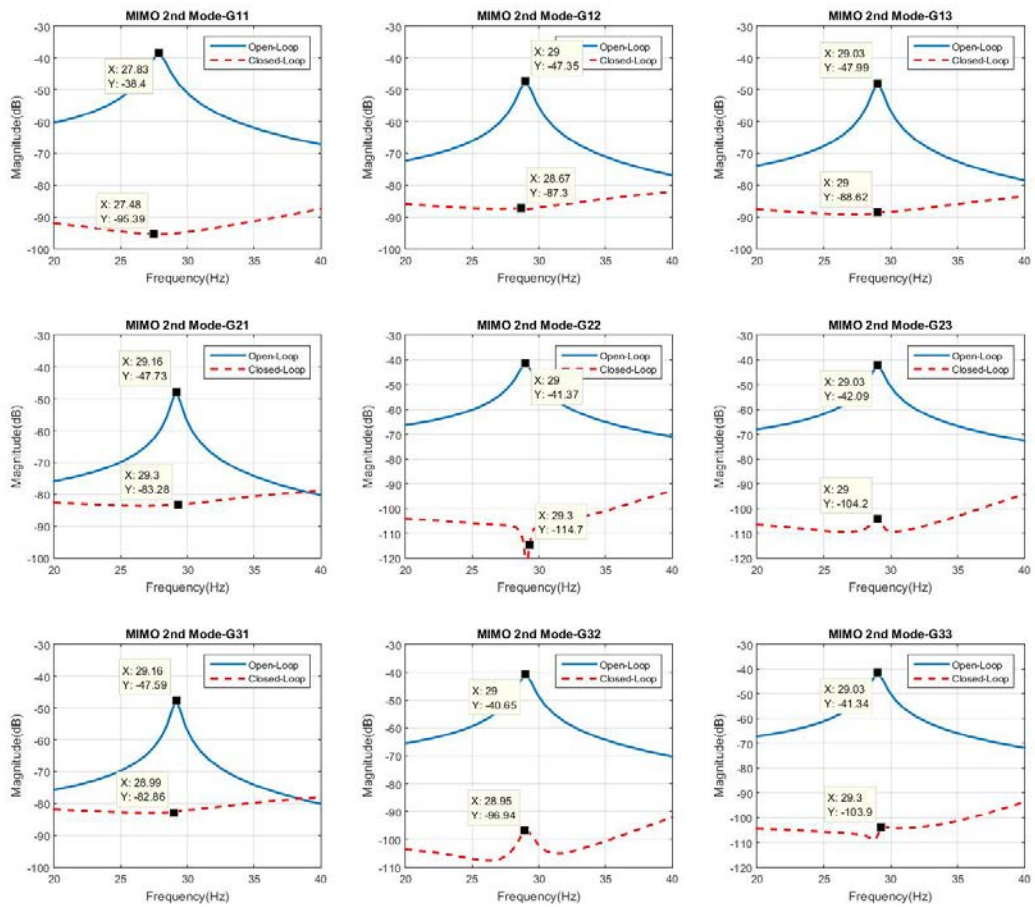


Figure 5.15 Control effects of MIMO PPF-Mode 2

Corresponding dB drop values are listed in Table 5.12.

Table 5.12 Vibration control result for MIMO-PPF mode 2

	G11	G12	G13
Open-loop (dB)	-38.4	-47.35	-47.99
Closed-loop (dB)	-95.39	-87.3	-88.62
dB drop (dB)	56.99	39.95	40.63
	G21	G22	G23
Open-loop (dB)	-47.73	-41.37	-42.09
Closed-loop (dB)	-83.28	-114.7	-104.2
dB drop (dB)	35.55	73.33	62.11
	G31	G32	G33
Open-loop (dB)	-47.59	-40.65	-41.34
Closed-loop (dB)	-82.86	-96.94	-103.9
dB drop (dB)	35.27	56.29	62.56

From table 5.12, it can be observed that MIMO-PPF controller for mode 2 achieved 35dB to 73dB vibration suppression on each simulated transfer function in MATLAB simulation. Also for the purpose of achieve the minimum energy cost (H_∞ value), vibration suppression levels are not as balance as in the SISO control system.

5.5.3 Third Mode Control

For third mode vibration control of the simulated MIMO system, also a 3 by 3 PPF matrix were designed, and as analyzed before, the frequencies of these controllers are equal to the frequencies of the third mode of each transducer, H_∞ optimized values of damping ratio and control gain are listed in Table 5.13.

Table 5.13 Parameters for MIMO-PPF controller mode 3

	G11	G12	G13
Control gain g	0.0887	0.0115	0.0221
Damping	0.4208	0.3757	0.6453
	G21	G22	G23
Control gain g	0.0067	0.0302	0.0408
Damping	0.3734	0.2476	0.5422

	G31	G32	G33
Control gain g	0.0149	0.0174	0.0355
Damping	0.6184	0.6246	0.8067

Bode plots of above PPF controllers are shown in Figure 5.16.

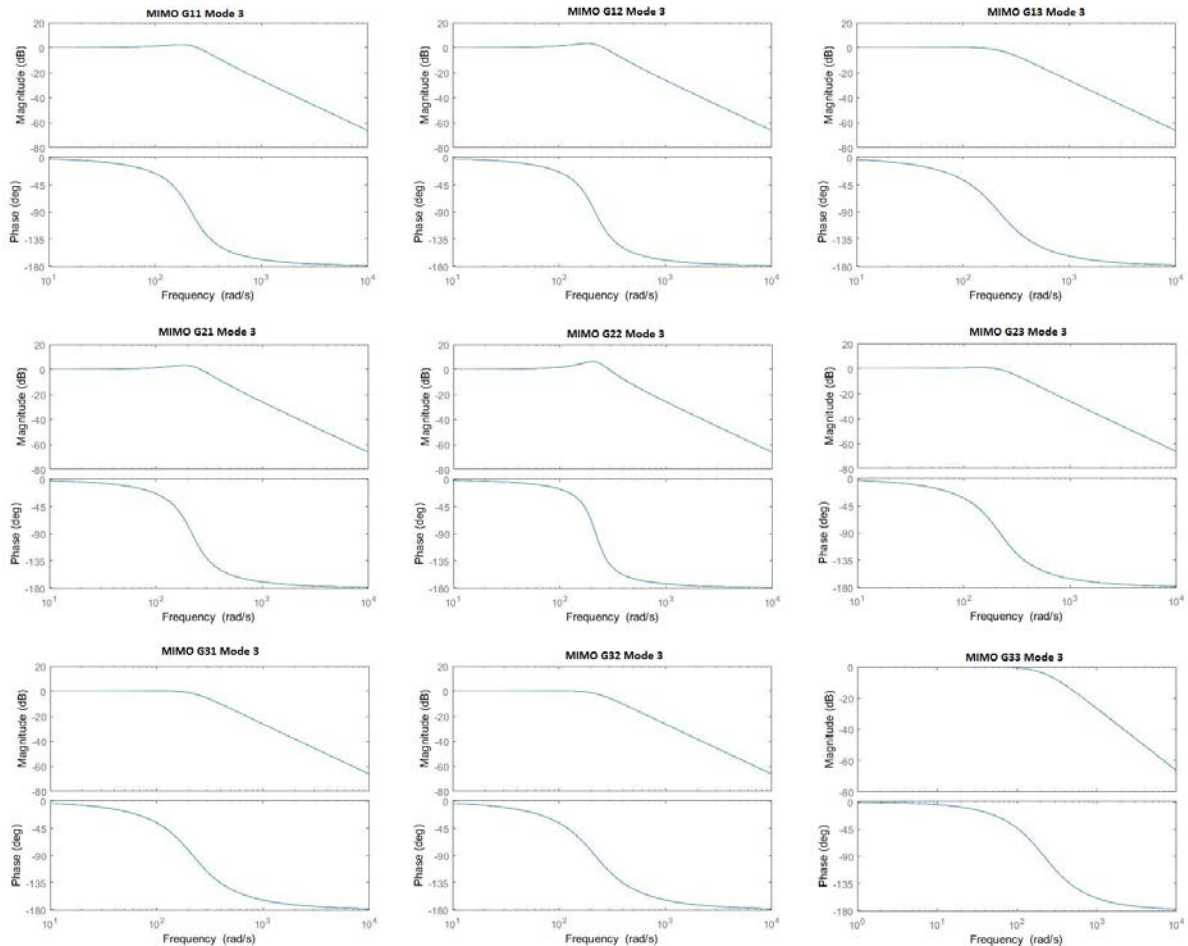


Figure 5.16 H_∞ optimized MIMO-PPF controller for mode 3

Substitute above PPF controller into the third mode of the simulated MIMO model, the simulated control effects on each transducer is shown in Figure 5.17.

Corresponding dB drop values are listed in Table 5.14.

From table 5.14, it can be seen that PPF controller achieved 21dB to 38 dB vibration suppression on each simulated transfer function in MATLAB simulation. Also for the purpose of achieve the minimum energy cost (H_∞ value), vibration suppression levels are not as balance as in the SISO control system.

Chapter 5: Controller Design

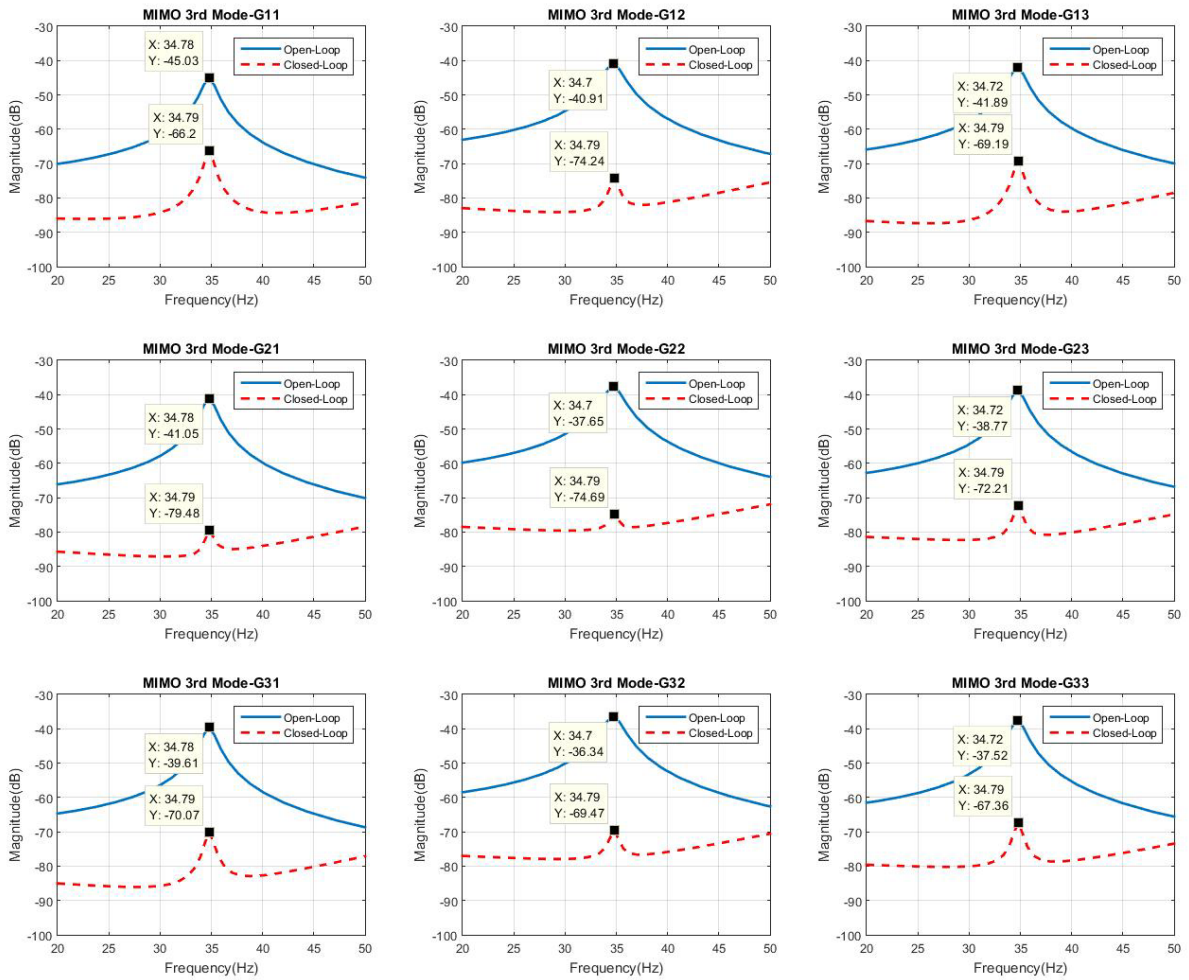


Figure 5.17 Control effects of MIMO-PPF mode 3

Table 5.14 Vibration control result for MIMO-PPF mode 3

	G11	G12	G13
Open-loop (dB)	-45.03	-40.19	-41.89
Closed-loop (dB)	-66.2	-74.24	-69.19
dB drop (dB)	21.17	34.05	27.3
	G21	G22	G23
Open-loop (dB)	-41.05	-37.65	-38.77
Closed-loop (dB)	-79.48	-74.69	-72.21
dB drop (dB)	38.43	37.04	33.44
	G31	G32	G33
Open-loop (dB)	-39.61	-36.34	-37.52
Closed-loop (dB)	-70.07	-69.47	-67.36
dB drop (dB)	30.46	33.13	29.84

5.5.4 Three Modes Control

Similar procedure as the SISO system control, after each individual mode achieved desired vibration depression, all above MIMO-PPF controllers were utilized to control the first three modes of vibration of the MIMO system simultaneously.

Firstly, three modes of MIMO-PPF controllers were implemented on the corrected model in MATLAB.

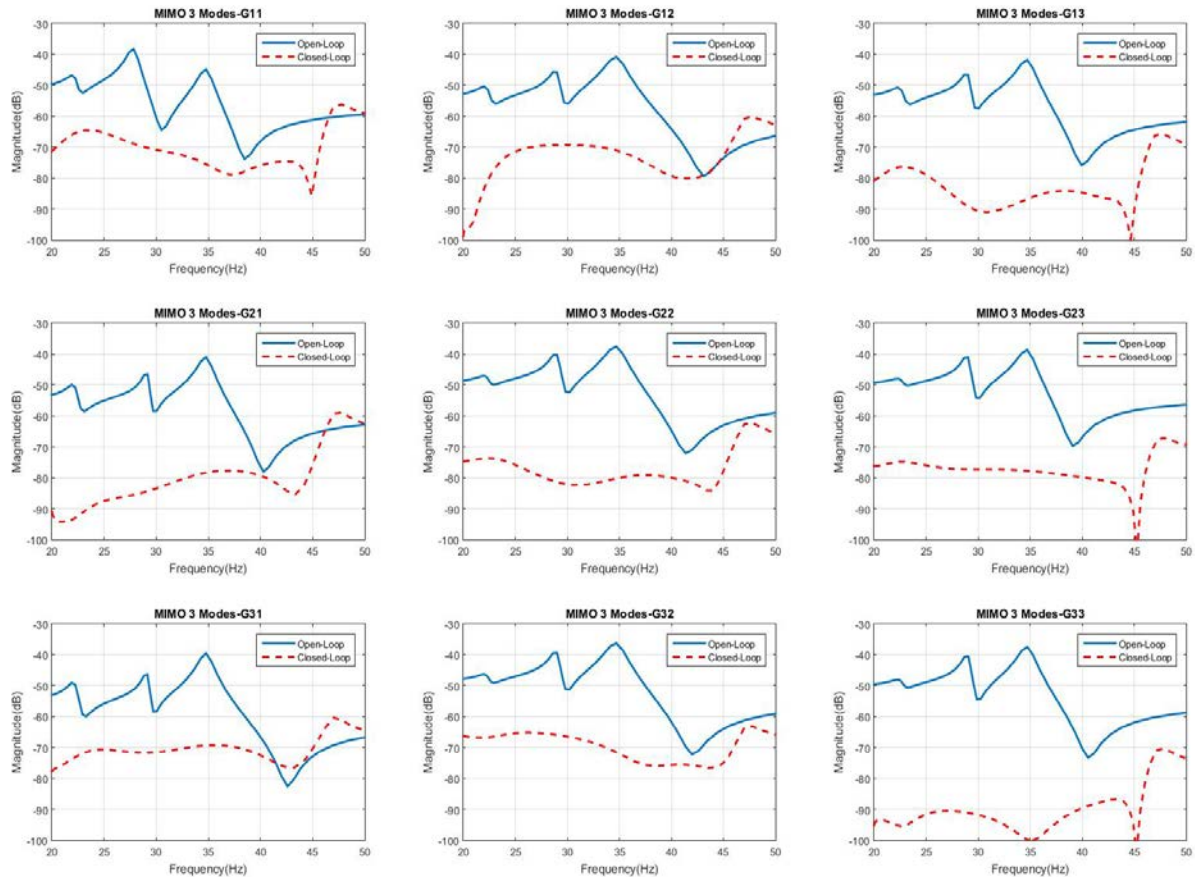


Figure 5.18 Control effects of MIMO-PPF three modes control on corrected model

Corresponding dB values of open-loop and closed-loop system and dB drop values are listed in table 5.15.

Table 5.15 Vibration control result for MIMO PPF first three modes

	G11			G12			G13		
	Mode 1	Mode 2	Mode 3	Mode 1	Mode 2	Mode 3	Mode 1	Mode 2	Mode 3
Open-loop	-46.75	-38.23	-44.85	-50.34	-45.75	-40.84	-50.74	-46.51	-41.8
Closed-loop	-65.03	-68.7	-74.14	-82.69	-69.32	-70.93	-76.61	-88.86	-86.16
dB drop	18.28	30.47	29.29	32.25	23.57	30.09	25.87	42.35	44.36

	G21			G22			G23		
	Mode 1	Mode 2	Mode 3	Mode 1	Mode 2	Mode 3	Mode 1	Mode 2	Mode 3
Open-loop	-49.91	-46.5	-40.98	-47.01	-40.18	-37.55	-47.92	-41.04	-38.64
Closed-loop	-93.87	-84.25	-78.51	-73.76	-81.35	-80.02	-74.89	-77.3	-77.72
dB drop	43.96	37.75	37.53	26.75	41.17	42.47	26.97	36.26	39.08
	G31			G32			G33		
	Mode 1	Mode 2	Mode 3	Mode 1	Mode 2	Mode 3	Mode 1	Mode 2	Mode 3
Open-loop	-49.06	-46.38	-39.58	-46.33	-39.4	-36.26	-48.62	-40.42	-37.44
Closed-loop	-73.81	-71.75	-69.54	-66.84	-65.69	-69.99	-95.06	-90.81	-99.34
dB drop	24.75	25.37	29.96	20.51	26.29	33.73	46.44	50.39	61.9

From Table 5.15, it can be concluded that three modes control on the simulated MIMO system achieved at least 20dB vibration suppression on each corrected transfer function. And from comparison of Table 5.8 (SISO PPF control result) and table 5.15 (MIMO PPF control result), it can be seen that MIMO PPF control achieved better vibration control performance on transducer 2 and transducer 3.

Then, three modes MIMO PPF controller were implemented on the true model that constructed in MATLAB. Control effects are illustrated in Figure 5.19.

From Figure 5.19, it can be concluded that MIMO-PPF controller implemented on true model also achieved similar control effect compared with effects that implemented on the corrected model. And similar to SISO system control, three modes PPF controllers also affect mode four and mode five but very little effect on the higher order modes, which is due to the reason that modes in this project are not well separated from each other.

From simulation results of SISO-PPF and MIMO-PPF controller, it can be concluded that the designed PPF controller achieved the desired value of vibration suppression. Next step is to implement these controllers on the physical plate structure to further evaluate control performance, which will be described in the next chapter.

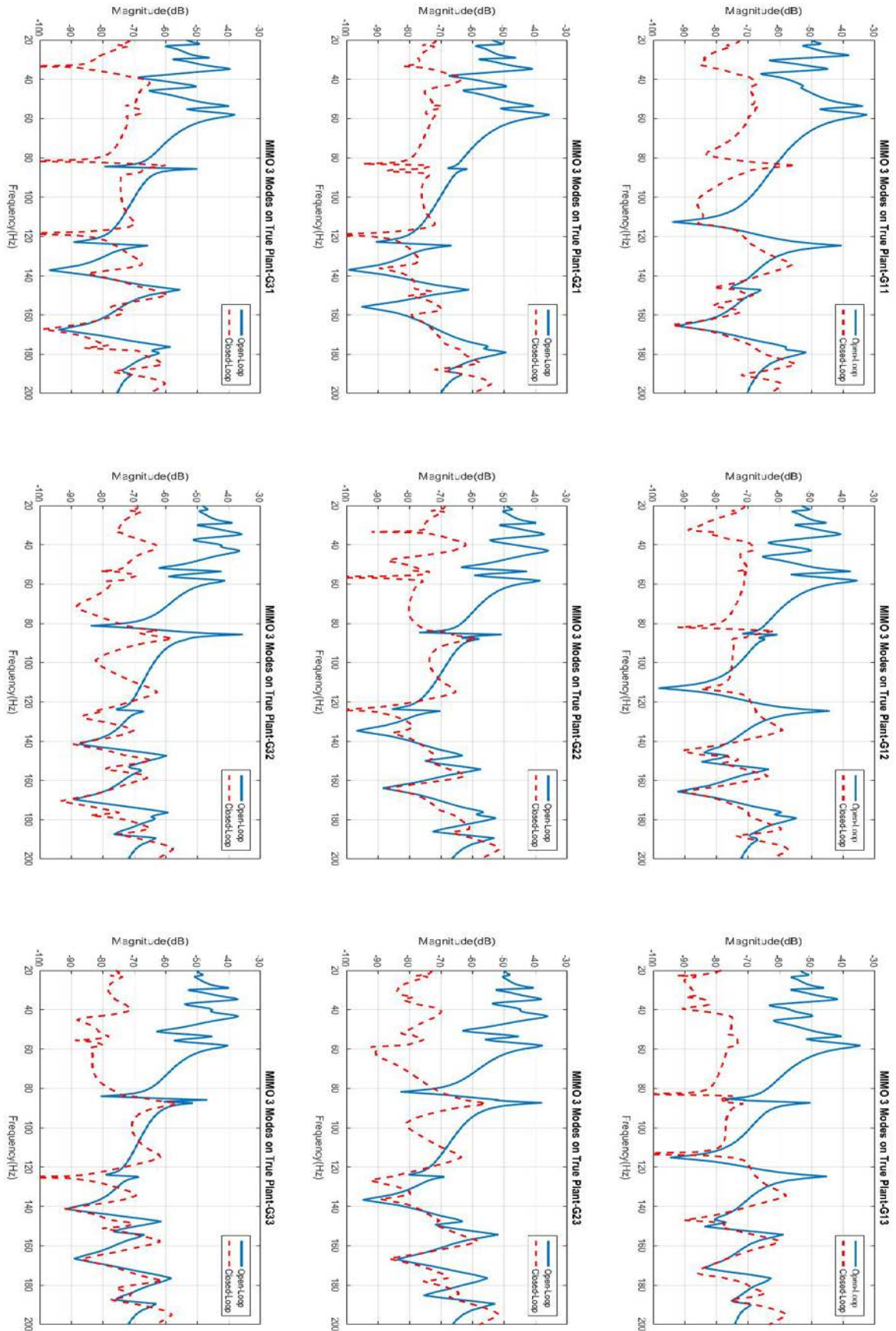


Figure 5.19 Control effects of MIMO-PPF First three modes on true model

Chapter 6 : PPF Control Experiment

After finalizing all optimal parameters of PPF controllers in Chapter 5, an experimental implementation of Multivariable SISO and MIMO PPF controller on the plate structure is presented in this Chapter. dSPACE module was utilized to run the controller. Firstly, the physical setup of the experiment is described, and then SISO PPF controllers MIMO PPF controllers are tested and analyzed respectively.

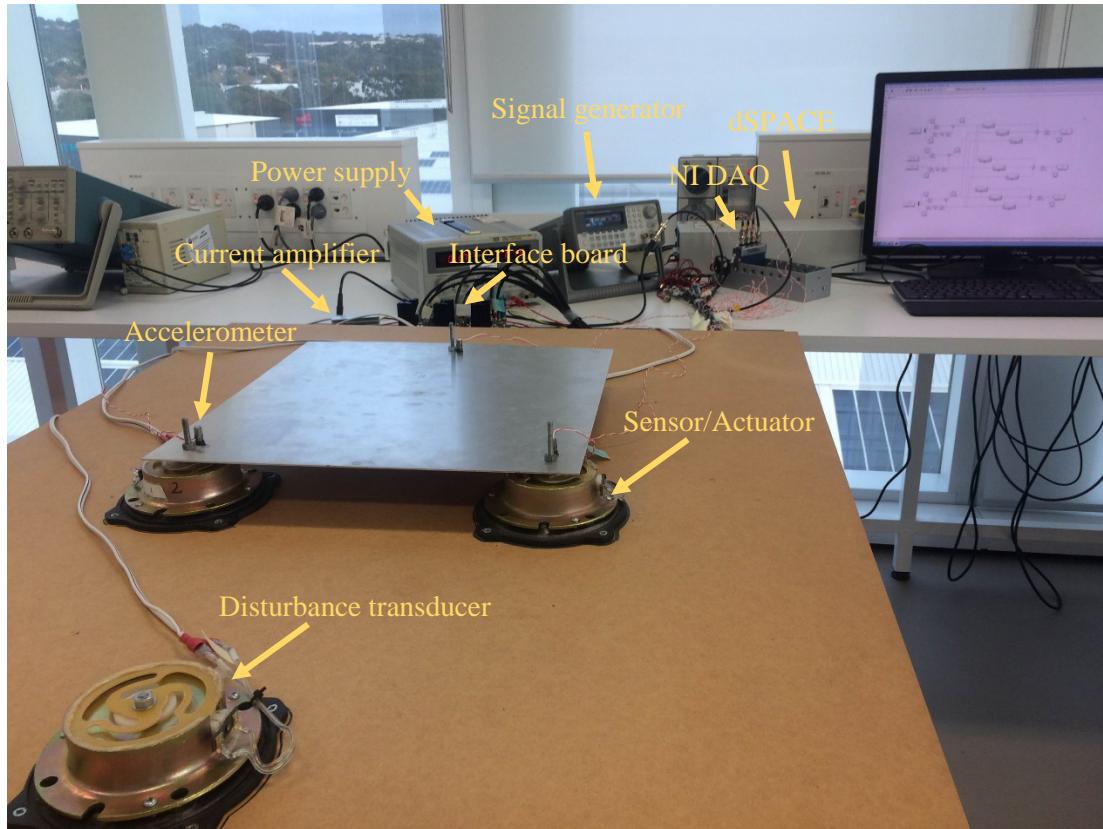
6.1 Experiment Setup

In this physical experiment, the plate structure, disturbance transducer as well as signal generator, accelerometers, interface circuitry board, dSPACE 1103 module and NI DAQ module were utilized to conduct the vibration control process, physical setup and block diagram of the hardware connection is shown in Figure 6.1.

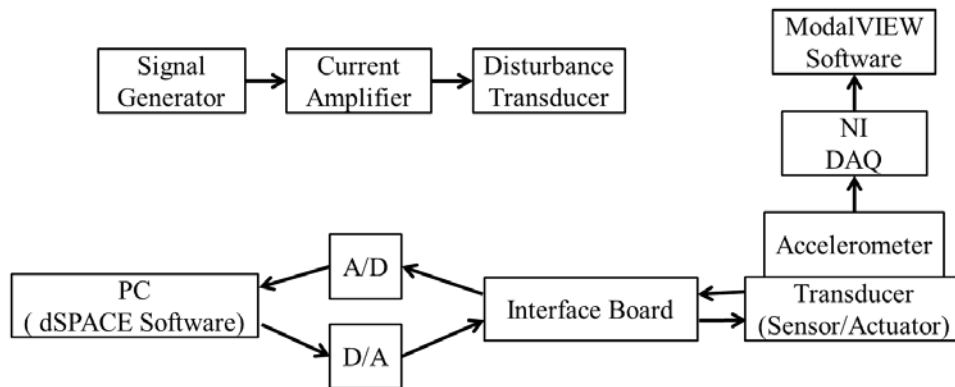
Figure 6.1 shows how the hardware was connected to realize the vibration control experiment. Standard sine signal generated by signal generator flow into disturbance transducer through current amplifier to provide a persistently external vibration disturbance to the plate structure.

The amplitude of the vibration at each transducer is reflected by amplitude of the induced voltages generated within the transducer which is used as sensor and actuator. The induced voltages are sensed by the interface board, then send to dSPACE through A/D convertor to generate control signal. The generated control signals then send back to interface board through D/A convertor to attenuate the induced voltage within each transducer, so that the corresponding amplitude of vibration will be attenuated. This is the closed-loop vibration control process.

As described before, the acceleration value can reflect the amplitude of the vibration, therefore accelerometers were used to produce the FRF curves which are considered as indicator of the vibration at each transducer. The values of each accelerometer are collected by NI DAQ9234 module, then send to ModalVIEW software to synthesize FRF curves.



(a) Physical setup of control experiment



(b) Block diagram of hardware connection for control experiment

Figure 6.1 Hardware setup and block diagram of control experiment

Based on the above configuration, open-loop and closed-loop control systems are measured and compared in the following sections.

6.2 Open-Loop System Measurement

Before implement PPF controllers on the plate structure, open-loop characteristics have to be measured first for the purpose of performance comparison when complete PPF control (closed-loop system).

Chapter 6: PPF Control Experiment

In this project, it concentrates on attenuate the vibration of the first three modes, also considering the lower frequency limitation of the transducers (20 Hz), FRF curves of open-loop system from 20 Hz to 50 Hz were plotted with the help of NI DAQ module and ModalVIEW software.

Measured open-loop FRF curves of three transducers are shown in Figure 6.2.

SISO-PPF controlled system and MIMO-PPF controlled system are tested and compared with open-loop system separately in the following two sections.

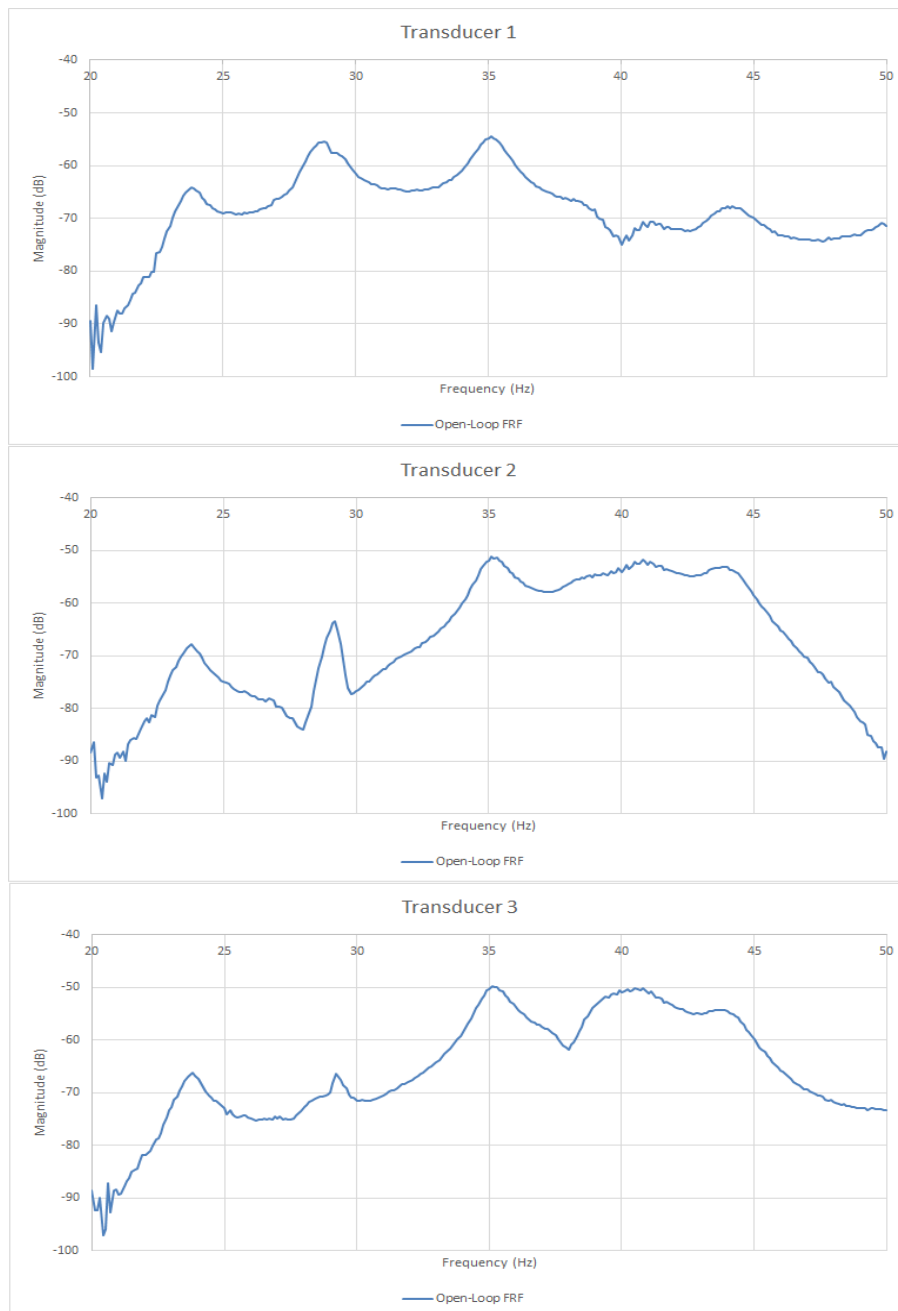


Figure 6.2 FRF curves of each transducer - Open-loop

6.3 SISO-PPF Control Experiment

In this section, the plate structure is considered as three SISO system, and SISO-PPF controllers designed in section 5.4 was implemented in physical experiment, according to control goal, the first three modes were intended to attenuate.

SIMULINK model of SISO-PPF controllers used in dSPACE environment was designed as Figure 6.3 shown.

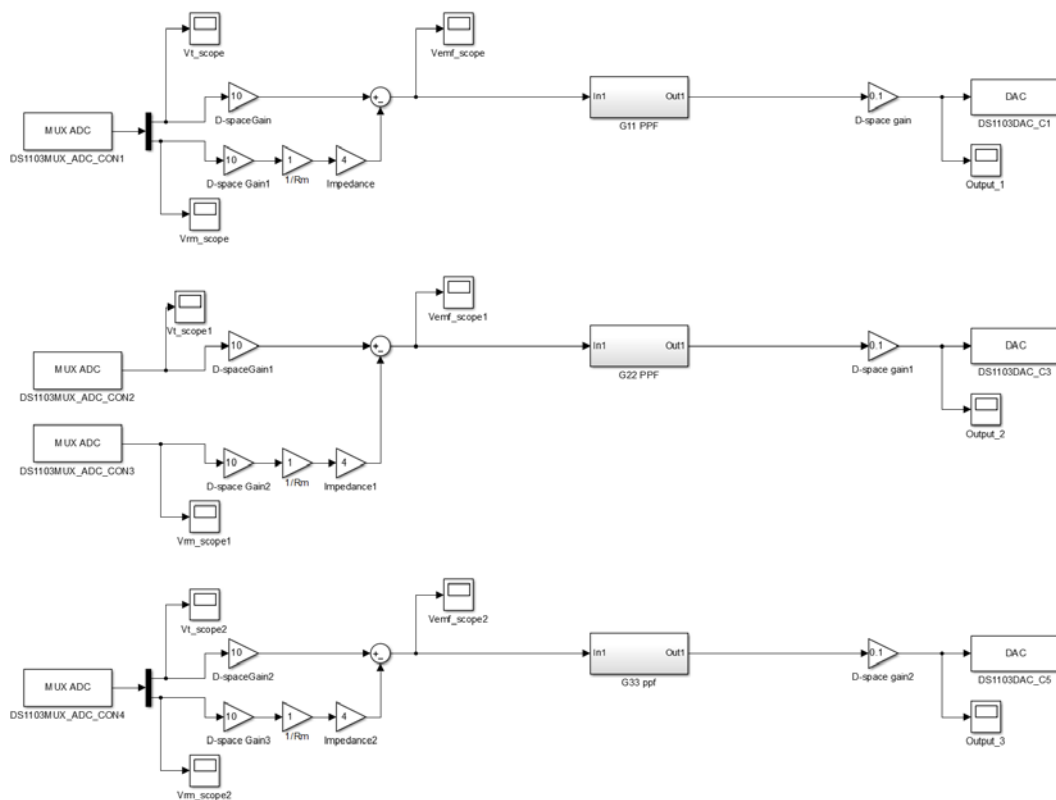


Figure 6.3 SIMULINK model of SISO PPF control experiment

Configuration of the subsystems shown in Figure 6.3 is displayed in Figure 6.4.

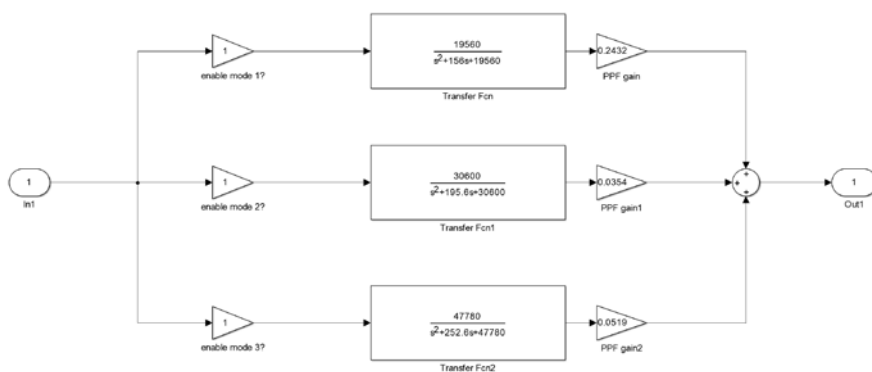


Figure 6.4 Configuration of subsystem

Chapter 6: PPF Control Experiment

From Figure 6.3, it can be seen that three PPF controlled systems are paralleled with each other, that is because in this section the plate structure is viewed as three SISO system, only affections of each transducer to itself were considered, affections of one transducer to another are considered as 0.

Figure 6.3 and 6.4 illustrate the data flow within dSPACE, it can be observed that the induced voltage convert to digital signal through A/D convertor, then this digital signal flow into PPF controller to compute control signal, finally the calculated control signal convert back to analogue signal through D/A convertor to control the external vibration.

Apply above PPF control SIMULINK model in dSPACE environment, the generated control signals are shown in Figure 6.5.

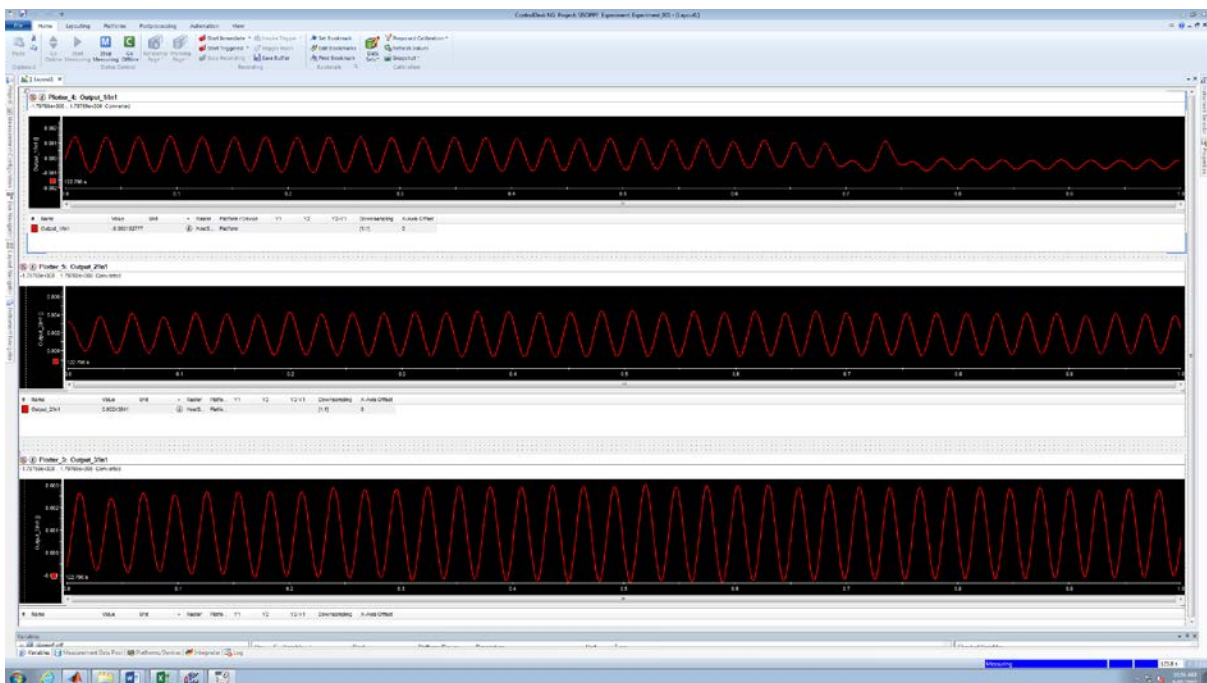


Figure 6.5 Control signal generated in dSPACE

It can be seen that the control signals are also sine wave signal as the disturbance transducer is driven by standard sine wave signal. These control signals were imposed on actuators to counteract induced voltage.

SISO-PPF control experiment result is shown in Figure 6.6.

Chapter 6: PPF Control Experiment

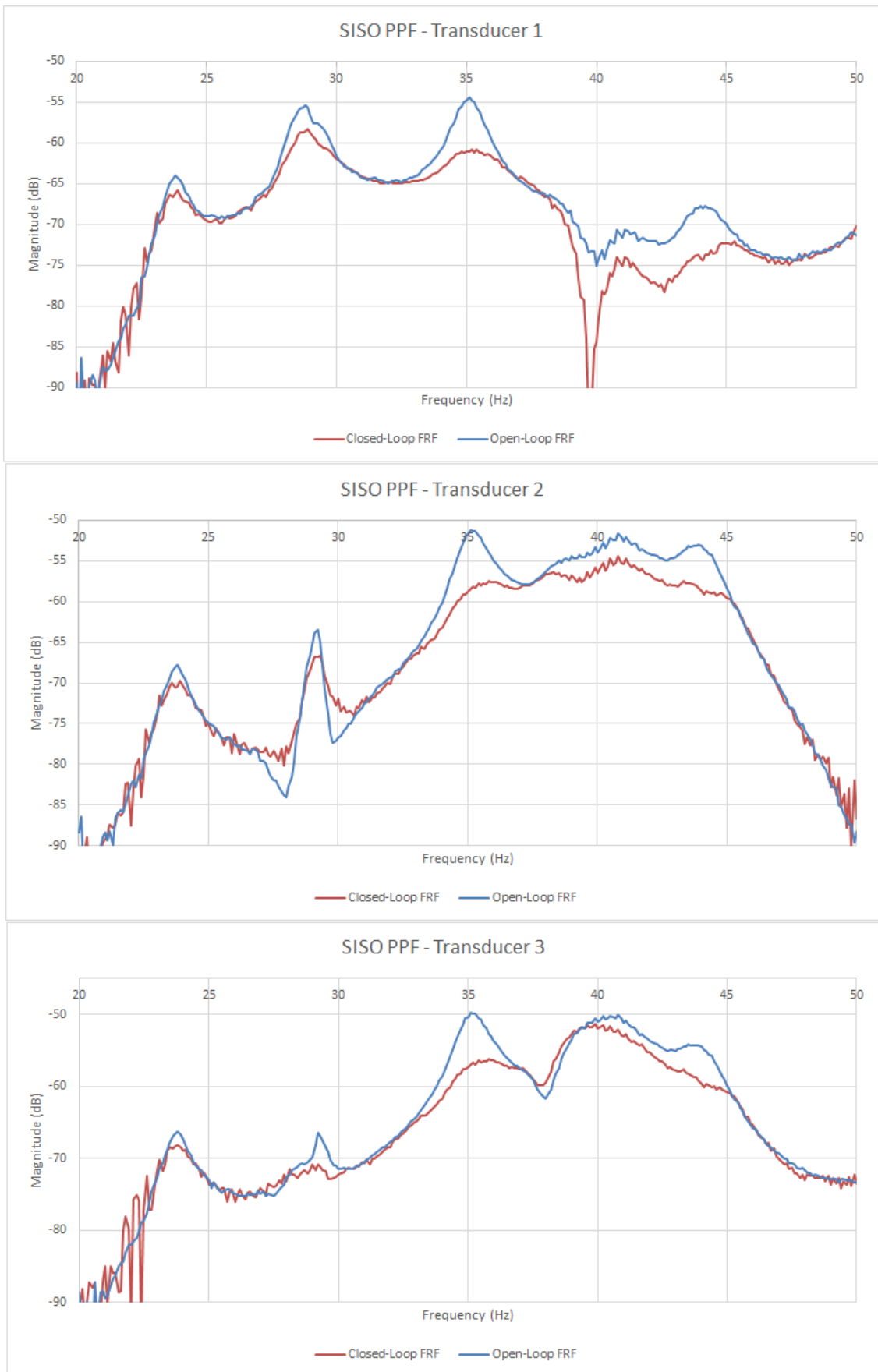


Figure 6.6 Comparison of FRF curves of open-loop and SISO-PPF closed-loop

As the vibration output was indicated by accelerometer, corresponding accelerations and dB values are listed in Table 6.1.

Table 6.1 Result of experiment of SISO-PPF controlled system

		Mode 1	Mode 2	Mode 3
Transducer 1	Open-loop Acceleration (m/s ²)	0.617	1.66	1.867
	Closed-loop Acceleration (m/s ²)	0.48	1.157	0.873
	Reduced Percentage	22.1%	30.3%	53.3%
	Open-loop (dB)	-64.0	-55.4	-54.4
	Closed-loop (dB)	-66.2	-58.6	-61.0
	dB drop (dB)	2.2	3.2	6.6
Transducer 2	Open-loop Acceleration (m/s ²)	0.399	0.66	2.698
	Closed-loop Acceleration (m/s ²)	0.294	0.451	1.167
	Reduced Percentage	26.3%	31.8%	56.8%
	Open-loop (dB)	-67.8	-63.4	-51.2
	Closed-loop (dB)	-70.4	-66.8	-58.5
	dB drop (dB)	2.6	3.4	7.3
Transducer3	Open-loop Acceleration (m/s ²)	0.477	0.468	3.193
	Closed-loop Acceleration (m/s ²)	0.382	0.284	1.373
	Reduced Percentage	19.9%	39.2%	57.1%
	Open-loop (dB)	-66.2	-66.4	-49.7
	Closed-loop (dB)	-68.2	-70.8	-57.1
	dB drop (dB)	2	4.4	7.4

From above Table 6.1 and Figure 6.6, it can be observed that the SISO-PPF controlled system achieved on average a 22.8% of vibration attenuation at first mode, corresponding dB value dropped by 2.3dB. At the second mode, on average a 33.8% of vibration attenuation was

achieved and corresponding dB drop value is 3.7dB. The biggest control effect occurred at the third mode, which achieved more than one half of vibration attenuation (55.7%), corresponding to 7.1dB. That is due to the higher frequency roll-off property of PPF controller, PPF controller designed for lower order mode also has some attenuation effect to higher order modes.

6.4 MIMO-PPF Control Experiment

In this section, the plate structure was considered as MIMO system with three-input three-output, MIMO-PPF controllers designed in section 5.5 were implemented in physical experiment, the first three modes were intended to control.

SIMULINK model of MIMO-PPF controlled system used in dSPACE environment was designed as Figure 6.7 shown.

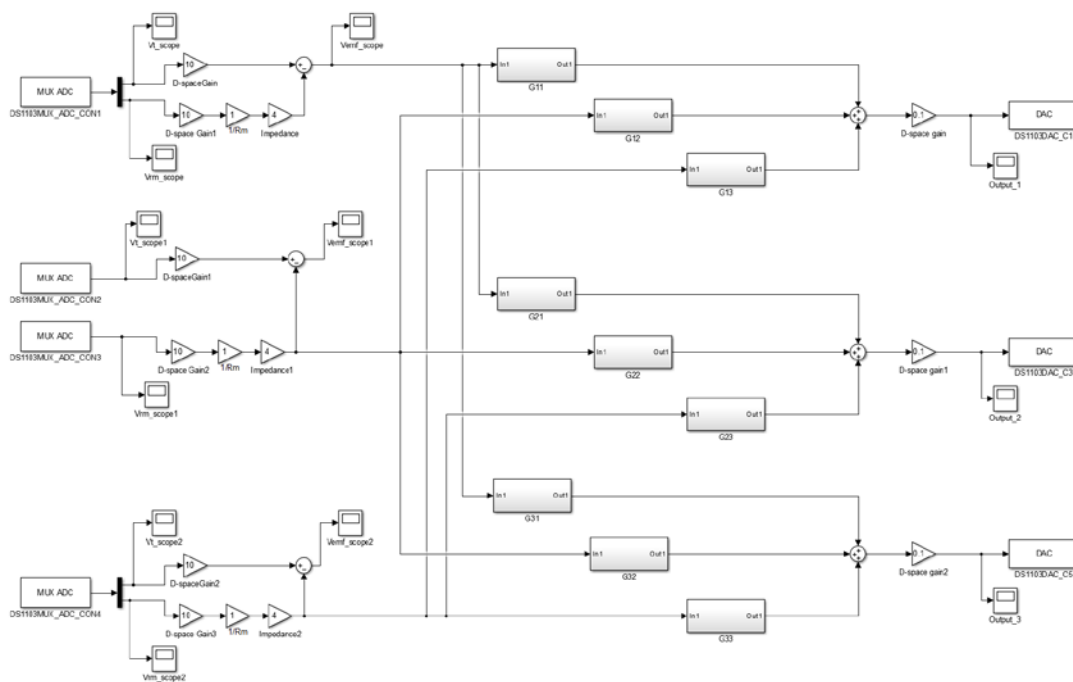


Figure 6.7 SIMULINK model of MIMO PPF control experiment

All the subsystems shown in Figure 6.7 has the same configuration as shown in Figure 6.4.

Data flow in the MIMO PPF control system is similar as in the SISO PPF control system.

From above configuration, it is seen that the generated control signal not only determined by one transducer any more, it is affected by the outputs of three transducers simultaneously and each control signal will act on three transducers concurrently.

MIMO-PPF control experiment result is shown in Figure 6.8.

Chapter 6: PPF Control Experiment

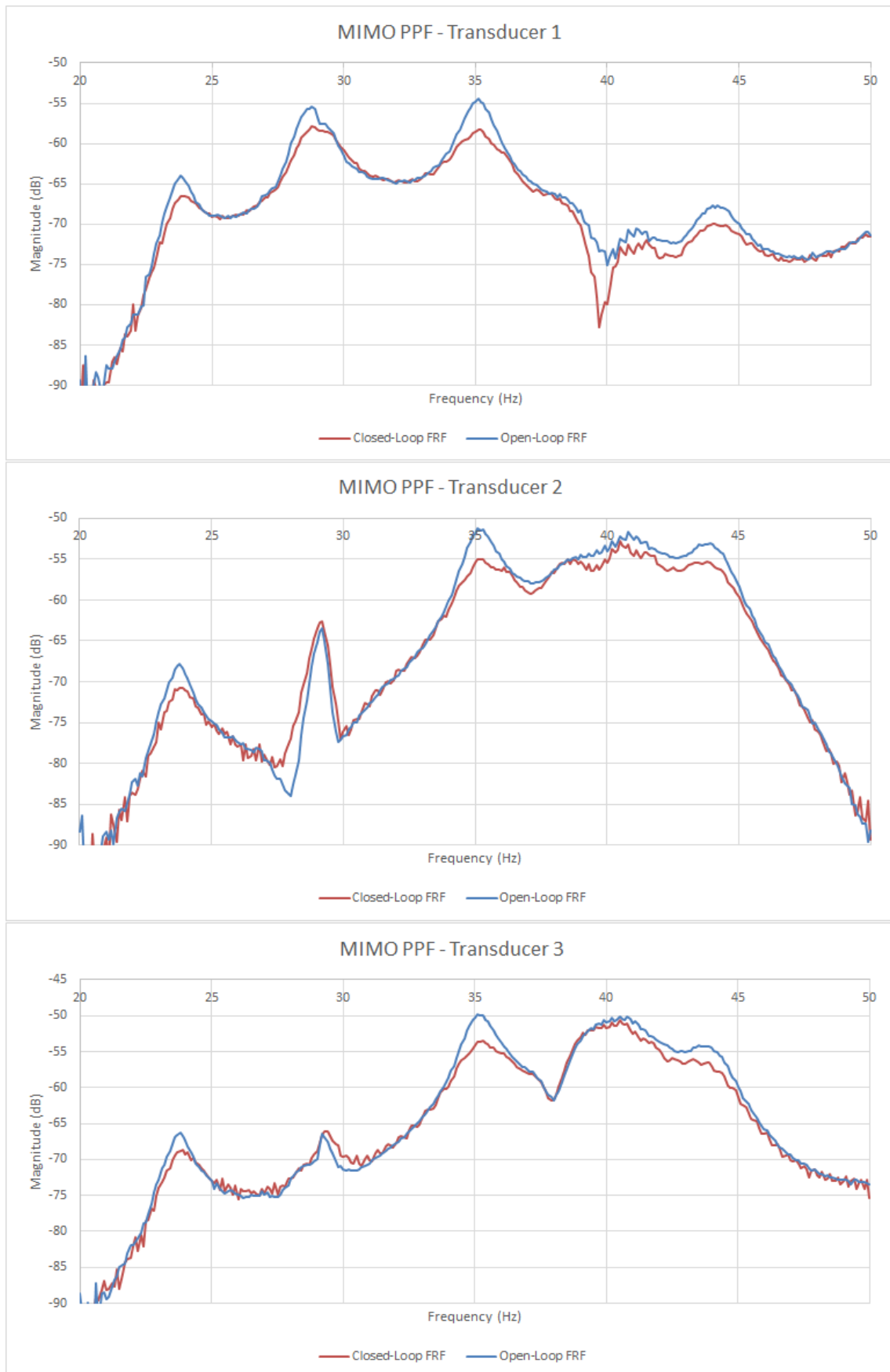


Figure 6.8 Comparison of FRF curves of open-loop and MIMO PPF closed-loop

Corresponding accelerations and dB values on each transducer are listed in Table 6.2.

Table 6.2 Result of experiment of MIMO-PPF controlled system

		Mode 1	Mode 2	Mode 3
Transducer 1	Open-loop Acceleration (m/s ²)	0.617	1.66	1.867
	Closed-loop Acceleration (m/s ²)	0.46	1.25	1.204
	Reduced Percentage	25.4%	24.6%	35.5%
	Open-loop (dB)	-64.0	-55.4	-54.4
	Closed-loop (dB)	-66.6	-57.9	-58.2
	dB drop (dB)	2.6	2.5	3.8
Transducer 2	Open-loop Acceleration (m/s ²)	0.399	0.66	2.698
	Closed-loop Acceleration (m/s ²)	0.283	0.72	1.75
	Reduced Percentage	29.0%	-9.1%	35.1%
	Open-loop (dB)	-67.8	-63.4	-51.2
	Closed-loop (dB)	-70.8	-62.7	-55.0
	dB drop (dB)	3	-0.7	3.8
Transducer3	Open-loop Acceleration (m/s ²)	0.477	0.468	3.193
	Closed-loop Acceleration (m/s ²)	0.356	0.459	2.055
	Reduced Percentage	25.5%	1.9%	35.6%
	Open-loop (dB)	-66.2	-66.4	-49.7
	Closed-loop (dB)	-68.8	-66.6	-53.6
	dB drop (dB)	2.6	0.2	3.9

From above Table 6.2 and Figure 6.8, it can be seen that the MIMO-PPF controlled system achieved on average a 26.6% of vibration attenuation at the first mode, corresponding dB value dropped by 2.7dB. At the second mode, on average a 5.8% of vibration attenuation was achieved and corresponding dB drop value is 0.7dB. Similar to SISO-PPF controlled system,

the biggest control effect occurred at the third mode, which achieved 35.4% of vibration attenuation, corresponding to 3.8dB. Mode 2 got the smallest control effect, that is probably because the first three modes are not well apart from each other, so that the spill-over effects of mode 1's PPF controller and mode 3's PPF controller counteract the control effect of mode 2's PPF controller.

6.5 Experiment Summary

From experiment results shown in section 6.3 and 6.4, it is seen that SISO-PPF controlled system achieved on average a 22.8% of vibration attenuation at the first mode, 33.8% of vibration attenuation at the second mode, and 55.7% of vibration attenuation at the third mode. And MIMO-PPF controlled system achieved on average a 26.6% of vibration attenuation at the first mode, 5.8% of vibration attenuation at the second mode, and 35.4% of vibration attenuation at the third mode. With further tuning parameters of PPF controller and improving the accuracy of the mathematical model, the experimental result can be improved.

It is understandable that experimental results may not be as good as those predicted by simulation, taking into account of the following reasons.

- (1) Except the persistent external vibration introduced by the disturbance transducer, there are also some unexpected or unknown noises in the environment, it is difficult to control this kind of noise, therefore, efficiency of the controllers would be reduced.
- (2) When considering the system as SISO system, only transfer function located on diagonal line are computed, but the other elements of the transfer matrix are actually not zero. This cannot be ignored when analyzing the efficiency of the controllers.
- (3) The spillover property of PPF controller determined that PPF control technique suit for well apart modes of vibration, in this plate structure, the first three modes are not well apart from each other, therefore, the control effect could be partly counteracted by the spillover effect.
- (4) There are many approximations during the mathematical modeling process, such as error introduced by the curve fitting method, the gain of the current amplifier PCB, and the impedance of the transducer, all these approximations have a negative effect on the precision of the mathematical model.

Chapter 7 : Conclusion

7.1 Project Conclusion

In this project, instead of numerically modelling the plate structure in ANSYS that conducted by previous students, theoretical analysis and physical experiment modelling techniques were utilized to derive the mathematical model by using modal analysis software, ModalVIEW. For controller designing purpose, the measured mathematical model was truncated to first three modes and model correction technique based on spatial H_2 norm was applied to minimize the truncation error. Then positive position feedback vibration control technique was selected to design controllers. As the plate structure was considered as SISO system and MIMO system respectively, SISO-PPF and MIMO-PPF controllers are designed corresponding to SISO system and MIMO system respectively. The designed PPF controllers were applied on the simulated mathematical model and then the physical plate structure to validate the control performance.

In the simulation stage, for both SISO system and MIMO system, PPF controllers are designed for each individual mode and corresponding control performances are validated. The results indicate that the simulated PPF controlled system of each single mode can achieve at least 20 dB on magnitude, which fulfilled the desired effect of vibration suppression. The designed PPF controllers are then imposed on the truncated and measured true model to control the vibration on the first three modes.

For SISO system, it can be seen that SISO-PPF control can achieve about 30 dB vibration suppression at the first three modes both on the corrected model and on the measured true model. Besides the first three modes, there are also some attenuation effect on the fourth and fifth modes, and no effect on the further higher frequency mode. This phenomenon indicates that PPF controller is suitable for well-separated modes. In this project, because modes are not well separated from each other, i.e. the natural frequency of each mode are not far away enough from the other modes, that is why the fourth and fifth modes affected by PPF controller but higher frequency modes do not.

For MIMO system, three modes control on the simulated corrected model achieved at least 20dB vibration suppression on each individual mode. And from comparison of Table 5.8 (SISO PPF control result) and table 5.15 (MIMO PPF control result), it can be seen that

Chapter 7: Conclusion

MIMO PPF control achieved better vibration control performance on transducer 2 and transducer 3. Similar control effects are achieved when perform MIMO-PPF controllers on the measured true model. And similar to SISO system control, three modes PPF controllers also affect mode four and mode five but very little effect on the higher order modes, which is due to the reason that modes in this project are not well separated from each other.

In the physical vibration control experiment, the plate structure also considered as three SISO systems and one MIMO system separately to validate the performances of designed PPF controllers. When it is considered as three SISO systems, the SISO-PPF controlled system achieved an average of 22.8% of vibration attenuation at first mode, an average of 33.8% at the second mode and an average of 55.7% at the third mode. The biggest control effect occurred at the third mode, which achieved more than one half of vibration attenuation. That is due to the higher frequency roll-off property of PPF controller, PPF controller designed for lower frequency mode also has some attenuation effect to higher frequency modes.

When the plate structure be considered as a MIMO system with three-input and three-output, the corresponding MIMO-PPF controlled system achieved on average a 26.6% of vibration attenuation at the first mode, on average a 5.8% of vibration attenuation at the second mode, and 35.4% of vibration attenuation at the third mode. Similar to SISO-PPF controlled system, the biggest control effect occurred at the third mode due to the higher frequency roll-off property of PPF controller. The second mode got the smallest control effect, that is probably because the natural frequencies of the first three modes are not well apart from each other, so that the spill-over effects of mode 1's PPF controller and mode 3's PPF controller counteract the control effect of mode 2's PPF controller.

From above analysis, it could be concluded that the initial design goal was basically realized, and with further improving accuracy of the simulated mathematical model and tuning the parameters of each PPF controller, the experimental vibration control performance is anticipated to be further improved.

From results of the control experiment, it is also indicated that PPF control technique is suitable for vibration with well-separated modes. If modes to be controlled are not well apart from each other, the spill-over effect of PPF controller will affect the vibration control result of the next mode, and the quick roll-off property can add extra vibration attenuation to the higher frequency modes.

7.2 Recommendations

As analyzed in Chapter 6, there are mainly two factors that can influence the efficiency of the controllers. Therefore, future work should mainly focus on two aspects, one is to improve precision of the mathematical model and another is to tune PPF parameters when doing physical experiment.

In terms of improving precision of the mathematical model, the most important part is to improve curve fitting method. There are many other curve fitting techniques both in frequency domain and time domain, different techniques can be utilized and compared for the purpose of get the optimal mathematical model.

Because of shortage of time, this author did not tune the parameters of PPF controller when doing physical vibration control experiment. Since this is an important step to improve control performance of the controller, this kind of works are highly suggested to do. Based on current simulation results, controller parameters can be slightly tuned to suit the dynamics of the plate structure.

Appendix A: Interface Board

The interface board in this project is used to communicate between transducer and dSPACE module.

The circuit schematics of the interface board used to communicate between transducer and dSPACE is shown in below Figure A.1. This circuit realized self-sensing technique which is described in chapter 3. In this circuit, low pass filters with cut-off frequency of 1591 Hz used to filter out high frequency noise signals, ZL represent impedance of the transducers. Chip OPA548 and UA741 are three voltage follower amplifiers used to calculate the induced voltage on the transducer ZL based on equation 3.3. Another function of this circuit is to impose the control voltage signal on transducer. Decoupling capacitors (C2, C3, C5, C6, C7) are used to reduce the noise signal on the power source and one 1A fuse is used to protect the circuit from overload damage.

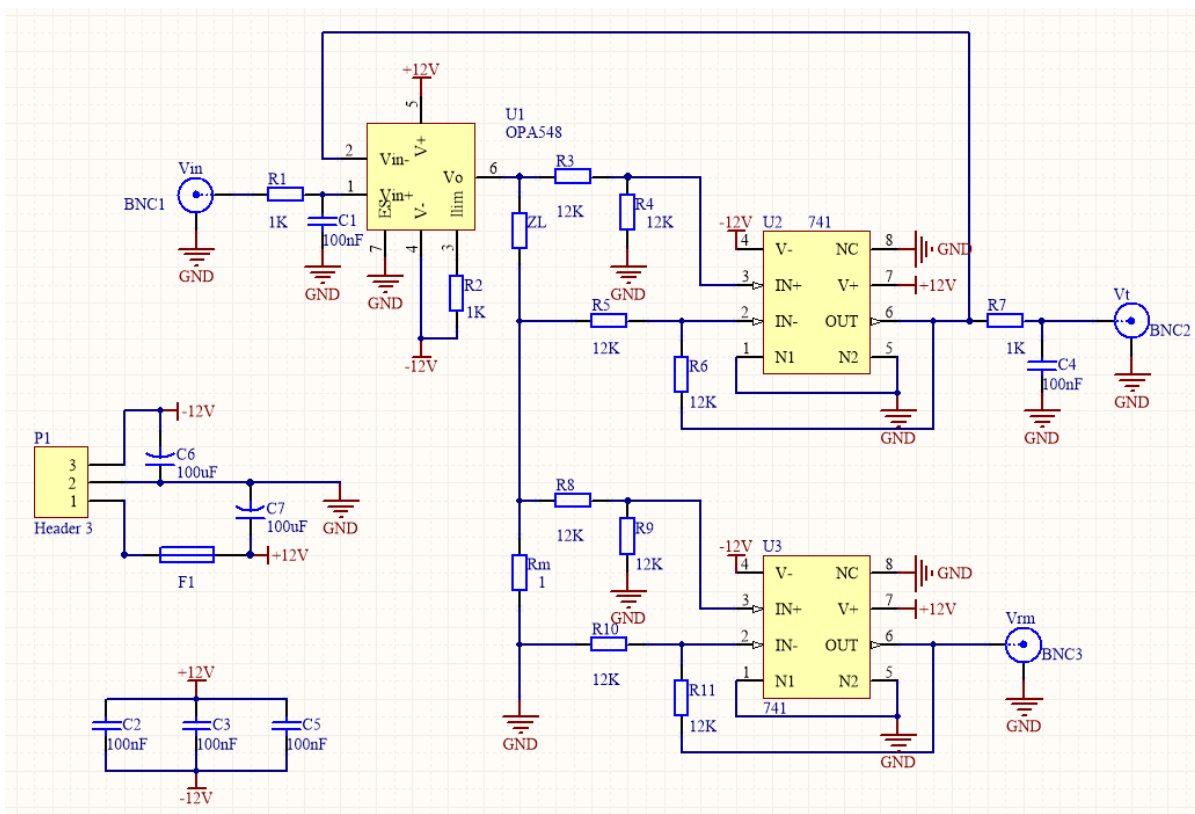


Figure A.0.1 Schematic circuit of interface board

Component list of this interface board is shown in Table A.1.

Table A.1 Component list of interface board

Item	Quantity	Designators	Name	Value	Footprint
1	1	U1	OPA548	-	TO-220
2	2	U2,U3	UA741	-	DIP-8
3	3	R1,R2,R7	Resistor	1k	Through hole
4	8	R3-R6,R8-R11	Resistor	12k	Through hole
5	1	Rm	Resistor	1R	Through hole
6	5	C1-C5	Capacitor	100nF	Through hole
7	2	C6,C7	Capacitor	100uF	Through hole
8	1	F1	Fuse	1A	Through hole

Component layout used in assembly stage is illustrated in Figure A.2.

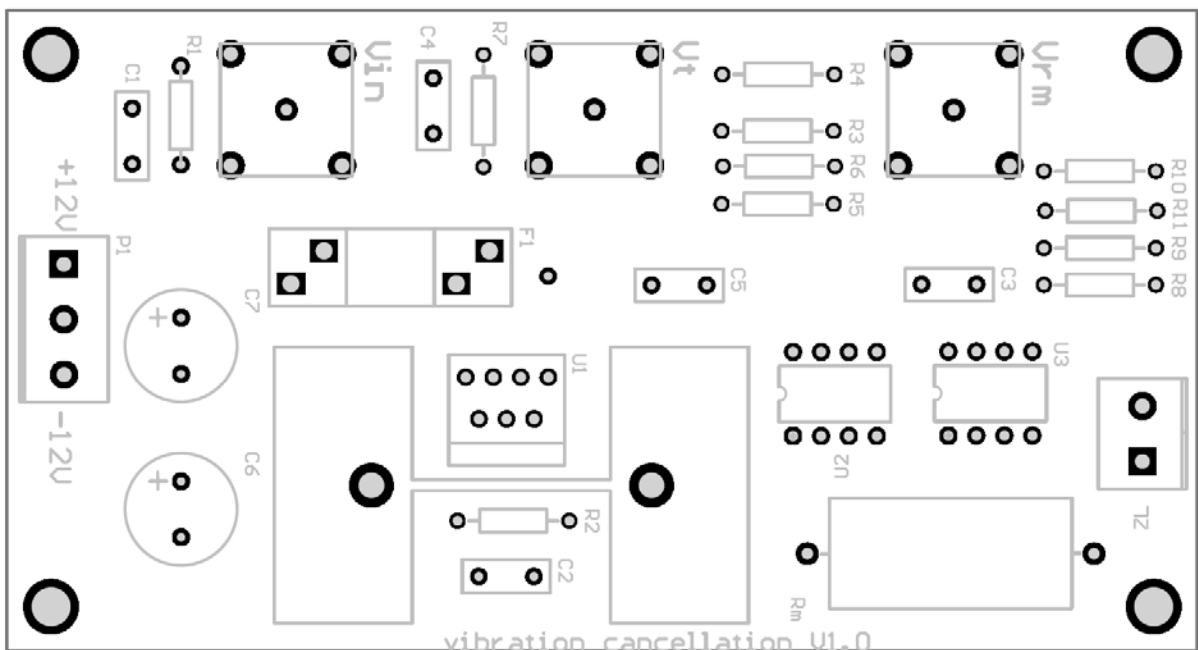


Figure A.0.2 Component layout of interface board

Appendix B: Modal Analysis Procedure in ModalVIEW Software

The detailed procedures to perform modal analysis in ModalVIEW software are provided in this appendix.

Generally, there are four steps to perform a modal analysis in ModalVIEW software:

- (1) Draw a structure
- (2) Perform FRF measure
- (3) Estimate modal parameter
- (4) Animate mode shape

First of all, a new project should be created by click File/Project/New in the project window, this will create a blank project, as shown in Figure A.3. There are quick start menus in the project window, which can open corresponding operating window.

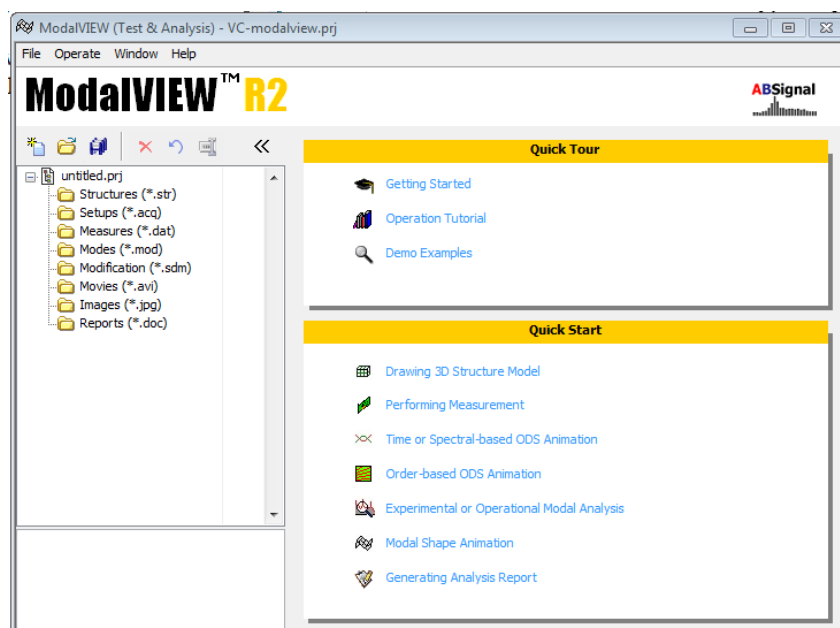


Figure A.0.1 Create a new project in ModalVIEW

Step 1: Draw the plate structure

- 1) Click **Drawing 3D Structure Model**, a blank structure view window will open, as shown in Figure A.4.

Appendix

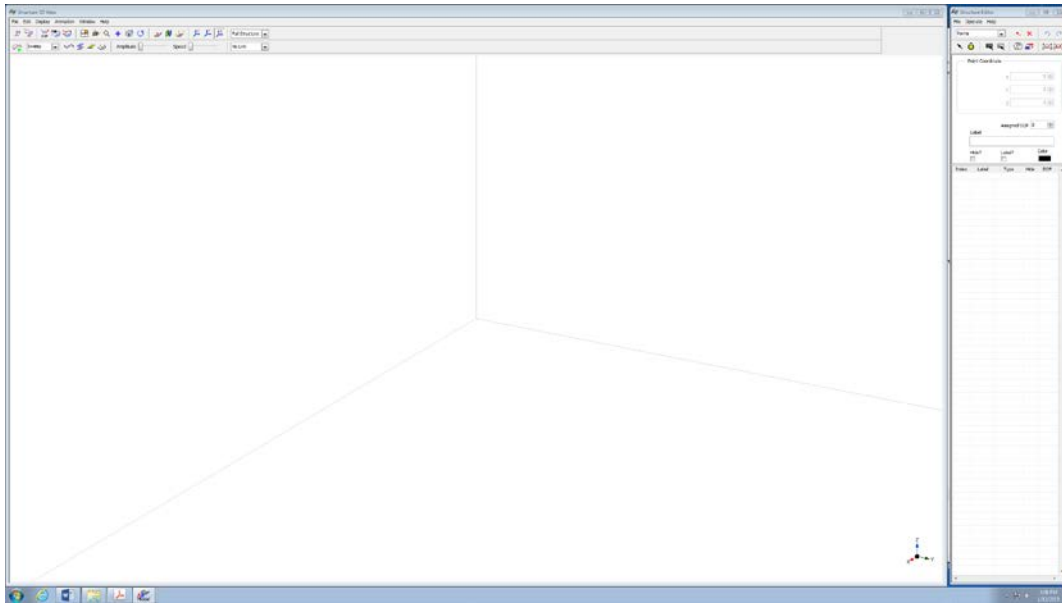


Figure A.0.2 Blank structure view window

- 2) In structure editor window, change object selection to substructures, as shown in Figure A.5.

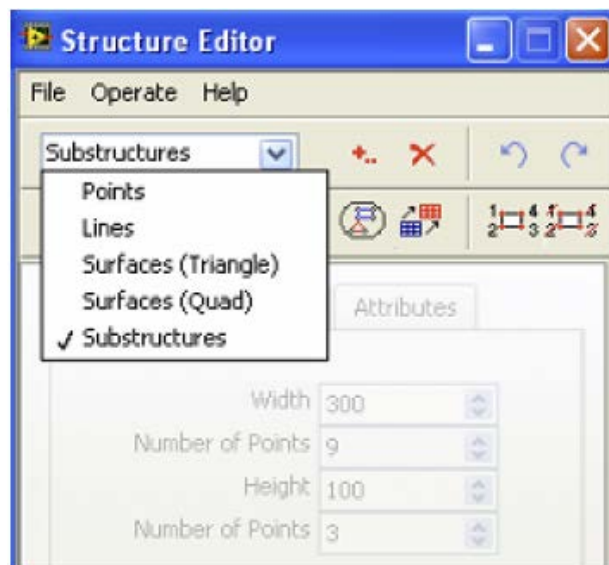



Figure A.0.3 Structure editor window

- 3) Click  to add a plate structure, and enter related information in the structure editor window.

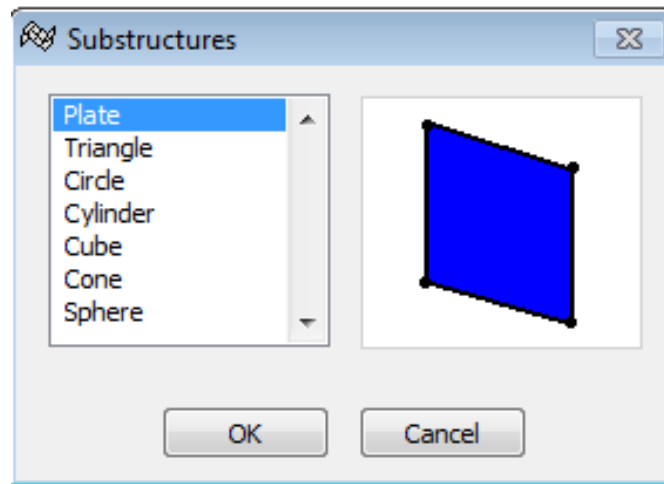
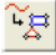


Figure A.0.4 Select plate structure

- 4) Click  button to set up measure properties in measure property window as shown in Figure A.7.

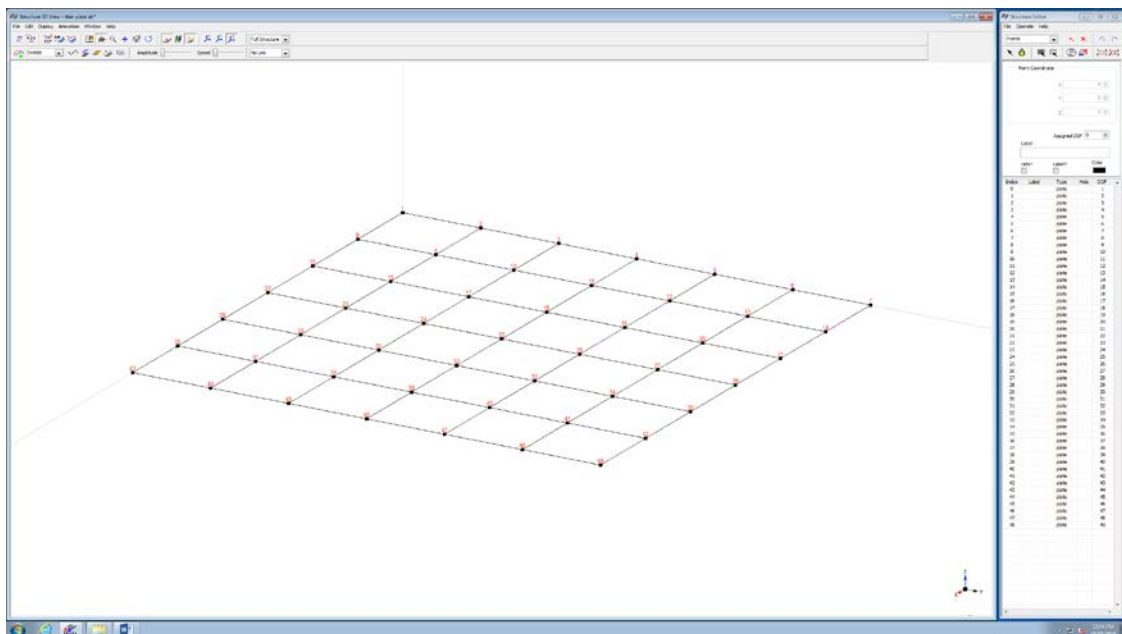


Figure A.0.5 Measure property window

- 5) Click File/Save menu, input file name “plate” and click OK.

Step 2: Measure FRF

- 1) Click Performing Measurement to open the measure window.

Appendix

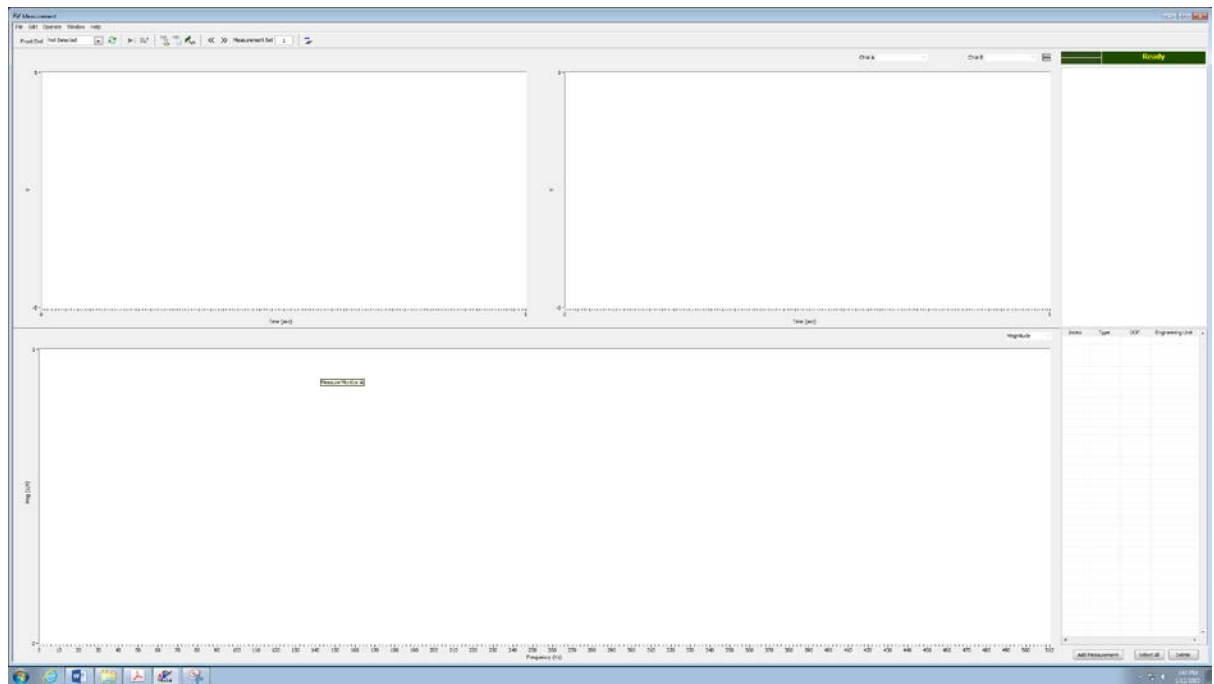


Figure A.0.6 Measure window

2) Select front end as NI9234.

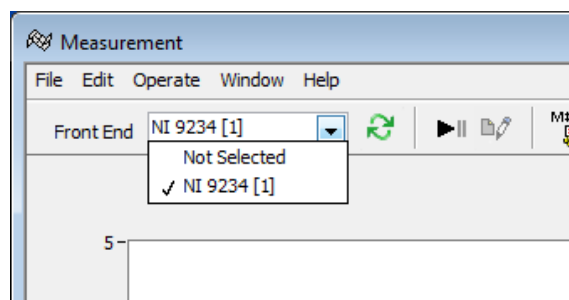



Figure A.0.7 Select front end

3) After front end being connected, click  to open DAQ setup window, as shown in figure A.10 and A.11.

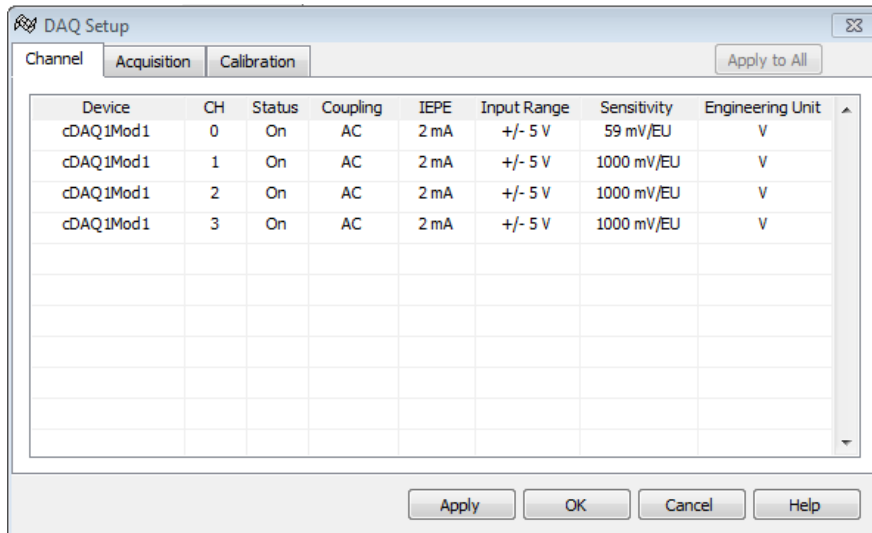


Figure A.0.8 DAQ setup window-Channel page

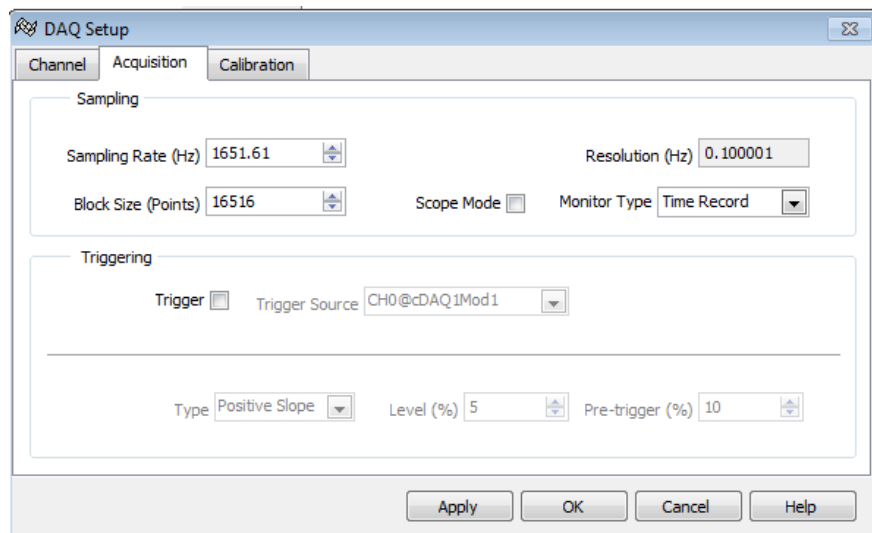
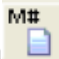


Figure A.0.9 DAQ setup window-Acquisition page

Under **Channel** tab, four channels have been displayed and enable. In this project, CH0 used for input reference signal, CH1-CH 3 are used for accelerometer signal. Sensitivity of CH0 set to 59mV/EU, that is because the input signal connected to an amplifier before into the transducer, this gain is 17 when $\pm 12V$ power supply input, therefore sensitivity is $1000/17=59mV/EU$.

Under **Acquisition** tab, choose block size to 16516, which will set the resolution to 0.1Hz.

- 4) Click Ok button to end DAQ setup.

- 5) Click test setup button  , to setup measurement scheme.

Appendix

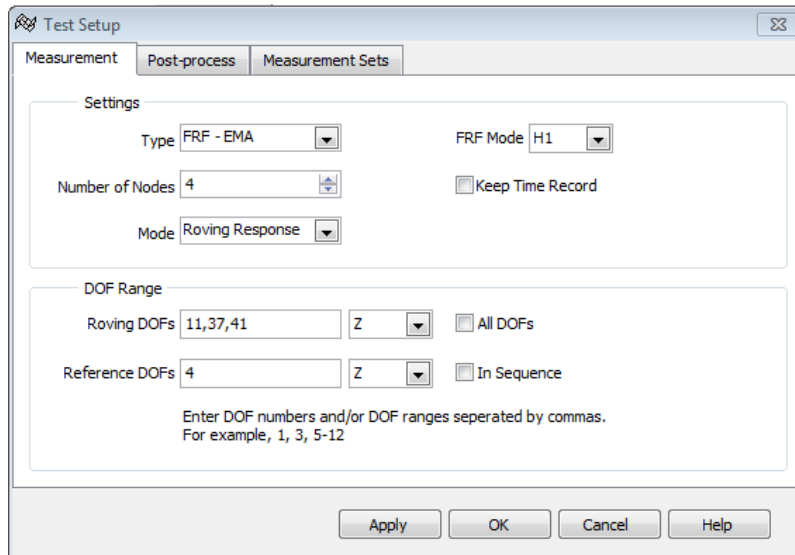


Figure A.0.10 Measurement scheme window-Measurement page

Under **Measurement** tab, set number of nodes to 4.

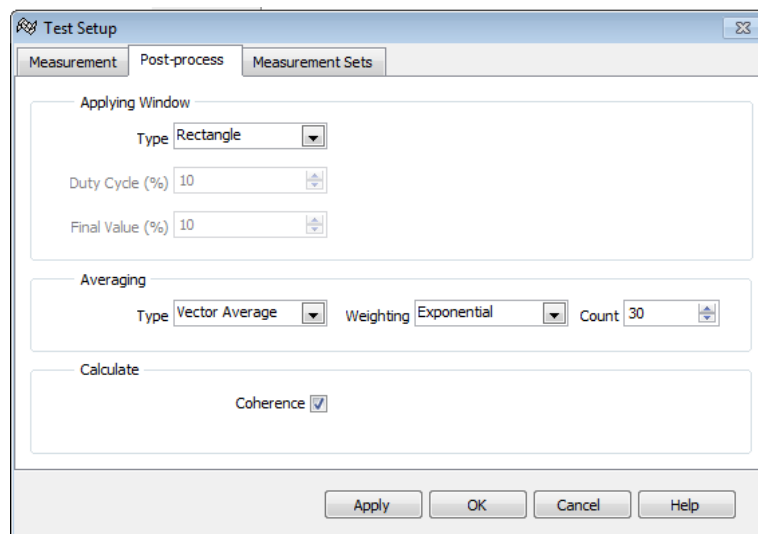


Figure A.0.11 Measurement scheme window-post-process page

Under **Post-process** tab, set Count number at least to 30.

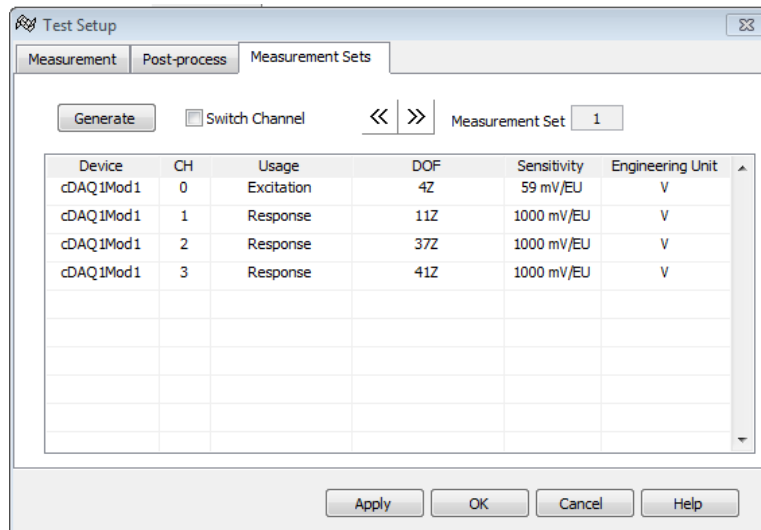



Figure A.0.12 Measurement scheme window-Measurement set page

Under **Measurement sets** tab, click Generate then click OK.

- 6) Make sure hardware are connected correctly and press  to start a measurement.
- 7) After finished measurement, save measurement data in the measurement window.

Step 3: Estimate modal parameters

- 1) Click **Experimental or Operational Modal Analysis** to open the FRF window and load the measured data, as shown in Figure A.15.

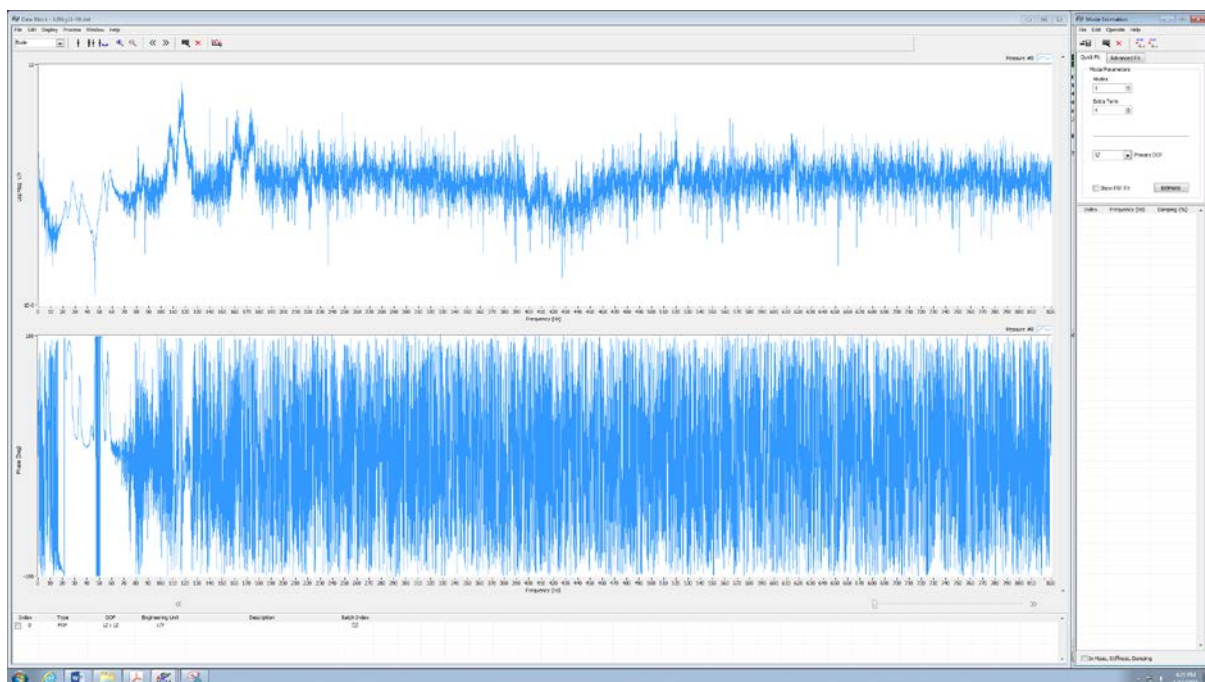


Figure A.0.13 FRF window

Appendix

- 2) Zoom in 20-60 Hz range as Figure A.16 shows, that is the frequency range we are interested in.

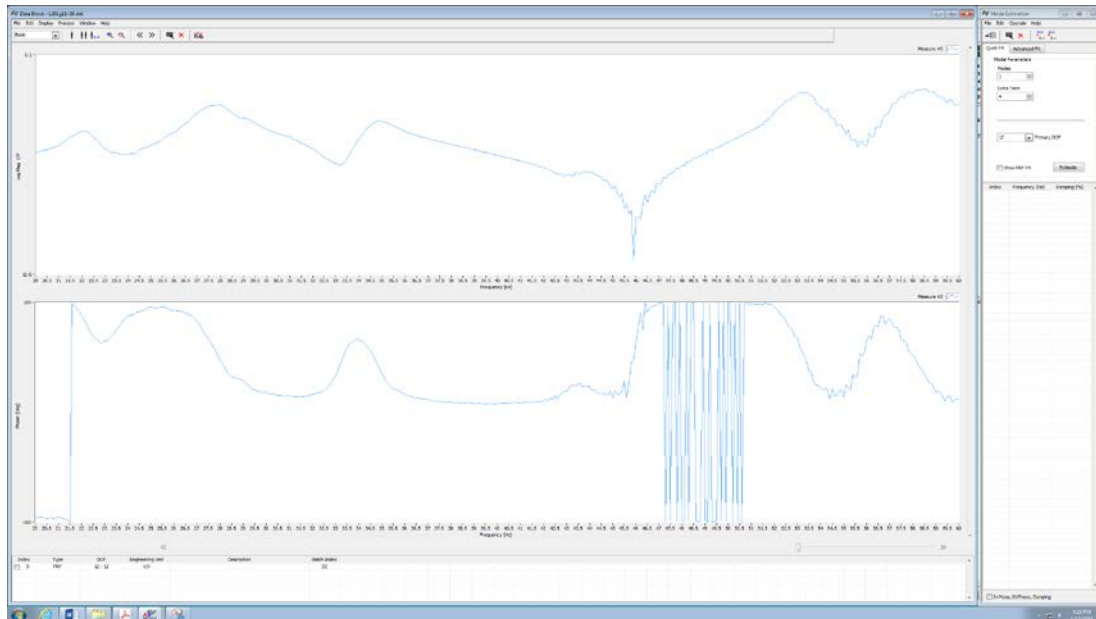


Figure A.0.14 Zoom in 20-60 Hz range

- 3) According to experiment bode plot, adjust mode number and Extra term number under Quick Fit tab, until an acceptable curve appears. The natural frequency and damping ratio of each mode are listed in the Mode Estimation window.

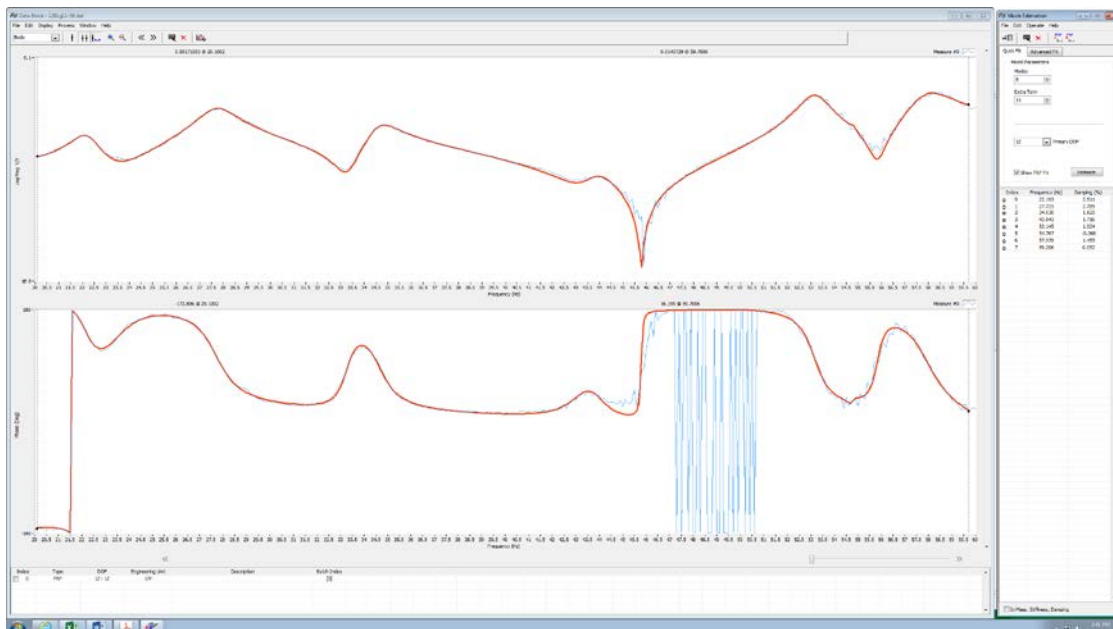


Figure A.0.15 Mode estimation window

Appendix

- 4) In Model Estimate window, click File/ Save Mode Table menu, and close the data review window.

Step 4: Animate mode shapes

- 1) Click quick start item **Modal Shape Animation** in project window.

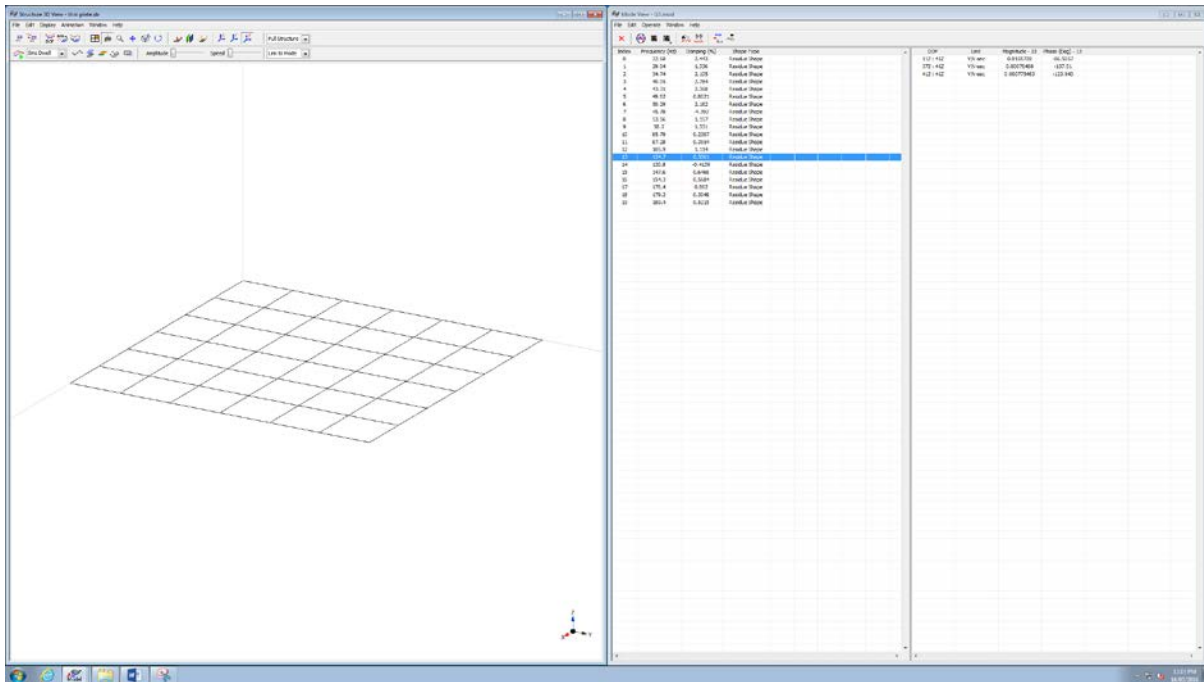


Figure A.0.16 Structure window

- 2) In the structure window, load corresponding structure, in the Mode View window, load the mode data saved in the previous step.
- 3) Click each frequency listed in the Mode View window, corresponding magnitude and phase value will appear on the right.

Index	Frequency (Hz)	Damping (%)	Shape Type	DOF	Unit	Magnitude	Phase (Deg)
0	22.68	2.493	Residue Shape				
1	29.04	1.256	Residue Shape				
2	34.74	2.105	Residue Shape				
3	40.05	2.784	Residue Shape				
4	43.31	2.568	Residue Shape				
5	49.62	0.8023	Residue Shape				
6	50.29	2.182	Residue Shape				
7	46.78	-4.392	Residue Shape				
8	53.56	1.157	Residue Shape				
9	58.2	1.331	Residue Shape				
10	85.79	0.2207	Residue Shape				
11	87.28	0.2054	Residue Shape				
12	105.9	1.114	Residue Shape				
13	124.8	0.112	Residue Shape				
14	130.9	-0.4139	Residue Shape				
15	147.6	0.6466	Residue Shape				
16	154.3	0.5684	Residue Shape				
17	176.4	0.8621	Residue Shape				
18	179.2	0.3048	Residue Shape				
19	189.4	0.5215	Residue Shape				

Figure A.0.17 Modal parameters

Appendix C: MATLAB Code

In this appendix, all the necessary MATLAB codes used in this projects are provided.

```
% %% Transfer function parameters %%%%
```

```
function modeinfo = getmodeinfo()

%natural frequency
modeinfo.f(1,1,:)=[22.26,27.84,34.79,43.77,53.7,58.06,124.7,147.2,176.3,179
.1,0,0,0,0,0];
modeinfo.f(2,1,:)=[22.26,29.16,34.79,43.77,53.7,58.06,85.62,124.7,147.2,176
.3,179.1,189.7,0,0,0];
modeinfo.f(3,1,:)=[22.26,29.16,34.79,43.77,53.7,58.06,85.62,124.7,147.2,176
.3,179.1,189.7,0,0,0];

modeinfo.f(1,2,:)=[22.36,29.01,34.72,43.01,53.55,58.23,85.69,87.77,124.6,14
7.4,154.3,176.3,179.2,189.3,0];
modeinfo.f(2,2,:)=[22.36,29.01,34.72,43.01,53.55,58.23,85.69,87.77,124.6,14
7.4,154.3,176.3,179.2,189.3,0];
modeinfo.f(3,2,:)=[22.36,29.01,34.72,40.36,43.01,53.55,58.23,85.69,87.77,12
4.6,147.4,154.3,176.3,179.2,189.3];

modeinfo.f(1,3,:)=[22.68,29.04,34.74,40.05,43.31,53.56,58.2,85.79,87.28,124
.7,147.6,154.3,176.4,189.4,0];
modeinfo.f(2,3,:)=[22.68,29.04,34.74,40.05,43.31,53.56,58.2,85.79,87.28,124
.7,147.6,154.3,176.4,189.4,0];
modeinfo.f(3,3,:)=[22.68,29.04,34.74,40.05,43.31,53.56,58.2,85.79,87.28,124
.7,147.6,154.3,176.4,189.4,0];

%natural frequency in radium
modeinfo.w=2*pi.*modeinfo.f;

%damping ratio
modeinfo.zeta(1,1,:)=[0.0211,0.01924,0.01866,0.01842,0.01047,0.01458,0.0034
44,0.005374,0.005288,0.005678,0,0,0,0];
modeinfo.zeta(2,1,:)=[0.0211,0.01036,0.01866,0.01842,0.01047,0.01458,0.0021
73,0.003444,0.005374,0.005288,0.005678,0.005049,0,0,0];
modeinfo.zeta(3,1,:)=[0.0211,0.01036,0.01866,0.01842,0.01047,0.01458,0.0021
73,0.003444,0.005374,0.005288,0.005678,0.005049,0,0,0];

modeinfo.zeta(1,2,:)=[0.0233,0.01489,0.02612,0.02635,0.007323,0.01117,0.002
43,0.002926,0.003087,0.00763,0.006028,0.005722,0.00596,0.004941,0];
modeinfo.zeta(2,2,:)=[0.0233,0.01489,0.02612,0.02635,0.007323,0.01117,0.002
43,0.002926,0.003087,0.00763,0.006028,0.005722,0.00596,0.004941,0];
modeinfo.zeta(3,2,:)=[0.0233,0.01489,0.02612,0.02708,0.02635,0.007323,0.011
17,0.00243,0.002926,0.003087,0.00763,0.006028,0.005722,0.00596,0.004941];

modeinfo.zeta(1,3,:)=[0.02443,0.01336,0.02105,0.02784,0.02368,0.01157,0.013
31,0.002307,0.003554,0.003561,0.006466,0.005684,0.00862,0.005215,0];
modeinfo.zeta(2,3,:)=[0.02443,0.01336,0.02105,0.02784,0.02368,0.01157,0.013
31,0.002307,0.003554,0.003561,0.006466,0.005684,0.00862,0.005215,0];
modeinfo.zeta(3,3,:)=[0.02443,0.01336,0.02105,0.02784,0.02368,0.01157,0.013
31,0.002307,0.003554,0.003561,0.006466,0.005684,0.00862,0.005215,0];
```


Appendix

```
% Mode shape a

modeinfo.a(1,1,:)= [2.0531,14.1454,9.9935,1.3535,45.6005,90.5574,39.5723,3.6
184,10.6088,36.0350,0.0000,0.0000,0.0000,0.0000,0.0000];
modeinfo.a(2,1,:)= [1.7447,2.8578,15.7963,8.8618,19.6973,63.5692,0.7478,1.91
86,7.9064,14.4058,46.6070,4.9308,0.0000,0.0000,0.0000];
modeinfo.a(3,1,:)= [2.2110,2.9036,18.6406,7.8030,22.1916,47.0703,3.9263,2.11
34,15.3631,14.3676,7.1169,1.5600,0.0000,0.0000,0.0000];

modeinfo.a(1,2,:)= [1.4362,4.2439,22.3877,11.3928,21.1431,50.3913,1.0975,0.4
314,23.0652,1.6163,7.3900,10.7335,25.8537,2.5571,0.0000];
modeinfo.a(2,2,:)= [1.3305,8.4493,32.5810,60.4619,11.2754,34.7368,3.9374,1.5
733,0.9947,8.5468,15.1288,14.2664,33.2144,29.4910,0.0000];
modeinfo.a(3,2,:)= [1.3818,9.1842,37.8622,14.8044,53.8024,11.7023,24.7710,23
.0951,0.7478,1.2397,13.1164,2.3683,14.7077,5.3835,8.6146];

modeinfo.a(1,3,:)= [1.4414,3.5449,16.1255,1.2186,10.5109,22.4672,66.2704,0.1
873,6.4106,24.4028,0.9908,11.8442,14.8695,2.9668,0.0000];
modeinfo.a(2,3,:)= [1.0484,6.9965,23.0971,9.0145,53.3759,12.7107,45.1412,1.6
235,26.6507,1.1986,6.7677,26.9108,36.3517,32.2121,0.0000];
modeinfo.a(3,3,:)= [1.1538,7.6262,26.6661,10.8387,47.5706,13.1665,32.9406,5.
8440,4.7128,1.2152,9.2563,4.1228,25.6780,9.2114,0.0000];

% calculate transfer function and export data into excel

function T=truncatedtf()

modeinfo=getmodeinfo();
s=tf('s');
p=1;

for i=1:3
    for j=1:3
        % tf for each mode
        for k=1:15

M(i,j,k)=modeinfo.a(i,j,k)/(s^2+2*modeinfo.zeta(i,j,k)*modeinfo.w(i,j,k)*s+
modeinfo.w(i,j,k)^2);
            end

            % All modes tf
            T(i,j)=M(i,j,1);
            for k=2:15
                T(i,j)=T(i,j)+ M(i,j,k);
            end

            %export data to excel
            pointsnum=linspace(40*pi,400*pi,1800);
            [mag,phase,w]=bode(T(i,j),pointsnum);
            mag=squeeze(mag);
            phase=squeeze(phase);
            w=squeeze(w);

            xlswrite('test.xlsx',w/2/pi,p,'a1')
```

Appendix

```
    xlsxwrite('test.xlsx',20*log10(mag),p,'b1')
    xlsxwrite('test.xlsx',phase,p,'c1')

    p=p+1;

end
end

% calculate truncation error

function err = modelcorrection()

modeinfo=getmodeinfo();

Wc=zeros(3,3);    % cut-off frequency
err=zeros(3,3);  % cut-off error

%%%%%%%%%%%%%%%%%%%%%%%%%%%%%%%%%%%%%%%%%%%%%%%%%%%%%%%%%%%%%%%%%%%%%%%%
%error from mode 3
%%%%%%%%%%%%%%%%%%%%%%%%%%%%%%%%%%%%%%%%%%%%%%%%%%%%%%%%%%%%%%%%%%%%%%%%
%

%calculate cut-off frequency
for i=1:3
    for j=1:3
        Wc(i,j)=(modeinfo.w(i,j,3)+modeinfo.w(i,j,4))/2;
    end
end

%calculate cut-off error
for i=1:3
    for j=1:3

        for k=4:15
            if modeinfo.f(i,j,k)>0

err(i,j)=err(i,j)+modeinfo.a(i,j,k)/modeinfo.w(i,j,k)*log((modeinfo.w(i,j,k)
)+Wc(i,j))/(modeinfo.w(i,j,k)-Wc(i,j)));
                end
            end
            err(i,j)=err(i,j)/(2*Wc(i,j));
        end
    end
end

% Calculate corrected tf
function G=correctedtftf()

modeinfo=getmodeinfo();
err=modelcorrection();
s=tf('s');
```

Appendix

```
% calculate transfer function
for i=1:3
    for j=1:3
        % tf for each mode
        for k=1:3 %interest mode number

M(i,j,k)=modeinfo.a(i,j,k)/(s^2+2*modeinfo.zeta(i,j,k)*modeinfo.w(i,j,k)*s+
modeinfo.w(i,j,k)^2);
        end

        % model correctted tf mode 1+mode 2+mode3
        G(i,j)=M(i,j,1)+M(i,j,2)+M(i,j,3)+err(i,j);

    end
end
```

```
%MIMO PPF
function mm=MIMOppf(x)

s=tf('s');

% get trsfer function
G=correcttedtf();
% get mode infomation
modeinfo=getmodeinfo();

%G(1,1)

w1=modeinfo.w(3,3,1); %frequency to be control
w2=modeinfo.w(3,3,2); %frequency to be control
w3=modeinfo.w(3,3,3); %frequency to be control
%ppf controller for mode 1
ppf11=x(1)*(w1^4)/(s^2+2*w1*x(2)*s+w1^2);
ppf12=x(3)*(w1^4)/(s^2+2*w1*x(4)*s+w1^2);
ppf13=x(5)*(w1^4)/(s^2+2*w1*x(6)*s+w1^2);

ppf21=x(7)*(w1^4)/(s^2+2*w1*x(8)*s+w1^2);
ppf22=x(9)*(w1^4)/(s^2+2*w1*x(10)*s+w1^2);
ppf23=x(11)*(w1^4)/(s^2+2*w1*x(12)*s+w1^2);

ppf31=x(13)*(w1^4)/(s^2+2*w1*x(14)*s+w1^2);
ppf32=x(15)*(w1^4)/(s^2+2*w1*x(16)*s+w1^2);
ppf33=x(17)*(w1^4)/(s^2+2*w1*x(18)*s+w1^2);

% %ppf controller for mode 2
ppf11=x(1)*(27.8^2)/(s^2+2*27.8*x(2)*s+27.8^2);
ppf12=x(3)*(w2^2)/(s^2+2*w2*x(4)*s+w2^2);
ppf13=x(5)*(w2^2)/(s^2+2*w2*x(6)*s+w2^2);

ppf21=x(7)*(w2^2)/(s^2+2*w2*x(8)*s+w2^2);
```

Appendix

```
ppf22=x(9)*(w2^2)/(s^2+2*w2*x(10)*s+w2^2);
ppf23=x(11)*(w2^2)/(s^2+2*w2*x(12)*s+w2^2);

ppf31=x(13)*(w2^2)/(s^2+2*w2*x(14)*s+w2^2);
ppf32=x(15)*(w2^2)/(s^2+2*w2*x(16)*s+w2^2);
ppf33=x(17)*(w2^2)/(s^2+2*w2*x(18)*s+w2^2);

% %ppf controller for mode 3
ppf11=x(1)*(w3^2)/(s^2+2*w3*x(2)*s+w3^2);
ppf12=x(3)*(w3^2)/(s^2+2*w3*x(4)*s+w3^2);
ppf13=x(5)*(w3^2)/(s^2+2*w3*x(6)*s+w3^2);

ppf21=x(7)*(w3^2)/(s^2+2*w3*x(8)*s+w3^2);
ppf22=x(9)*(w3^2)/(s^2+2*w3*x(10)*s+w3^2);
ppf23=x(11)*(w3^2)/(s^2+2*w3*x(12)*s+w3^2);

ppf31=x(13)*(w3^2)/(s^2+2*w3*x(14)*s+w3^2);
ppf32=x(15)*(w3^2)/(s^2+2*w3*x(16)*s+w3^2);
ppf33=x(17)*(w3^2)/(s^2+2*w3*x(18)*s+w3^2);

%ppf matrix
ppf=[ppf11,ppf12,ppf13;ppf21,ppf22,ppf23;ppf31,ppf32,ppf33];

%closed loop tf
Gcl=feedback(G,ppf,+1);

% change to statespace form
Gcl=ss(Gcl);

%calculate H infinity norm
mm=norm(Gcl,inf)

end

% % MIMO PPF optimize
% %%%%%%%%%%%%%%%%%%%%%%%%%%%%%%%%%%%%%%%%%%%%%%%%%%%%%%%%%%%%%%%%%%%%%%%%%%
A=[];
b=[];
Aeq=[];
beq=[];
lb=zeros(1,18);
%ub=[1/2.0531,1, 1/1.4362,1, 1/1.4414,1, 1/1.7447,1,
1/1.3305,1, 1/1.0484,1, 1/2.2110,1, 1/1.3818,1, 1/1.1538,1];
%%mode 1
%ub=[1/14.1454,1, 1/4.2439,1, 1/4.2439,1, 1/2.8578,1,
1/8.4493,1, 1/6.9965,1, 1/2.9036,1, 1/9.1842,1, 1/7.6262,1];
%%mode 2
ub=[1/9.9935,1, 1/22.3877,1, 1/16.1255,1, 1/15.7963,1,
1/32.581,1, 1/23.0971,1, 1/18.6406,1, 1/37.8622,1,
1/26.6661,1]; %%mode 3
%ub=ones(1,18);

x=ga(@MIMOppf,18,A,b,Aeq,beq,lb,ub)
```

Bibliography

- [1] Billah, K.Y. and Scanlan, R.H., 1991. Resonance, Tacoma Narrows bridge failure, and undergraduate physics textbooks. *American Journal of Physics*, 59(2), pp.118-124.
- [2] Groothuis, S.S. and Roesthuis, R.J., 2010. Vibration Cancellation Using Synthetic Shunt Impedances (Internship thesis, Flinders University-Adelaide Australia).
- [3] Pratama, G., 2010. Characterization of vibration of two-dimensional rectangular plate (honours thesis, Flinders University-Adelaide Australia).
- [4] Yu, S., 2012. Mechanical Structure Modelling and Vibration Control (bachelor thesis, Flinders University-Adelaide Australia).
- [5] Nguyen, T., 2015. *Vibration Cancellation in Plate Structures* (honours thesis, Flinders University-Adelaide Australia).
- [6] Ogata, K., 2001. *Modern control engineering*. Prentice Hall PTR.
- [7] Ljung, L., 1998. *System identification* (pp. 163-173). Birkhäuser Boston.
- [8] Stoer, J. and Bulirsch, R., 2013. *Introduction to numerical analysis* (Vol. 12). Springer Science & Business Media.
- [9] Hrovat, D., Barak, P. and Rabins, M., 1983. Semi-active versus passive or active tuned mass dampers for structural control. *Journal of Engineering Mechanics*, 109(3), pp.691-705.
- [10] Soong, T.T. and Costantinou, M.C. eds., 2014. *Passive and active structural vibration control in civil engineering* (Vol. 345). Springer.
- [11] LIPTAK, B., 2013. Feedback and FeedforWard Control. *Process Control: Instrument Engineers' Handbook*, p.55.
- [12] Morari, M. and Zafiriou, E., 1989. *Robust process control* (Vol. 488). Englewood Cliffs, NJ: Prentice hall.
- [13] Goh, C.J., 1983. *Analysis and control of quasi distributed parameter systems* (Doctoral dissertation, California Institute of Technology).
- [14] Fanson, J.L., 1987. *An experimental investigation of vibration suppression in large space structures using positive position feedback*.

Bibliography

- [15] Ewins, D.J., 1984. *Modal testing: theory and practice* (Vol. 15). Letchworth: Research studies press.
- [16] Moheimani, S.R., Fleming, A.J. and Halim, D., 2003. *Spatial control of vibration: theory and experiments* (Vol. 10). World Scientific.
- [17] Kwak, M.K. and Heo, S., 2007. Active vibration control of smart grid structure by multiinput and multioutput positive position feedback controller. *Journal of Sound and Vibration*, 304(1), pp.230-245.
- [18] Moheimani, S.R., Vautier, B.J. and Bhikkaji, B., 2006. Experimental implementation of extended multivariable PPF control on an active structure. *IEEE Transactions on Control Systems Technology*, 14(3), pp.443-455.
- [19] Song, G., Schmidt, S.P. and Agrawal, B.N., 2002. Experimental robustness study of positive position feedback control for active vibration suppression. *Journal of guidance, control, and dynamics*, 25(1), pp.179a-182.
- [20] Burl, J.B., 1998. *Linear optimal control: H (2) and H (Infinity) methods*. Addison-Wesley Longman Publishing Co., Inc..
- [21] Haug, E.J., 1989. *Computer aided kinematics and dynamics of mechanical systems* (Vol. 1, pp. 48-104). Boston: Allyn and Bacon.
- [22] Mori, S., Nishihara, H. and Furuta, K., 1976. Control of unstable mechanical system Control of pendulum†. *International Journal of Control*, 23(5), pp.673-692.
- [23] Dorf, R.C. and Bishop, R.H., 1998. *Modern control systems*.
- [24] Kalman, R.E., Falb, P.L. and Arbib, M.A., 1969. *Topics in mathematical system theory* (Vol. 33). New York: McGraw-Hill.
- [25] Lu, Z.J., Honeywell Inc., 1996. *Method of incorporating independent feedforward control in a multivariable predictive controller*. U.S. Patent 5,561,599.
- [26] Skogestad, S. and Postlethwaite, I., 2007. *Multivariable feedback control: analysis and design* (Vol. 2). New York: Wiley.
- [27] LaSalle, J.P. and Lefschetz, S., 1961. *Stability by Liapunov's direct method: with applications* (Vol. 4, pp. vi+-134). New York: Academic Press.
- [28] De Silva, C.W., 1989. *Control sensors and actuators* (Vol. 6). Englewood Cliffs, NJ: Prentice Hall.

Bibliography

- [29] Goodwin, G.C., Graebe, S.F. and Salgado, M.E., 2001. *Control system design* (Vol. 240). New Jersey: Prentice Hall.
- [30] Ferrari, G. and Amabili, M., 2015. Active vibration control of a sandwich plate by non-collocated positive position feedback. *Journal of Sound and Vibration*, 342, pp.44-56.
- [31] Moheimani, S.R. and Heath, W.P., 2002. Model correction for a class of spatio-temporal systems. *Automatica*, 38(1), pp.147-155.
- [32] Shahian, B. and Hassul, M., 1992. *Computer-aided control system design using MATLAB*. Prentice Hall Professional Technical Reference.